

## Journal Pre-proof

Gold nanoparticles: New routes across old boundaries

Yogita Kumari, Gurmandeep Kaur, Rajesh Kumar, Sachin Kumar Singh, Monica Gulati, Rubiya Khursheed, Ayinkamiye Clarisse, K. Gowthamarajan, V.V.S. Narayana Reddy Karri, Ravichandran Mahalingam, Dipanjoy Ghosh, Ankit Awasthi, Rajan Kumar, Ankit Kumar Yadav, Bhupinder Kapoor, Pankaj Kumar Singh, Kamal Dua, Omji Porwal



PII: S0001-8686(19)30134-4

DOI: <https://doi.org/10.1016/j.cis.2019.102037>

Reference: CIS 102037

To appear in: *Advances in Colloid and Interface Science*

Revised date: 16 September 2019

Please cite this article as: Y. Kumari, G. Kaur, R. Kumar, et al., Gold nanoparticles: New routes across old boundaries, *Advances in Colloid and Interface Science*(2018), <https://doi.org/10.1016/j.cis.2019.102037>

This is a PDF file of an article that has undergone enhancements after acceptance, such as the addition of a cover page and metadata, and formatting for readability, but it is not yet the definitive version of record. This version will undergo additional copyediting, typesetting and review before it is published in its final form, but we are providing this version to give early visibility of the article. Please note that, during the production process, errors may be discovered which could affect the content, and all legal disclaimers that apply to the journal pertain.

© 2018 Published by Elsevier.

## Gold Nanoparticles: New Routes Across Old Boundaries

Yogita Kumari<sup>a</sup>, Gurmandeep Kaur<sup>a</sup>, Rajesh Kumar<sup>a</sup>, Sachin Kumar Singh<sup>a</sup> \*, Monica Gulati<sup>a</sup>, Rubiya Khursheed<sup>a</sup>, Ayinkamiye Clarisse<sup>a</sup>, K. Gowthamarajan<sup>b</sup>, V.V.S. Narayana Reddy Karri<sup>b</sup>, Ravichandran Mahalingam<sup>c</sup>, Dipanjoy Ghosh<sup>a</sup>, Ankit Awasthi<sup>a</sup>, Rajan Kumar<sup>a</sup>, Ankit Kumar Yadav<sup>a</sup>, Bhupinder Kapoor<sup>a</sup>, Pankaj Kumar Singh<sup>d</sup>, Kamal Dua<sup>e</sup>, Omji Porwal<sup>f</sup>

<sup>a</sup>School of Pharmaceutical Sciences, Lovely Professional University, Phagwara-144411, Punjab, India

<sup>b</sup>Department of Pharmaceutics, JSS College of Pharmacy, JSS Academy of Higher Education and Research (Deemed to be University), Ootacamund, Tamilnadu.

<sup>c</sup>Reech Pharma, LLC. 37200 Central Court Newark, CA 94560 United States

<sup>d</sup>Department of Pharmaceutics, National Institute of Pharmaceutical Education and Research, Hyderabad, India

<sup>e</sup>Discipline of Pharmacy, Graduate School of Health, University of Technology Sydney, Australia

<sup>f</sup>Department of Pharmacognosy, Faculty of Pharmacy, Ishik University, Erbil, Kurdistan, Iraq

\* Corresponding Author:

Dr. Sachin Kumar Singh

Associate Professor

School of Pharmaceutical Sciences, Lovely Professional University,  
Phagwara (Punjab)- 144411, India.

E-mail address: [singhsachin23@gmail.com](mailto:singhsachin23@gmail.com); [sachin\\_pharma06@yahoo.co.in](mailto:sachin_pharma06@yahoo.co.in);  
[sachin.16030@lpu.co.in](mailto:sachin.16030@lpu.co.in)

Tel.: +919888720835; Fax: +91 1824501900

Funding: This paper was not funded

**Abstract**

In recent years, gold nanoparticles have emerged as unique non-invasive drug carriers for targeting drugs to their site of action. Their site specificity has helped in increasing drugs' efficacy at lower dose as well as reduction in their side effects. Moreover, their excellent optical properties and small size offer their utilization as diagnostic tools to diagnose tumors as well as other diseases. This review focuses on various approaches that have been used in last several years for preparation of gold nanoparticles, their characterization techniques and theranostic applications. Their toxicity related aspects are also highlighted. Gold nanoparticles are useful as theranostic agents, owing to their small size, biocompatible nature, size dependent physical, chemical and optical properties etc. However, the challenges associated with these nanoparticles such as scale up, cost, low drug payload, toxicity and stability have been the major impediments in their commercialization. The review looks into all these critical issues and identifies the possibilities to overcome these challenges for successful positioning of metallic nanoparticles in market.

**Keywords:** Gold nanoparticles; Turkevich method; Green synthesis; Characterization; Theranostics

## 1. Introduction

Over past 35 years, nanoparticles (NPs) have been used as a potential drug delivery system in medical as well pharmaceutical applications. Metallic NPs are nano sized entities composed of pure metals like gold, silver, platinum and zinc, having size range of 1-100 nm. Due to their unique properties like small size, biocompatibility [1], bioavailability of entrapped drugs [2] and easy functionalization with ligands as well as antibiotics [3], they are considered as excellent carriers for biomedical applications like diagnosis [4], therapeutics [5], imaging [6] and site-specific delivery of drug [7]. Metallic NPs have gained more interest and publicity in current scenario because of their huge potential in nanotechnology [8]. In past few years, various types of NPs have been introduced like gold, silver, platinum, zinc and copper out of which, gold is highly preferred due to its favorable physical, chemical and optical properties. Gold NPs (AuNPs) exhibit various shapes such as spherical, rod shaped, wire, triangular, octahedral, and tetrahedral [9]. Spherical AuNPs exhibit various colors ranging from brown to orange to red to purple in aqueous solution with increase in core size from 1 to 100 nm, and generally show a size-relative absorption peak from 500 to 550 nm. This absorption band arises from the collective oscillation of the conduction electrons due to the resonant excitation by the incident photons. This phenomenon however, is absent in both small nanoparticles ( $d < 2$  nm) and the bulk material. This phenomenon is not only dependent on size, but is also influenced by shape, solvent, surface ligand, core charge, temperature and the proximity of other nanoparticles. The aggregation of nanoparticles results in significant red-shifting of SPR frequency, broadening of surface plasmon band and changing the solution color from red to blue due to the interparticle plasmon coupling [10]. AuNPs are widely used now days in various biomedical applications due to their ease of synthesis and conjugating properties [11].

AuNPs are preferred as a good candidate for labeling technique because of their capability to interact with visible light [10]. They are used as a photo thermal agent that causes destruction of adjacent cancer cells by producing enough heat. Due to their unique properties, AuNPs have been used as biosensors for the detection of toxins [11]. Major advantage of using AuNPs as drug carriers is their easy surface modification so that they can be attached with different ligands for targeted drug delivery. The inorganic outer layer of the NPs has a better impact for various biomedical applications which includes drug delivery, imaging and sensing. Size and shape of AuNPs play an important role in cellular uptake. NPs conjugated with cell penetrating peptides were transported into the cytoplasm which showed their ability to behave as a functional unit for delivery of drugs to various sites [12]. Surface modification of AuNPs with peptides have been shown to allow their release into the cellular matrix. High stability of gold-ligand complex outside the cells resulted in higher glutathione concentration, which makes AuNPs suitable carrier for cellular delivery of drug. NPs incorporated with anti-epidermal growth factor receptor exhibited greater absorption in cancer cells as compared to normal cells. AuNPs conjugated with gemcitabine and C225 (ligand conjugated AuNPs) were successfully used to treat pancreatic cancer cells [13].

One of the major advantages of AuNPs is their stability against oxidation [14] and degradation *in vivo* [15], which enables them to be used as potential therapeutic and diagnostic tools. In 1925, efficacy of gold to alleviate rheumatoid arthritis was tested in clinical trials. During the same year, very first clinical testing of gold for its bacteriostatic effect was performed [16]. These studies allowed the introduction of gold complexes as a remission inducing agent by a French physician. However, clinical use of sulphur-gold was found to be limited because of its toxicity. This led to introduction of auranofin (lipophilic gold components) which can be given orally [17]. In a recent study, delivery of AuNPs conjugated with TNF (tumor necrosis factor) *in vivo*, showed less toxicity and more

effectiveness than the parent TNF. Recently it was found that AuNPs inhibited VPF/VEGF-165 mediated endothelial cell proliferation *in vitro* and reduced ascites accumulation *in vivo*. These AuNPs bound with heparin binding domain inhibited different growth factors such as VEGF-121 and epidermal growth factor resulting in reduction of angiogenesis and edema formation [18].

Despite having various advantages in various biomedical applications, commercialization of the same has not fully been exploited. This is attributed to the challenges involved in the synthesis of AuNPs. The current paper focuses on properties of AuNPs, different techniques of synthesis, their theranostic applications and various limitations such as challenges associated with their synthesis and toxicity aspects. Various modification associated with different methods and techniques used to characterize them are also discussed.

## **2. Properties of Gold NPs**

Optoelectronic properties related to shape and size are amongst the dominant characteristics including excellent biocompatibility, large surface to volume ratio and minor toxicity that mark AuNPs as a significant tool in bio nanotechnology field [19, 20]. Main physical characteristics of AuNPs include Surface Plasmon Resonance (SPR) along with the capacity for fluorescence quenching depending on their own morphological properties (*viz.* solvent, core charge, solvent, surface ligand, temperature) and physiology [21]. The optical intrinsic features of AuNPs related to their physiology and morphology allow them to be complex therapeutic clinical agents.

The spherical AuNPs aqueous solution exhibits a colors range (orange, brown and red to purple) along with core size growth variation from 1 to 100 nm and shows the absorption peak from 500 to 550 nm depending upon their size [22]. The absorption band ascends from

collective oscillation of conduction band electrons as a result of excitation due to incident photons are termed as “Surface Plasmon Band” (SPB) [23].

Surface plasmon resonance (SPR) is the resonant oscillation of conduction electrons at the interface between negative and positive permittivity material stimulated by incident light

Nevertheless, there is absence of the band in both minor NPs ( $d < 2$  nm) as well as in the bulky material. This phenomenon depends on solvent, size, surface ligand, shape, temperature, core charge and it is sensitive to other NPs proximity [24].

NPs aggregation leads to major red-shift of SPR frequency while there is a change in color of the solution from red to blue as a result of interparticles Plasmon coupling. The outstanding quenching capacity of AuNPs towards proximal fluorophores derives from the deactivation pathway which is based on the proper overlapping among the excited fluorophores emission spectrum and the AuNPs [25].

This fluorescence resonance energy transfer (FRET) phenomenon is observed even in the presence of 1 nm AuNPs due to the fact that radiative and non-radiative decay rates of fluorescent molecules are both distinctly affected by the NPs. AuNPs can act like electron acceptors in order to quench the fluorophores of the photon induced electron transfer (PET) procedure. The modulation of this process is by discharging/charging the gold core that might be used in fabrication of sensor [26].

### **3. Preparation of AuNPs**

Two major approaches i.e. top down and bottom up are used for fabrication of AuNPs [27]. For top down techniques, a bulk state gold is systematically broken down to generate AuNPs of desired dimensions. In this case, particle arrays and formation are controlled by a pattern or matrix. In case of bottom up approach, atoms are arranged to form nano size particles. Top down method includes bulk metal grinding/mechanical milling, sputtering, laser ablation,

thermal decomposition and lithography. Bottom up uses colloidal techniques including methods such as Turkevich [28] and Brust[29] and green method [30]. Various approaches used to prepare AuNPs are shown in Fig.1.

Journal Pre-proof



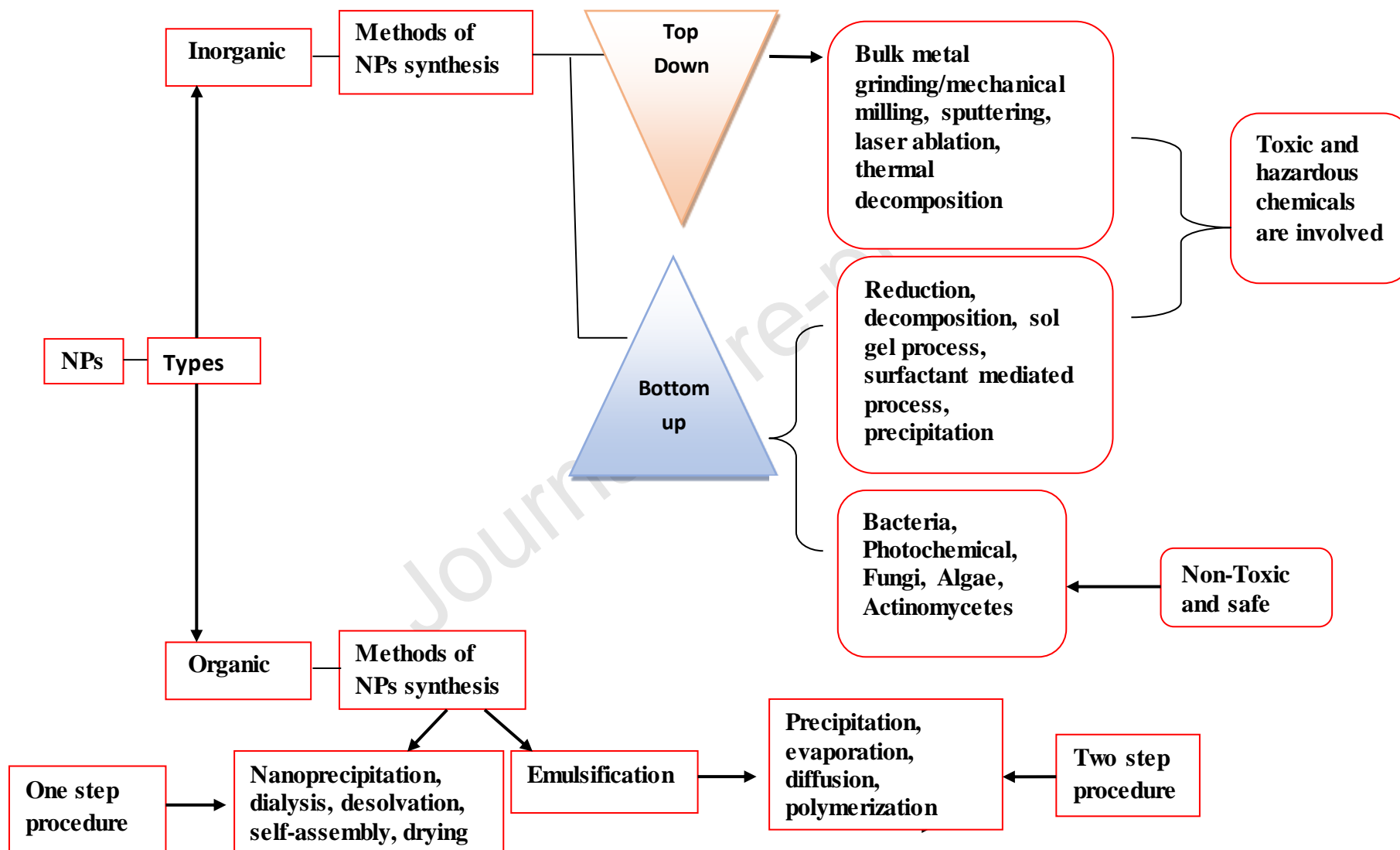


Fig.1. Overall scheme for synthesis of AuNPs involving top down and bottom up approaches

### 3.1. Chemical method

Chemical method is also known as liquid phase synthesis method. Hydrochlorauric acid ( $\text{HAuCl}_4$ ) is used as gold precursor. In this method, AuNPs are firstly reduced with the help of reducing agents such as sodium citrate, borohydrides, hydrogen peroxide. After reduction, they are stabilized with the help of stabilizing agents such as thiols, amines, tetraacetylammonium bromide (TOAB) etc. Stabilizing agents prevent aggregation of NPs by forming protective layer on the surface of the NPs and help them to disperse. Among the stabilizers, citrate acts as both reducing and stabilizing agent [31]. Some chemical methods involve use of matrix that acts as support for synthesis of NPs.

**3.1.1. Turkevich method (TM)** -This method was designed by John Turkevich in 1951 [28]. It is one of the most commonly used methods for synthesizing AuNPs of spherical shape within the range of 10-20 nm using sodium citrate as reducing agent as well as stabilizing agent. Since it involves the use of citrate as reducing agent, this method is also called citrate reduction method [32].

Turkevich et al., (1951) prepared colloidal gold using different solutions of reducing agents viz Faraday solution, Bredige solution and sodium citrate solution in aqueous medium. A) Faraday solution was prepared by addition of a saturated solution of white phosphorous into diethyl ether followed by its dilution with three times the volume of diethyl ether. To this solution chloroauric acid containing Au ( $\text{HAuCl}_4$ ) and 0.1N KOH were added. This solution was treated with either phosphorous solution or phosphorous ether solution. After adding phosphorous ether, the solution first changed its color firstly to pink, then grey, purple and then to red and finally a deep red product was obtained. Solution was boiled and stream of air was drawn through it to oxidize the remaining phosphorous. Both the solutions prepared were examined by electron microscope

which revealed that both contained extremely fine AuNPs [28]. The major limitation of TM method was its failure to produce Au NPs with large diameters ( $d_c > 50\text{nm}$ ) and with acceptable monodispersity. This issue was overcome by controlling the reaction conditions (temperature, pH, stirring speed, etc.), stoichiometry of the reagents (gold salt to sodium citrate ratio), and addition of additives [32]. The modifications introduced to overcome the limitations of TM method are discussed below.

B) In another method, Bredige solution was prepared by striking an arc from two gold wires under very dilute sodium hydroxide solution with a 115 V, 60-cycle potential. The reaction yielded purple cloud. The reaction was continued until a fairly intense purple colour had developed. The results of scanning electron microscopy revealed that the obtained particles ranged in diameter from **30-100 Å**. However, the particles were found agglomerated due to their small size [32].

C) In another method,  $\text{HAuCl}_4$  solution containing Au was heated to the boiling point then 1% sodium citrate solution was added to the boiling solution with mechanical stirring. After one-minute, grayish pink to grayish blue tone was observed which gradually darkened and deep wine-red color was observed as a final color. Electron microscopic examination of AuNPs prepared by using all the before mentioned solutions revealed that this colloid is highly reproducible and could provide spherical particles (mean diameter is  $200 \pm 15 \text{Å}$ ). Use of sodium citrate as reducing agent was thus found to result in the formation of spherical AuNPs. From the study it could be concluded that characteristics of AuNPs were dependent upon two main factors, one “nucleation”, in which a new phase of discrete particles is being generated in a single-phase system and second “growth” which is defined as a process in which additional material deposits on these particles leading to increase in their size [32].

**Frens et al.**, (1973) modified the TM, however, the basic principle was kept same. Frens studied the effect of reactants concentration (sodium citrate and  $\text{HAuCl}_4$ ) on nucleation and growth formation of particles. From the experiment, it was concluded that size of NPs depends upon number of nuclei which grows into NPs and also reported that reduction of  $\text{HAuCl}_4$  using sodium citrate is a promising step for formation of monodispersed AuNPs having different particle size [33].

**Ojea-Jimenez et al.**, 2011 reported an experimental method to determine the effect of decarboxyacetone (DCA) as a stabilizer on the synthesis of AuNPs. This method led to formation of AuNPs with better size distribution and uniform shape by changing the sequence of reagent addition. It was observed that change in the sequence of reagent addition led to red shift of the Plasmon band from 518 nm to 527 nm [34].

**Zhao et al.**, (2013) also reported *in-situ* synthesis (in the reaction mixture) of AuNPs using sodium citrate as reducing as well as stabilizing agent [35]. The synthesized NPs were functionalized with drugs and used further for various diagnostic applications [36]. More spherical shaped particles were synthesized when a slight modification was made in TM [37]. It was also noted that upon reduction of temperature, the shape of the particles became irregular [38].

Spherical shaped citrate stabilized AuNPs with core diameter of 5 nm were reported by Piella et al [38], 13 nm were reported by Schulz et al. [39] 18 nm and between 19 nm to 100 nm were prepared and reported by Bastus et al. [40]. Citrate stabilized AuNPs of 5 nm core diameter were synthesized by reacting 2.2 mM sodium citrate, 0.1 mL of 2.5 mM tannic acid (used for homogeneous growth of seeds) and 1 mL of 150 mM potassium carbonate in a 250 mL three necked round bottom flask connected with the condenser to prevent the evaporation of the

solvent. The solution was heated on a heating mantle with vigorous stirring. Upon temperature of solution reaching to 70°C, 25 mM HAuCl<sub>4</sub> (1 mL) was quickly injected. Within 2 minutes the colour of solution changed to purple and then to red. The solution was kept heated for 5 min more at 70°C for complete reduction of gold ions [38]. The reaction is shown in Fig.2.

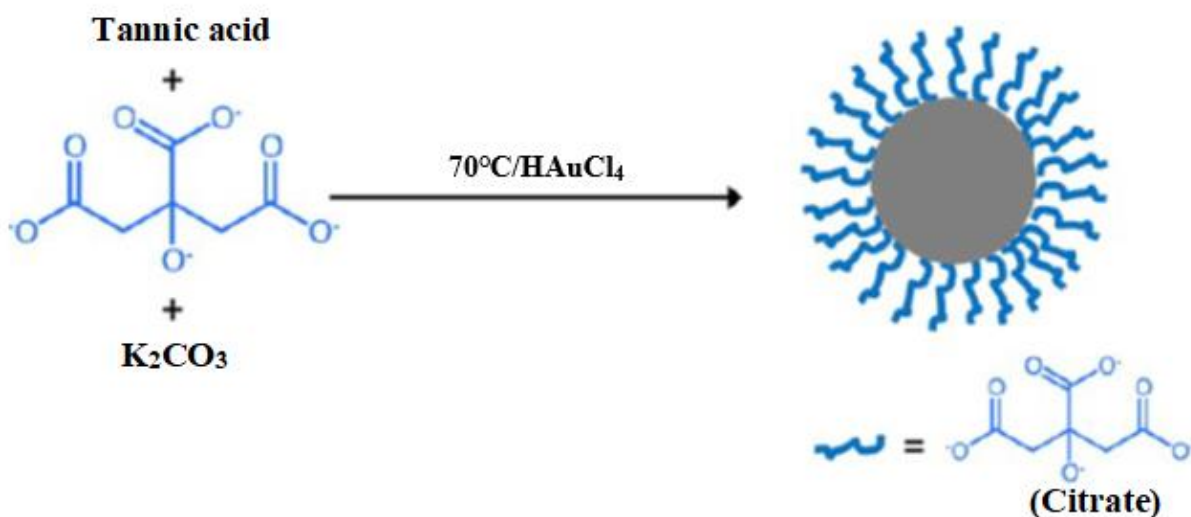


**Fig.2.** Synthesis of Cit-Au NPs in water with 5 nm core diameter. Reprinted with permission from [32] Copyright 2017, American Chemical Society.

Citrate stabilized spherical AuNPs with a core diameter equal to 13 nm were synthesized by reacting 3.5 mL of 60 mM sodium citrate and 1.5 mL of 60 mM citric acid in 100 mL of boiling water in a three necked round bottom flask connected with the condenser on a heating mantle stirred at 450 rpm for 30 min. In order to get narrow size distribution, the pH of solution was kept constant by the addition of citrate buffer and heating time was kept 30 min. To the above prepared solution, 0.1 mL of ethylene diamine tetra-acetic acid was injected rapidly. This was followed by addition of 1 mL of 25 mM aqueous solution of hydrogen tetrachloroaurate (III). A wine-red solution of citrate stabilized AuNPs were obtained. After cooling down the reaction

mixture to 95°C, the flask containing citrate AuNPs was immersed in ice to stop the reaction. This yielded spherical AuNPs of 13 nm core diameter [39].

Spherical citrate stabilized AuNPs with core diameter 18 nm were prepared by boiling the reaction mixture containing 150 mL of a 1.32 mM sodium citrate solution and 1.5 mL of 25 mM of HAuCl<sub>4</sub> in a three necked round bottom flask connected with condenser. Red colour citrate AuNPs of 18 nm core diameter were obtained [40]. These 18 nm spherical citrate AuNPs were used as seed solution to prepare nanoparticles above 18 nm and between 100 nm core diameter. To the seed solution, 25 Mm HAuCl<sub>4</sub> (1 mL) was injected and the solution was stirred for 30 min. This process was repeated thrice (total three injections of gold salts per growth step). The temperature of reaction mixture was kept to 90°C during the entire process. This solution (55 mL) was diluted using 53 mL of Milli-Q water. To this, 2 mL of 60 mM sodium citrate was added. The solution was stirred at 90°C for another 15 min. By three consecutive gold additions (0.025 mM, 1 equivalent each) separated by 30 min interval, citrate gold nanoparticles with 25 nm core diameter were obtained. Later they were grown to 50 nm and 100 nm using the aforementioned steps [32, 40].

**3.1.2. Brust-Schiffrin method-** The two phase Brust-Schiffrin method, reported in 1994, was the first method where thiol-stabilized AuNPs were prepared via in situ synthesis [29]. The method is advantageous due to facile synthesis of AuNPs at ambient condition, relatively high thermal stability, easy functionalization and modification by ligands. Synthesis using this method led to formation of thermally stable AuNPs having size range of 1.5-5.2 nm. In this method, HAuCl<sub>4</sub> aqueous solution was transferred to organic phase (toluene) using phase transfer catalyst tetra octyl ammonium bromide (TOAB). Further reduction was done using sodium borohydride (NaBH<sub>4</sub>) in the presence of thiol group derivative such as alkanethiol or dodecanethiol which

resulted in change in color of the solution from orange to deep brown and this confirmed the formation of AuNPs. The method of Brust-Schiffrin is described in detail by Perala and Kumar [19, 41]. It was reported that under invariable conditions of synthesis, the continuous nucleation of synthesis, the continuous nucleation-growth process leads to complete coating of equally sized particles by a thio ligand. The scheme for synthesis of gold nanoparticles coated by the thio ligand according to Brust-Schiffrin is shown in Fig.3. This method was further modified in 1995. Synthesis of stable gold nanoparticles was reported using p-mercaptophenol. The preparation of the p-mercaptophenol-derivatized material was carried out in a single-phase system to avoid the extraction of p-mercaptophenol into the alkaline aqueous phase. Hydrogen tetrachloroaurate trihydrate and p-mercaptophenol were dissolved in methanol in presence of acetic acid and aqueous sodium borohydride. The role of acetic acid was to prevent the deprotonation of p-mercaptophenol. Brown colour gold clusters of size 2 nm were obtained. The solution was stirred for 30 minutes below 50°C under reduced pressure to remove solvent. The residue was washed thoroughly with diethyl ether to remove excess p-mercaptophenol followed by water to remove borates and acetates. The solvent was removed under reduced pressure to give the pure product as a dark-brown solid [42].

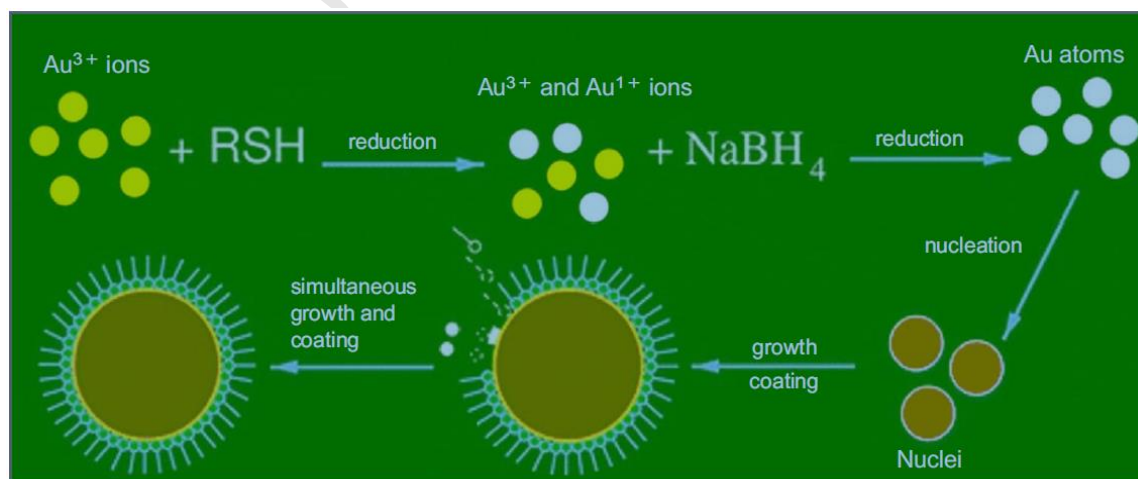


**Fig.3.** Brust-Schiffrin method to prepare this stabilized AU-NPs. Reprinted with permission from [41]. Copyright 2017, American Chemical Society.

### **3.1.3. Synthesis of Dodecanethiol-Stabilized Hydrophobic Au NPs ( $\approx 4$ or $7$ nm core diameter)**

This method is also a modification of Brust-Schiffrin method. Initially,  $0.9$  mM aqueous solution of  $\text{HAuCl}_4$  was prepared by dissolving  $300$  mg of  $\text{HAuCl}_4$  in  $25$  mL of water. The organic phase was prepared by dissolving  $2.17$ g ( $3.9$  mM) of TOAB in  $80$  mL of toluene. Both the solutions were transferred in the separating funnel and shaken for  $5$  min. This caused the migration of  $\text{AuCl}_4^-$  ions into the organic phase of toluene, causing formation of TOAB ion pairs. The aqueous solution was discarded and organic phase was transferred to a  $250$  mL round flask. Parallel to this, aqueous solution of sodium borohydride ( $\text{NaBH}_4$ ) was prepared. The AuNPs were obtained by dropwise addition of sodium borohydride solution for  $1$  min. with vigorous stirring to the organic phase containing precursor of gold. Thus, reduction of Au (III) to Au (0) forming AuNPs took place. After few seconds of addition of sodium borohydride, the colour changed was observed from deep orange (Au (III) precursor) to red violet indicating formation of TOAB conjugated AuNPs (TOAB-AuNPs). The stirring was continued for complete reduction of remaining gold ions. The aqueous phase was discarded and organic phase was separated out using separating funnel and washed with  $10$  mM  $\text{HCl}$  (aq.),  $10$  mM  $\text{NaOH}$  (aq.), and three times with  $25$  mL Milli-Q water to dissolve residual precursors and salts. Once again, the entire solutions i.e. organic phase and combined aqueous solutions of washings (i.e.  $\text{HCl}$ ,  $\text{NaOH}$  and water) were added to the separating funnel and organic phase was collected, whereas, aqueous phase was discarded. A deep-red organic solution was transferred to the round bottom flask and stirred overnight to get thermodynamically stable nanoparticles (TOAB-AuNPs). The scheme for preparation of TOAB-AuNPs is shown in Fig.4. These TOAB-AuNPs were further stabilized



using dodecanethiol (DDT) through ligand exchange procedure. To carry out this, 1-DDT (10 mL) was added to TOAB-AuNPs (80 mL) in toluene. The solution was heated to 65°C and stirred for 2h in order to displace TOAB by the mercapto group of DDT molecule to get DDT-stabilized AuNPs (DDT-AuNPs). The solution was centrifuged and supernatant was collected. The precipitate was discarded. The supernatant was the uniform suspension of DDT-AuNPs. This was precipitated using methanol as a non-solvent and the solution was centrifuged to get the precipitate of DDT-AuNPs and the supernatant was discarded. The collected precipitate was resuspended in chloroform and precipitated using methanol and recentrifuged. Finally, the precipitate was resuspended in chloroform to obtain final solution of DDT-AuNPs [32]. The entire scheme for synthesis of DDT-AuNPs is shown in Fig.4.

**3.1.4. Seed growth method-**The seed growth method is another popular technique for synthesis of AuNPs that has been used for more than a century. Seed growth method causes enlargement of the particles step by step and it is easier to control size and shapes of formed AuNPs. Using TM and Brust's method, only spherical AuNPs were synthesized but using seeded growth method, different shapes of NPs (sphere, oval and rod) were produced. In first step, seeds of Au salts were produced by reducing  $\text{HAuCl}_4$  with strong reducing agent such as  $\text{NaBH}_4$ . Then the seeds produced were added to the solution of Au salt in the presence of ascorbic acid. In addition to that the structure directing agents were also added to prevent aggregation and nucleation (phase transformation from solute in solution to crystal lattice). The reducing agents used in the second step were always mild ones that reduce Au (III) to Au (0) only in the presence of Au seeds as catalyst. Thus, the reduced Au (0) were only assembled on the surface of the Au seeds, and no new nucleation occurred in solution. The first step of this reaction was faster than the

second step. In seed growth method, the ratio of stabilizer and reducing agent controlled the surface properties, size and shape of the AuNPs [43].

Jana et al. (2001), reported wet chemical synthesis of cylindrical gold nanorods with high aspect ratio of  $4.6 \pm 1.2$ ,  $13 \pm 2$ , and  $18 \pm 2.5$  using citrate-capped AuNPs (3.5 nm diameter) as seed in presence of an aqueous micellar template. The AuNPs seed was prepared by reduction of  $\text{HAuCl}_4$  with borohydride. The ratio of seed to metal salt was varied to control the aspect ratio of the nanorods [44].

Journal Pre-proof

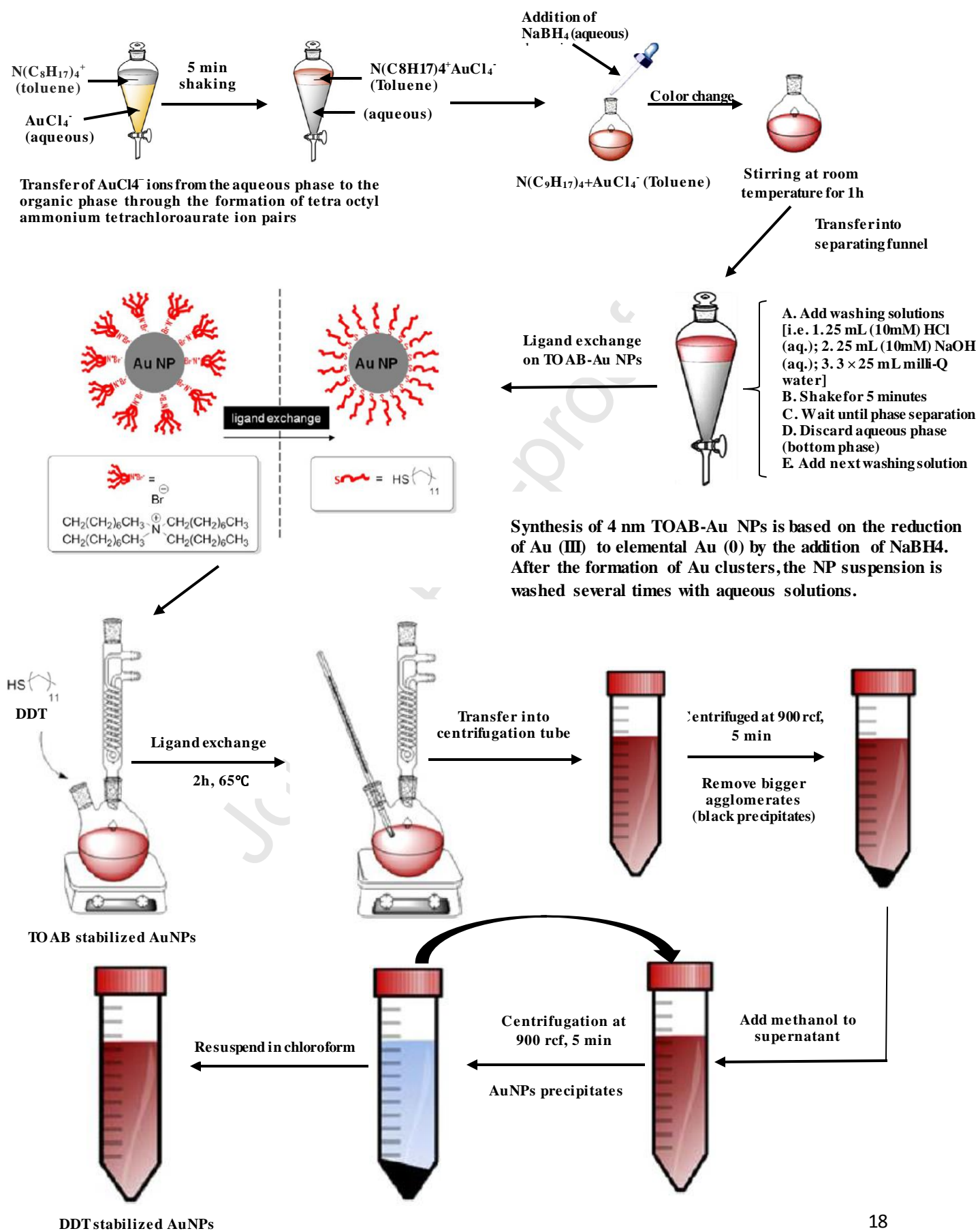


**Fig.4.** Scheme for synthesis of DDT-AuNPs. Reprinted with permission from [32]. Copyright 2017, American Chemical Society.

### 3.1.4.1. Synthesis of CTAB stabilized gold nanorods

Gold nanorods having various longitudinal surface plasmon resonance have been prepared using seed-mediated wet synthesis method [32]. At first stage a seed solution was prepared in presence of cationic surfactant hexadecyl trimethyl ammonium bromide (CTAB) and silver ions (silver nitrate). The reported core diameter of these seed AuNPs was about 4 nm. This seed solution was further injected to the growth solution that contains more gold ions, silver ions and CTAB. These gold ions in the growth solution were partially reduced to Au (I) to allow complete reduction to Au (0) at the surface of the added seeds only to promote growth of gold nanorods and for preventing undesired nucleation and formation of nanospheres as side product. It is important to note that the shape yield and length to width ratio of nanorods is controlled by concentration of silver ions in solution. CTAB acts as shape directing agent as well as capping agent to form CTAB-capped gold nanorods [45]. The unidirectional growth of nanorods was controlled by CTAB. However, apart from concentration of silver nitrate and CTAB, other reaction conditions were also responsible for yielding nanorods having different surface plasmon resonance. These reaction conditions include volume of hydrochloric acid, pH, and volume of acetic acid solution. [32]

It has been reported that traditional protocol that has been used to prepare gold nanoparticles using high concentration of CTAB (upto 0.1M) were cytotoxic. Hence, they could not find their potential for biomedical applications. Attempts have been made by researchers to reduce the concentrations of CTAB.

Nikoobakht and El-Sayed (2003), prepared gold nanorods with aspect ratios ranging from 1.5 to 10. The surface plasmon absorption maxima of these nano rods were observed between 600 and 1300 nm using hexadecyltrimethylammonium bromide (CTAB)-capped seed. The formation of reproducible gold nanorods having aspect ratios ranging from 1.5 to 4.5 took place using CTAB alone. Whereas a binary mixture of benzyl dimethyl hexadecyl

ammonium chloride (BDAC) and CTAB were used to produce longer gold nanorods having aspect ratios ranging from 4.6 to 10 [46].

In 2012, Murray and co-workers reported that presence of aromatic additives such as 5-bromosalicylic acid (5-BS). Using 5-BS the amount of CTAB required to control shape of gold nanorods reduced to half [45]. In 2013, Murray and co-workers prepared gold nanorods using a mixture of CTAB and sodium oleate. The amount of CTAB required in this synthesis was 0.037M, which was very less than the traditional method [47].

#### **3.1.4.2. Synthesis of ascorbic acid stabilized gold nanostars**

This is another example for seed growth method. The gold nanostars were prepared using spherical gold nanoparticles as seeds and using silver ions as blocking facet agents. The silver ions acted as growth promotor of spherical nanoparticles. The reduction of gold salt using ascorbic acid promotes the seed growth rather than independent nucleation.

The Au nanostars were prepared by mixing 20 mL of aqueous solution of  $\text{HAuCl}_4$  ( $5\mu\text{M}$ ), 0.03 mL of aqueous solution of 1M HCl ( $0.03\text{mM}$ ) and 1.5 mL of AuNPs of 13 nm diameter (as seed solution). To the above solution, 0.15 mL of 1 mM silver nitrate solution and 0.15 mL of 66.67 mM ascorbic acid were added. This was followed by simultaneous addition of aqueous solution of 10 mg/mL  $\alpha$ -methoxy- $\omega$ -thiolpoly (ethylene glycol) and 0.05 mL of 2 M sodium hydroxide (Fig.5). Afterwards, the solution was immersed in ice to terminate the reaction. This yielded ascorbic acid stabilized nano stars. [32]

#### **3.1.5. Synthesis of hexanoic acid stabilized AuNPs ( $\approx 4$ nm core diameter)**

Hexanoic acid stabilized AuNPs (HA-AuNPs) were prepared by reacting 231 nM solution of HA (HA solution was prepared in toluene) with 97.2 mM solution of tetra butyl ammonium borohydride (TBAB) at room temperature in a 25 mL round bottom flask. TBAB solution was prepared in didodecyl dimethyl ammonium bromide (DDAB). To the above reaction mixture, 25  $\mu\text{M}$  solution of  $\text{AuCl}_4$  prepared in DDAB stock and 2 mL solution of DDAB

stock prepared in toluene were added vigorously. The flask was shaken vigorously for 1h at room temperature to yield HA-AuNPs [32].

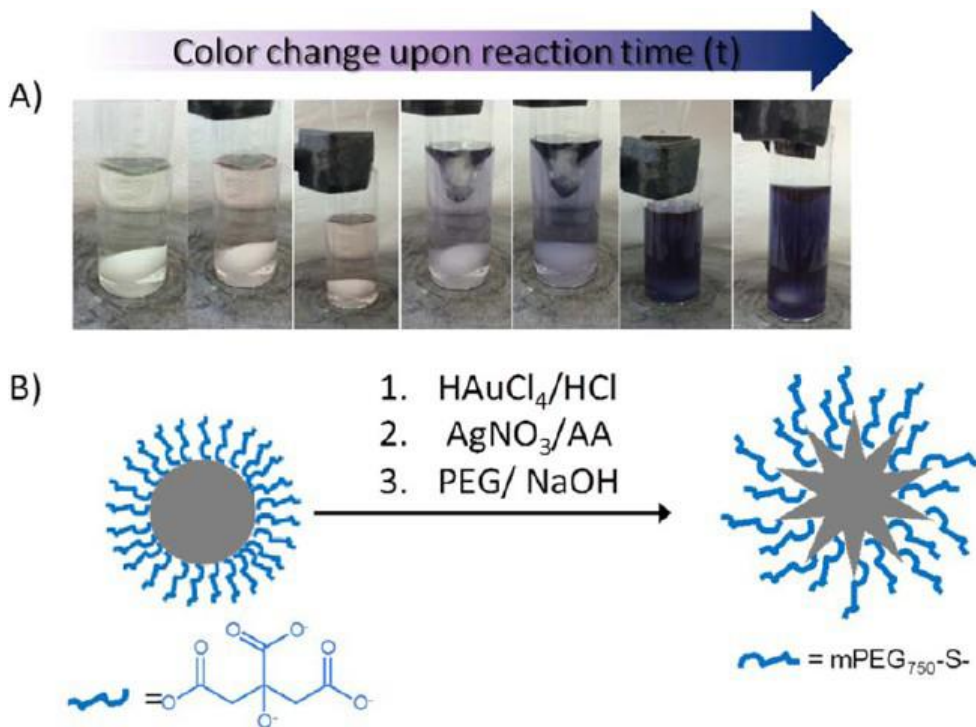


**Fig.5.** (A) Synthesis process of PEG-coated star-shaped Au NPs. After addition of  $\text{AgNO}_3$  and AA, the solution color changed from soft red to light blue in a few seconds and then to dark blue, which is indicating the formation of gold nanostars. (B) The cartoon demonstrates the seed mediated growth of spherical gold NPs (seeds) into star-shaped Au NPs. The final surface functionalization of the resulting NPs is PEG-SH, as mediated by displacement of physically adsorbed citrate ions by chemically assembled PEG-S-molecules via the strong S-Au bond. Reprinted with permission from [32]. Copyright 2017, American Chemical Society.

### 3.1.6. Synthesis of decanoic acid stabilized AuNPs ( $\approx 7$ nm core diameter)

Decanoic acid stabilized AuNPs (DA-AuNPs) were prepared by reacting 250  $\mu\text{M}$  solution of DA (DA solution was prepared in toluene) with 97.2 mM solution of tetra butyl ammonium borohydride (TBAB) at room temperature in a 25 mL round bottom flask. TBAB solution was prepared in didodecyl dimethyl ammonium bromide (DDAB). To the above reaction mixture, 25  $\mu\text{M}$  solution of  $\text{AuCl}_4$  prepared in DDAB stock and 2 mL solution of DDAB

stock prepared in toluene were added vigorously. The flask was shaken vigorously for 1h at room temperature to yield DA-AuNPs [32].

**3.2. Green method of synthesis of AuNPs using plant extracts and microbes-** Chemical method employs use of toxic chemical and solvents for synthesis. These chemicals have adverse effect on the environment and social health. They may also lead to cytotoxicity as they get adsorbed on the surface of NPs using synthesis. Hence, to overcome all these limitations, researchers have developed a new method known as green method which employs use of plant extracts (Fig.6) [48] and microorganisms for the synthesis of AuNPs (Fig.7) [49]. Although such type of synthesis also involved chemical reaction (reduction) but due to use of natural products the synthesis is called as green synthesis. Phytoconstituents present in plant and microorganisms are responsible for the reduction and stabilization of NPs. In addition to that AuNPs synthesized using green method do not require functionalization agent to become active [50]. List of various plant sources used by different researchers for the synthesis of AuNPs are listed in Table 1.

### **3.3. Synthesis of AuNPs using synthetic polymers**

AuNPs are also synthesized by the reduction of  $\text{HAuCl}_4$  with low-molecular-mass compounds and the subsequent adsorption of biopolymers [60]. These biopolymers include, PVP (reduction with potassium bitartrate, ascorbic acid, sodium diphenylaminosulfonate, sodium borohydride or, sodium citrate [61], polyacrylamide (reduction with sodium borohydride) [62], polyethylene glycol (PEG) (reduction with hydroxylamine) [63], styrene-vinylpyridine copolymer (reduction with hydrazine) [60], polyethyleneimine (PEI) or poly(vinyl alcohol) (reduction with sodium borohydride or ascorbic acid), polydithiafulvene [64], sodium polyacrylate [65], poly(ethylene oxide) - poly(propylene oxide) block copolymer [66], polyacrylamide [67], poly-allylamine [68], polyphenols [69], poly(L-lysine) [70] and polydi-methylaminoethyl methacrylate [71]. In addition, surfactants such as

acetylene glycol [72], oleylamine [73], oxyethylene-diamine [74], Tween 80 and organic compounds such as disulfanylsuccinic acid [75] or cycloketones [76]. In these cases, the stability of AuNPs greatly depends upon the molecular mass. Higher molecular mass yielded more stable AuNPs. For example, in case of PEG the stability of AuNPs follows the given order:

PEG 20000 > PEG 8000 > PEG 3350 > PEG 1450

Journal Pre-proof



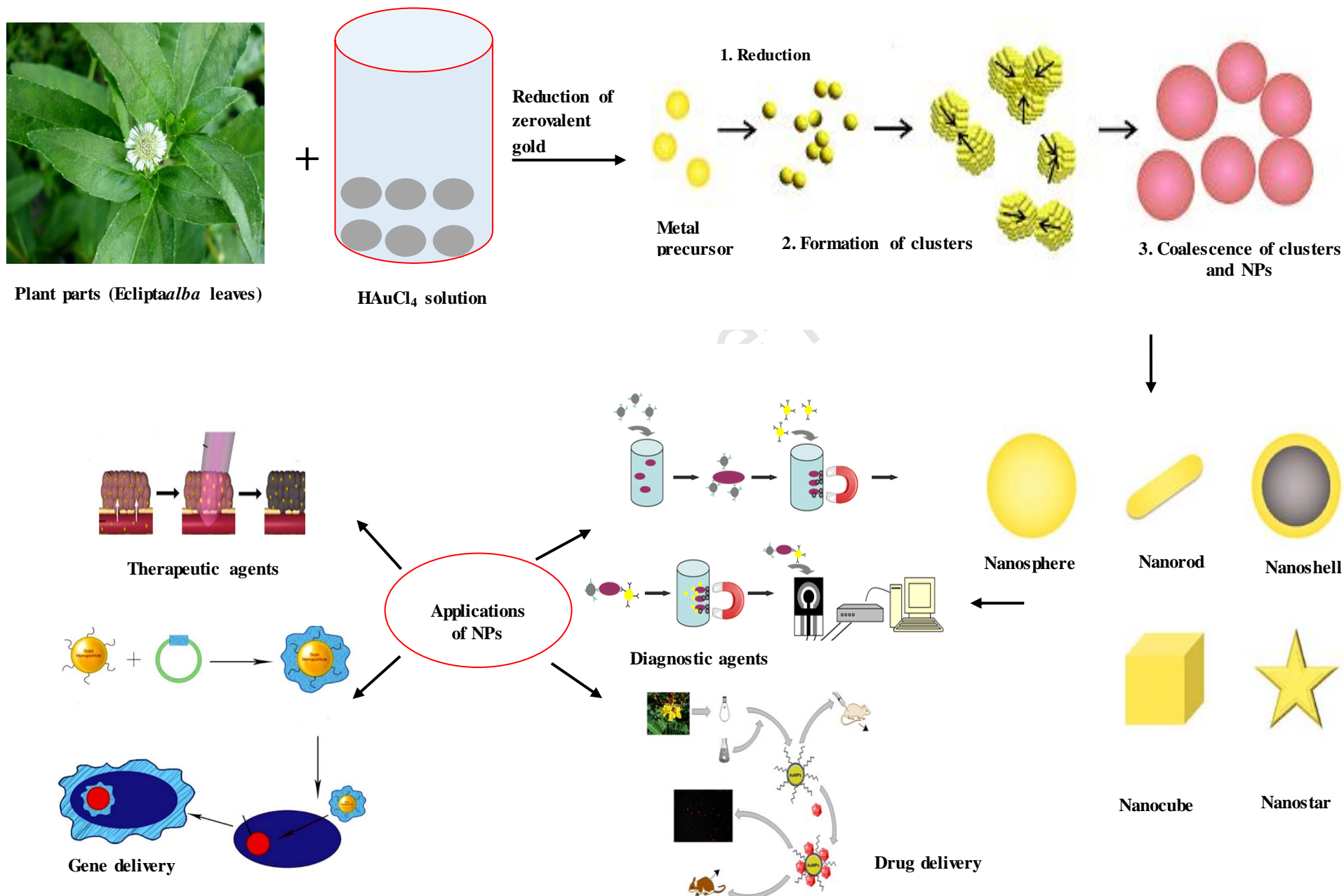
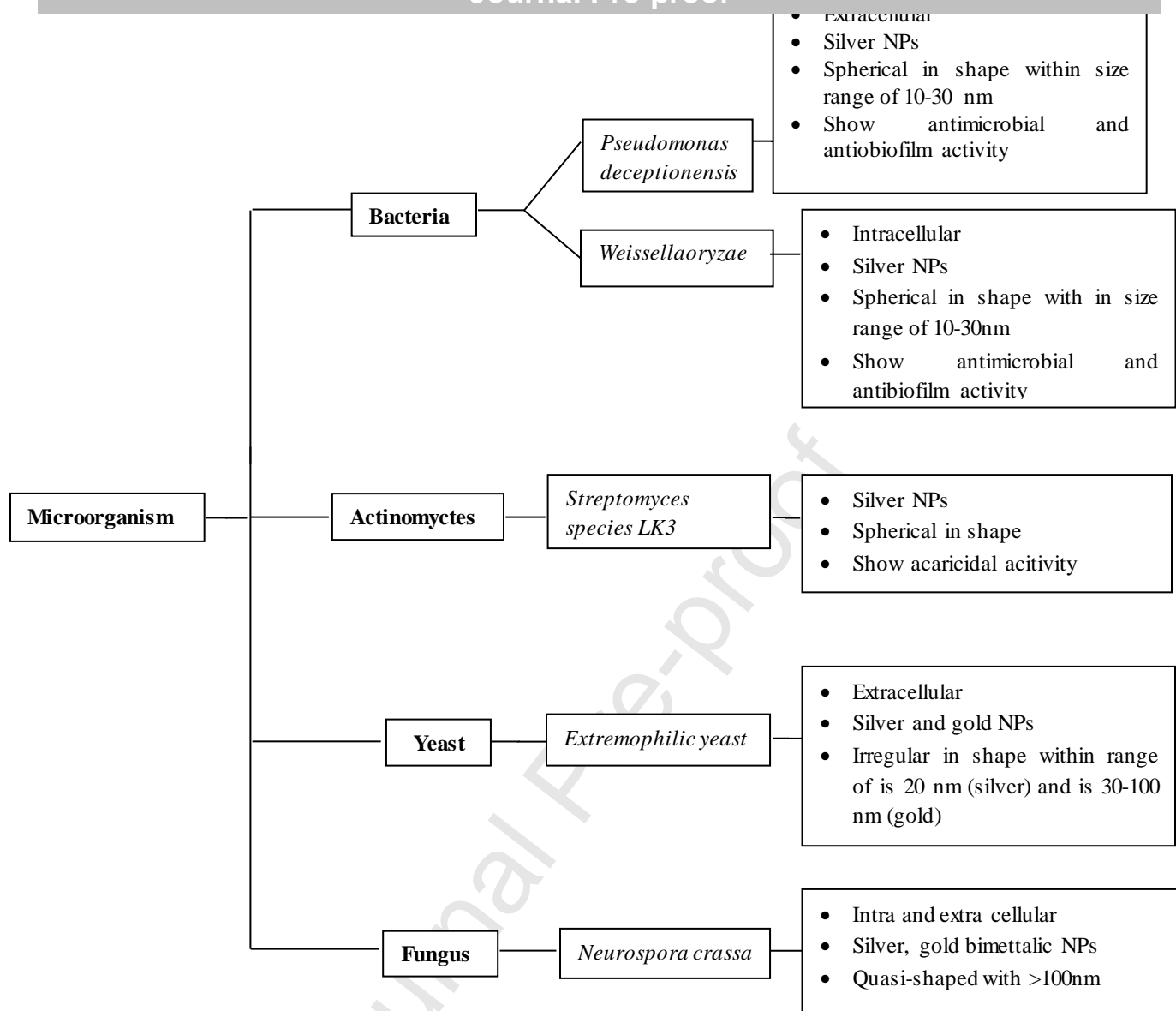
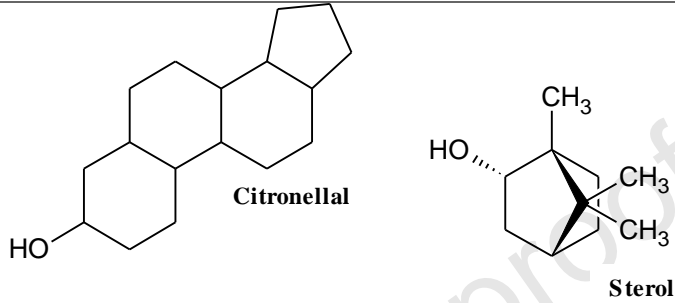
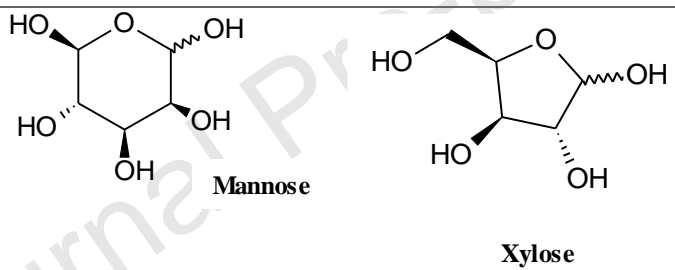
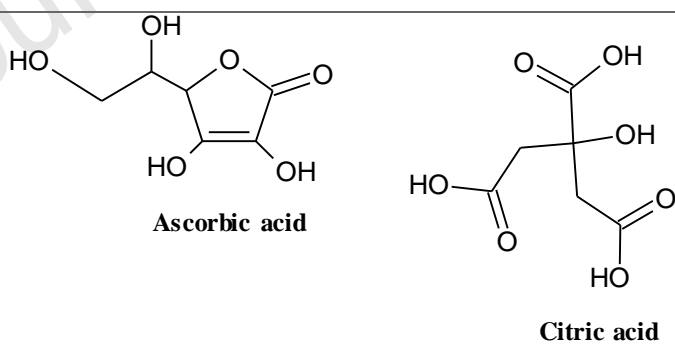


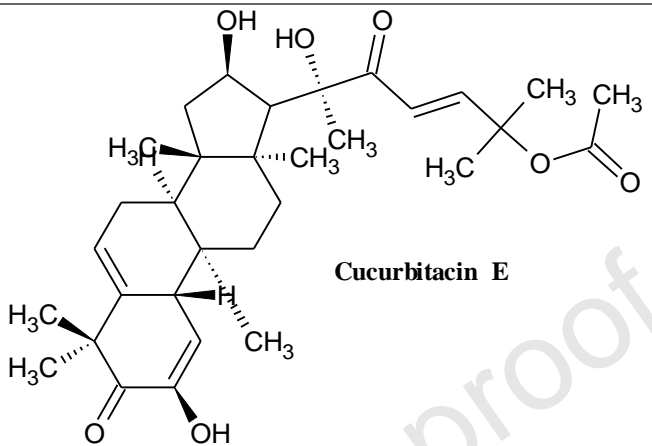
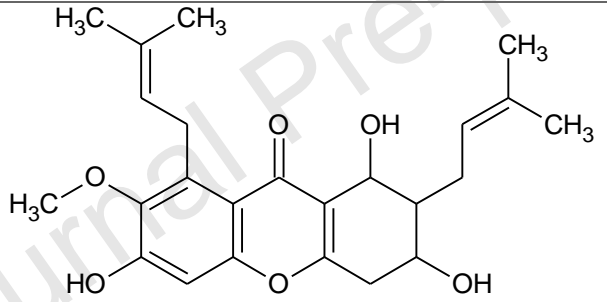
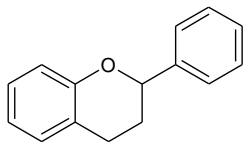
Fig. 6. Synthesis of AuNPs using green method.

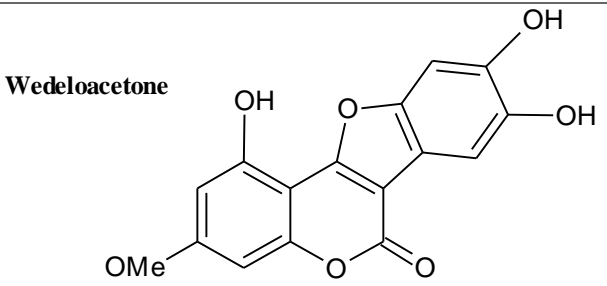
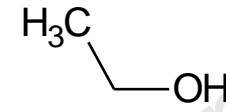
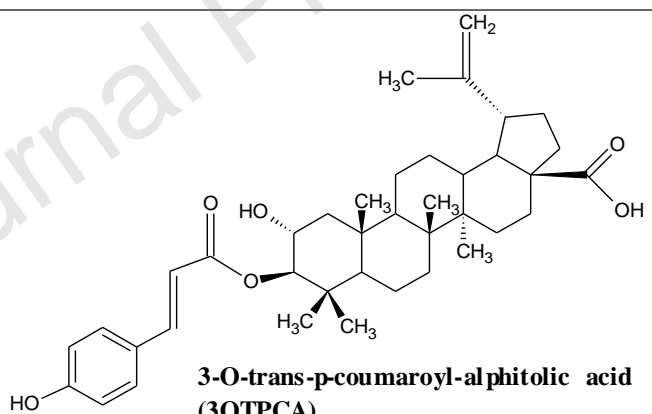


**Fig.7.** List of various microorganisms involved in the synthesis of AuNPs.

**Table 1:** Plant sources used by different researchers for the synthesis of AuNPs.

S. N.	Biological Source	Type of extract	Reducing/ stabilizing agent	Outcomes	Reference
1.	<i>Aloe Vera</i>	Aqueous extract	 <p>Citronellal</p> <p>Sterol</p>	Size: 4.4nm Shape: Spherical $\lambda$ max: 540nm	[51]
2.	<i>Turbinaria conoides</i> (Sea weeds)	Aqueous extract	 <p>Mannose</p> <p>Xylose</p>	Size: 6-10nm Shape: spherical, pseudo spherical $\lambda$ max: 520nm	[52]
3.	<i>Citrus limon</i> <i>Citrus sinensis</i> <i>Citrus reticulata</i>	Citrus extract	 <p>Ascorbic acid</p> <p>Citric acid</p>	Size: 15-80 nm Shape: variable	[53]

4.	<i>Malva crispa</i> , <i>Curbita pepo</i>	Aqueous extract	 <p><b>Cucurbitacin E</b></p>	Size :10-100nm Shape: spherical	[54]
5.	<i>Garcinia mangostana</i> fruit peels	Aqueous extract	 <p><b><math>\alpha</math>-mangostin</b></p>	Size: 32.96-5.25nm Shape: spherical $\lambda_{\text{max}}$ : 520nm	[55]
6.	<i>Hibiscus rosa seniesis</i>	Aqueous extract	 <p><b>Flavonoids</b></p>	Size:16-30nm Shape: spherical $\lambda_{\text{max}}$ : 530nm	[56]

7.	<i>Eclipta alba</i>	Aqueous extract	<b>Wedeloacetone</b> 	Size: 10-25nm Shape: spherical, hexagonal $\lambda_{\text{max}}$ : 530nm	[57]
8.	<i>Nyctanthes arbortristis</i> flower	Ethanolic extract	<b>Ethanol</b> 	Size: 19.8nm Shape: spherical	[58]
9.	<i>Zizyphus mauritiana</i>	Leaf extract	<b>3-O-trans-p-coumaroyl-aphitolic acid (3OTPCA)</b> 	Size: 20-40nm Shape: spherical	[59]

Using PEG, the AuNPs of 15-20 nm core diameter can be produced with the help of ultrasonic treatment. The reduction of  $\text{HAuCl}_4$  was carried out at room temperature with vigorous stirring. In the case of PEG with molecular weight of 20,000, the solution colour changed after 8 min, and the process was completed in 8 h. The reaction mixture first assumed a pale pink colour, which then turned into bright red [60].

### 3.4. Preparation of AuNPs using biomolecules

The AuNPs have also been reported to be prepared by using small biopolymers alone or in combination with other reducing agents [61]. The biopolymers include, chitosan, dextran, aminodextran, gum arabic, pectins, starch, glucose, proteins, oligopeptides, bovin serum albumin (BSA), gelatine, collagen, casein, tryptone, trypsin, alpha-amylase, aspartic acid, tyrosine, tryptophan, glutamic acid, glycyl-L-tyrosine, sodium glutamate, cystine, L-leucine etc [60]. Some organic compounds such as amino alcohols [77] glycerol [78], oxocarboxylic acid [79], luminol [80], nitriloacetic acid [81], nicotinamide adenine dinucleotide [82] and sodium rhodizonate [60], have been reported to prepare AuNPs by reducing  $\text{HAuCl}_4$ . AuNPs of 6 to 16 nm core diameter have been prepared by reduction of  $\text{HAuCl}_4$  by chitosan and sodium borohydride [83]. Chitosan coated AuNPs conjugated to ampicillin have shown very good antibacterial activity [84]. Chitosan-AuNPs complex conjugated to insulin have been reported for trans-mucosal drug delivery [85]. AuNPs of 18-40 nm core diameter have been prepared by reducing  $\text{HAuCl}_4$  by amino dextrin [60]. The size of AuNPs was controlled by controlling parameters such as temperature, pH of solution and  $\text{Au}^{3+}$  to aminodextran ratio. A combination of sodium borohydride, haemoglobin and BSA as reducing agent have been reported to yield very stable AuNPs [86]

### 3.5. Role of therapeutic agents in preparation of AuNPs

Targeted delivery of drugs can be achieved by conjugating therapeutic agents with AuNPs. In such cases the therapeutic agents play a dual role. They act reducing agents in the formation of AuNPs and act as therapeutic agents because of conjugation with the NPs, get delivered to the target sites [60]. They can be used alone or in combination with other reducing agents. The drugs that have been reported in the preparation of AuNPs include, dopamine hydrochloride (neurotransmitter used for treating neurological disease), insulin, silymarin (hepatoprotective agent), 5-aminolevulinic acid (anti-atherosclerotic), epigallocatechin 3-gallate (anti-atherosclerotic), folic acid (vitamin B<sub>9</sub>), 3-hydroxymethylindole (antitumor agent), antibiotics (ampicillin, amoxicillin, streptomycin and kanamycin) [60]. AuNPs of 3 nm core diameter have been produced by reduction of H<sub>2</sub>AuCl<sub>4</sub> using dopamine hydrochloride and Triton X-100 [87]. AuNPs of 20 nm core diameter were prepared using silymarin as reducing and stabilizing agent [83]. Folic acid stabilized AuNPs of 18 nm core diameter have been reported to yield very good nutraceutical activity [88]. Cephalosporin conjugated AuNPs of 20-50 nm core diameter have been reported to provide very good antimicrobial activity [89]. Insulin conjugated AuNPs along with chondroitin sulfate have shown good reduction in blood glucose level [90].

#### **4. Characterization of AuNPs using different techniques**

Two main properties of AuNPs such as core size and protecting ligands influence their character. While uncapped AuNPs have a core diameter range between 2 and 150 nm whereas, thiolate-stabilized AuNPs have diameter less than 10 nm. Smallest AuNPs having discrete size and structures are known as monolayer-protected gold clusters (MPCs). These MPCs have quantum properties like tunable band gaps, optical absorbance bands and quantized charging. Larger particles exhibit properties of bulk gold like SPB having wavelength of 520 nm. Therefore, characterization of AuNPs core size and capping agents has great advantage for AuNPs-based

applications. Various techniques used for characterization of AuNPs are shown in Fig.8 [91]. UV-vis spectroscopy is employed for measuring size depending upon the presence or absence of SPB, transmission electron microscopy (TEM) is used for imaging of the gold core, whereas, NMR or IR allows characterization of protecting ligands and TGA is used to find the amount of gold and ligand present in NPs. Mass spectrometry is unique as it is capable of performing the entire task (core size measurement, characterization of ligands and calculating molecular formula) [92].

#### **4.1. UV-visible spectroscopy**

UV-visible spectroscopy is a very helpful technique, which can be used to estimate size, concentration and aggregation level of AuNPs. The extinction spectra of AuNPs analyzed by UV-visible spectroscopy can be determined using Mie theory. According to Mie theory, AuNPs have potential effect on SPR and correspondent extinction spectra. Plasmons are formed due to coherent displacement of negatively charged clouds of electrons from their equilibrium position around a lattice made of positively charged ions. The external electric field of the electromagnetic radiation excites the surface of real materials that causes formation of specific plasmon modes. Thus, the electron gas with respect to their equilibrium position around positively charged ions gets displaced. This causes formation of propagating surface plasmon polaritons (PSPP). In case of metallic NPs, the electric field of incident light can penetrate the metal and polarize the conduction electrons. Localized surface plasmons (LSPs) is observed in NPs with size much smaller than photon wavelength. LSPs are non-propagating excitations because the resulting plasmon oscillation is distributed over the whole particle volume. Hence, the LSPs in a NP can be considered as a mass-spring harmonic oscillator driven by the energy resonant light wave, where the electron cloud oscillates like a simple dipole in parallel direction



to the electric field of the electromagnetic radiation. Only light with frequency in resonance with the oscillation is able to excite the LSP [93]

The Localized Surface Plasmon Resonance (LSPR) spectrum depends upon the size and shape of AuNPs. The peak absorbance SPR wavelength increases with particle diameter because the distance between particles decreases due to aggregation [94]. Enhanced SPR peak intensity for smaller nanoparticles (40 nm) compared to larger ones (80 nm) has been reported by Zeng and co-workers [95]. Zuber et al. [94] reported shift in SPR maximum towards longer wavelength with increase in size of AuNPs due to the differences in the frequency of surface plasmon oscillations of the free electrons. The absorbance was also found to be increased with increase in size of NPs due to the enhanced mean free path of the electrons in the larger NPs. The SPR peak maximum shifted from 514 nm for 5 nm NPs, through 519 nm for 20 nm NPs to 526 nm for 50 nm NPs.

The shape of the Au NPs influences the width, position, and number of SPRs [96]. AuNPs of different shapes such as nanorods [97], nanospheres [98], porous nanospheres [99], nanoshells and nanorices [100], nanocorals [101], nanotriangles [102], nanostars/nanourchins [103], nanocages [104], nanocubes and nanododecahedra [105] of varying sizes have been reported by different authors that showed different optical extinction (transmission) or scattering (dark-field) spectra. It is important to note the number, position, and intensity of SPR can be modified by reduction in symmetry of NPs [96]. It is reported that porous nanospheres and nanocorals of 25 nm showed only one SPR band near to 520 nm (Fig.9A and 9B), whereas, the porous nanospheres of size 50 nm showed two SPR bands between 800 to 820 nm (Fig.9C) [98, 99, 101].

Zijlstra et al. [97] reported red shift of SPR wavelength of nanorods with increase in their dimension from  $37 \times 19$  nm (aspect ratio  $2 \pm 1$ ),  $50 \times 12$  nm (aspect ratio  $4.2 \pm 1$ ), and  $50 \times 8$  nm (aspect ratio  $6 \pm 2$ ), as shown in Fig. 9D.

Barbosa et al [102], investigated of  $\text{HAuCl}_4$  concentration to Au seed concentration (R) on morphology and tip plasmon resonance frequency of Au nanostars prepared in concentrated solutions of poly(vinylpyrrolidone) in N, N-dimethylformamide. The size of nanostars was also varied from 2 to 30 nm and it was observed that the size significantly influenced the dimensions and number of spikes of nanostars. A bathochromic shift was observed in the UV-visible spectra of nanostars with increase in R value (Fig.10).

Nanoshell plasmon resonances is caused due to interaction between the essentially fixed frequency plasmon response of a sphere and that of a cavity. The sphere and cavity plasmons are electromagnetic excitations at the outer and inner interfaces of the metal shell, respectively. Due to the finite thickness of the shell layer, the sphere and cavity plasmons interact with each other and hybridize in a way analogous to the hybridization between atomic orbitals. This interaction results in the splitting of the plasmon resonances into two new resonances, the lower energy symmetric or “bonding” plasmon and the higher energy antisymmetric or “antibonding” plasmon. The strength of the interaction between the sphere and cavity plasmons is controlled by the thickness of the metal shell layer [106]. The corresponding optical extinction (transmission) or scattering (dark-field) spectra of nanoshells and nanorice are shown in Fig 11. Soares et al. [102] reported the visible extinction spectrum of gold nanotriangles (prepared by catalytic method using CTAB as capping agent and tin porphyrin as catalyst) two peaks, one at 520 nm and other at 730 nm (Fig.12). Wu et al [105] synthesized seed mediated gold nanocrystals of cubic and dodecahedral shape in the size range of 30-75 nm using cetyltrimethylammonium

chloride (CTAC) surfactant and sodium bromide. In both the cases, red-shift was observed with increase in the size of nanocrystals (Figs.13). Luan et al [104] reported the vis-NIR spectrum of aqueous suspension of gold Nano rattles (nanocages) at 700 nm (Fig. 14).

*Silva et al.*, 2010 reported influence of UV visible light on photocatalytic activity of titania containing AuNPs. Samples containing AuNPs were found to exhibit photocatalytic activity (generation of O<sub>2</sub> from water) when exposed to both UV and visible light [107].

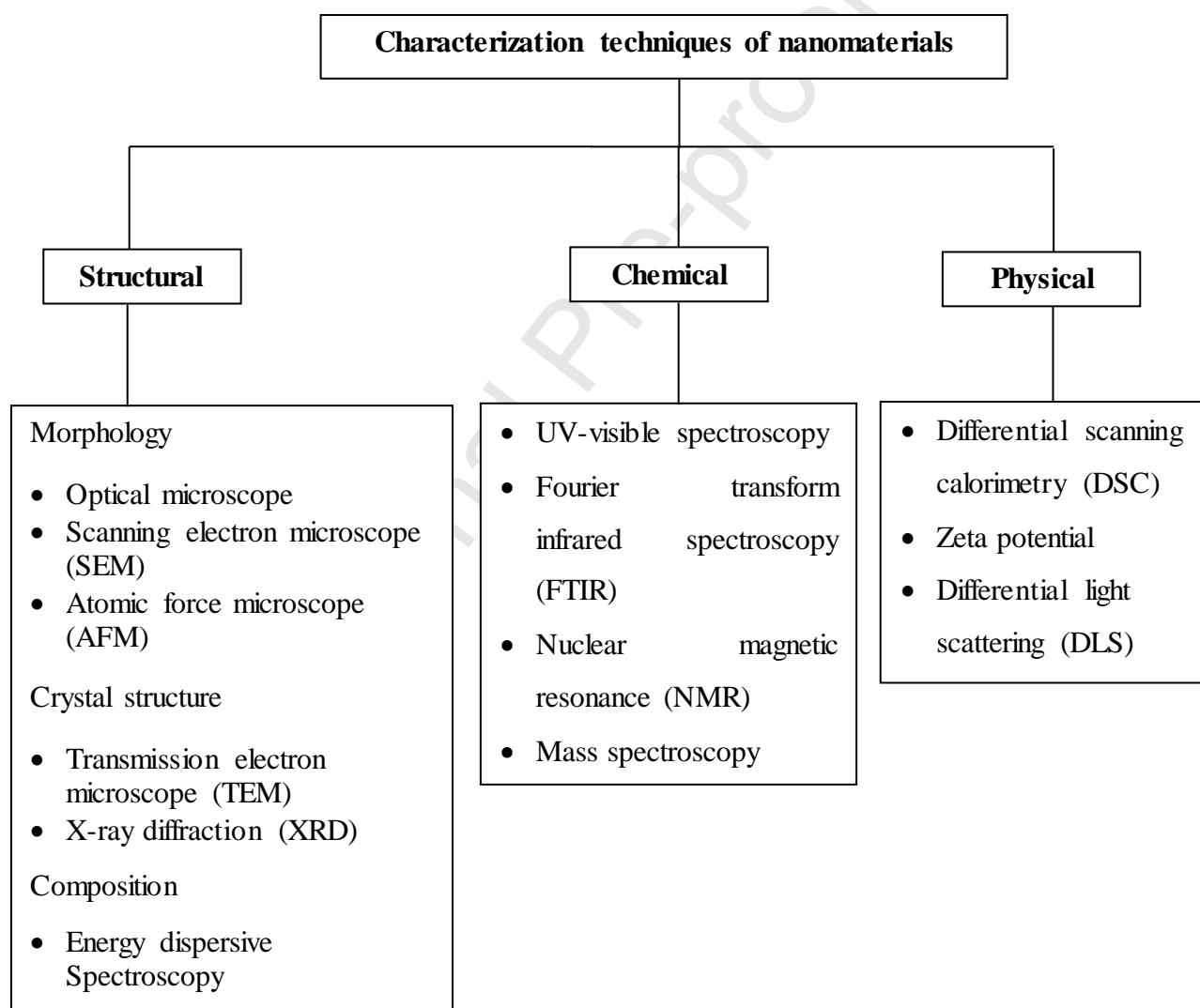


**Fig.8.** Various techniques used for characterization of AuNPs.

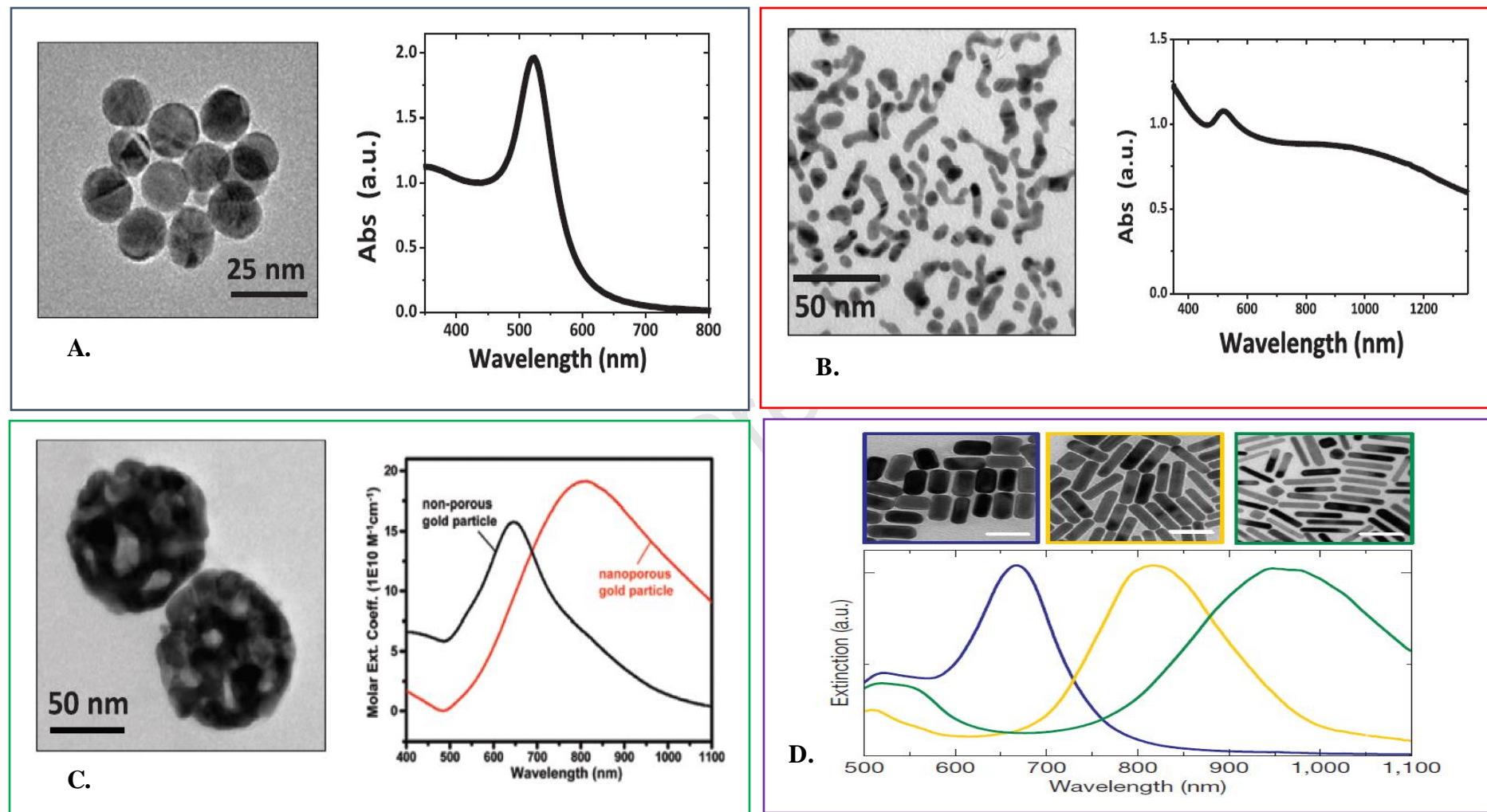


**Fig.9.** AuNPs with different shape resembling different SPR A. nanosphere [98](Copyright (2013) American Chemical Society) B. Nanocorals [101](Copyright The Royal Society of Chemistry), C. Porous nanospheres [99] (Copyright The Royal Society of Chemistry.), and D. nanorods [97].

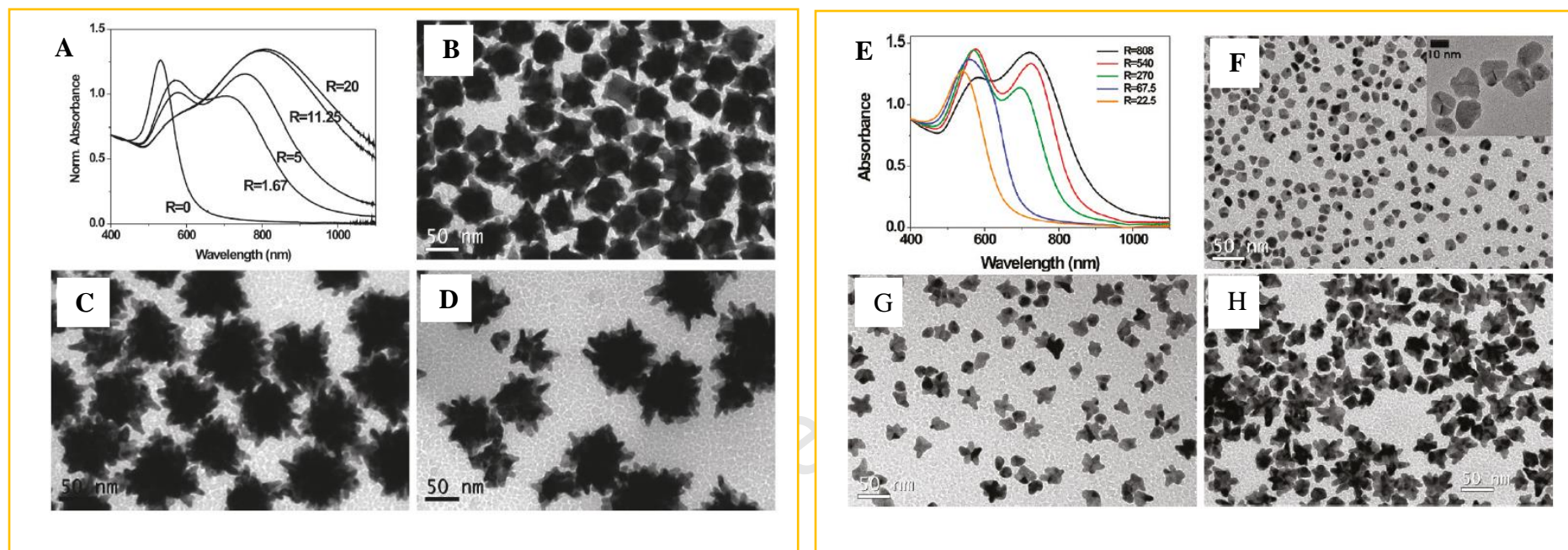


**Fig.10.** (A) Vis-NIR spectra of Au colloids obtained using 30 nm Au nanoparticles as seeds. In the graph, the ratio of Au salt concentration to Au seed concentration ( $R$ ) is displayed. (B-D) corresponding TEM images of samples prepared at  $R$  values of 1.67, 11.25, and 20, respectively. (E) Vis-NIR spectra of Au nanostars obtained for different  $R$  values, using 2.5 nm Au nanoparticles as seeds. (F-H) Corresponding TEM images of samples with  $R$  values of 67.5 (F), 270 (G), and 808 (H) [103] Copyright (2010) American Chemical Society.



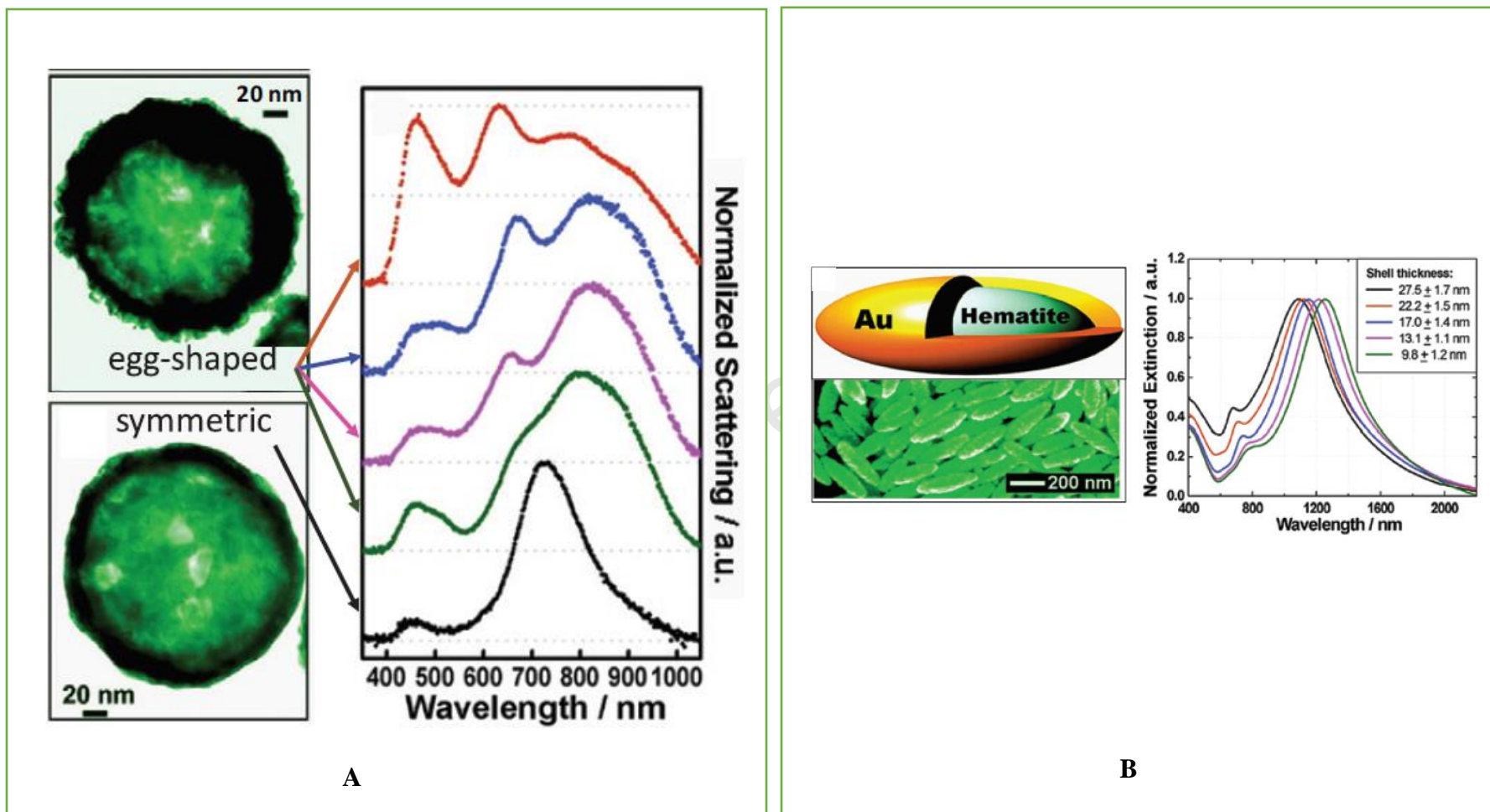


**Fig.11.** Optical extinction (transmission) or scattering (dark-field) spectra of nanoshells (A) and nanorice (B). [100] (Copyright (2007) American Chemical Society).

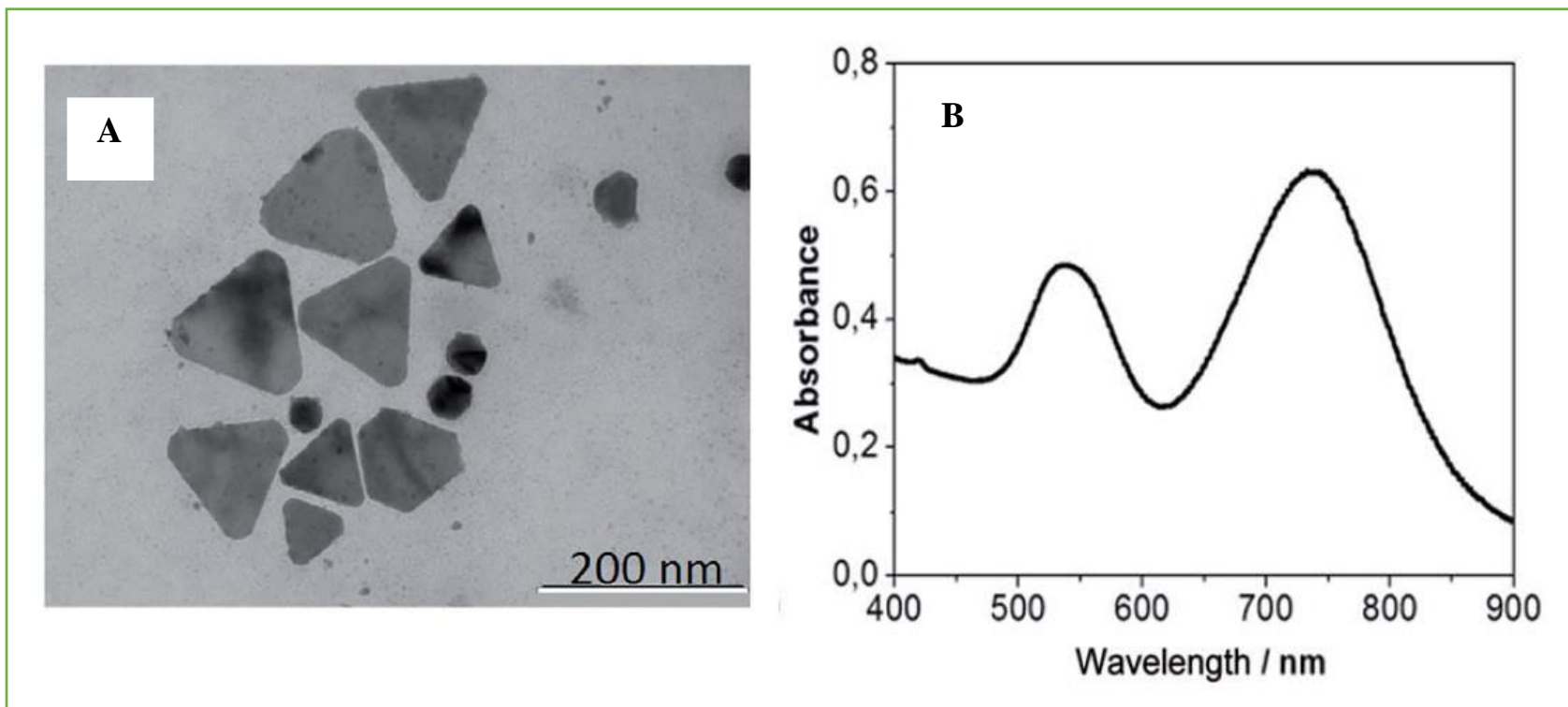


**Fig.12.** (A) TEM image of CTAB-AuNTs. (B) Visible extinction spectrum of a sample of CTAB-AuNTs in aqueous solution. [102] (Copyright The Royal Society of Chemistry).

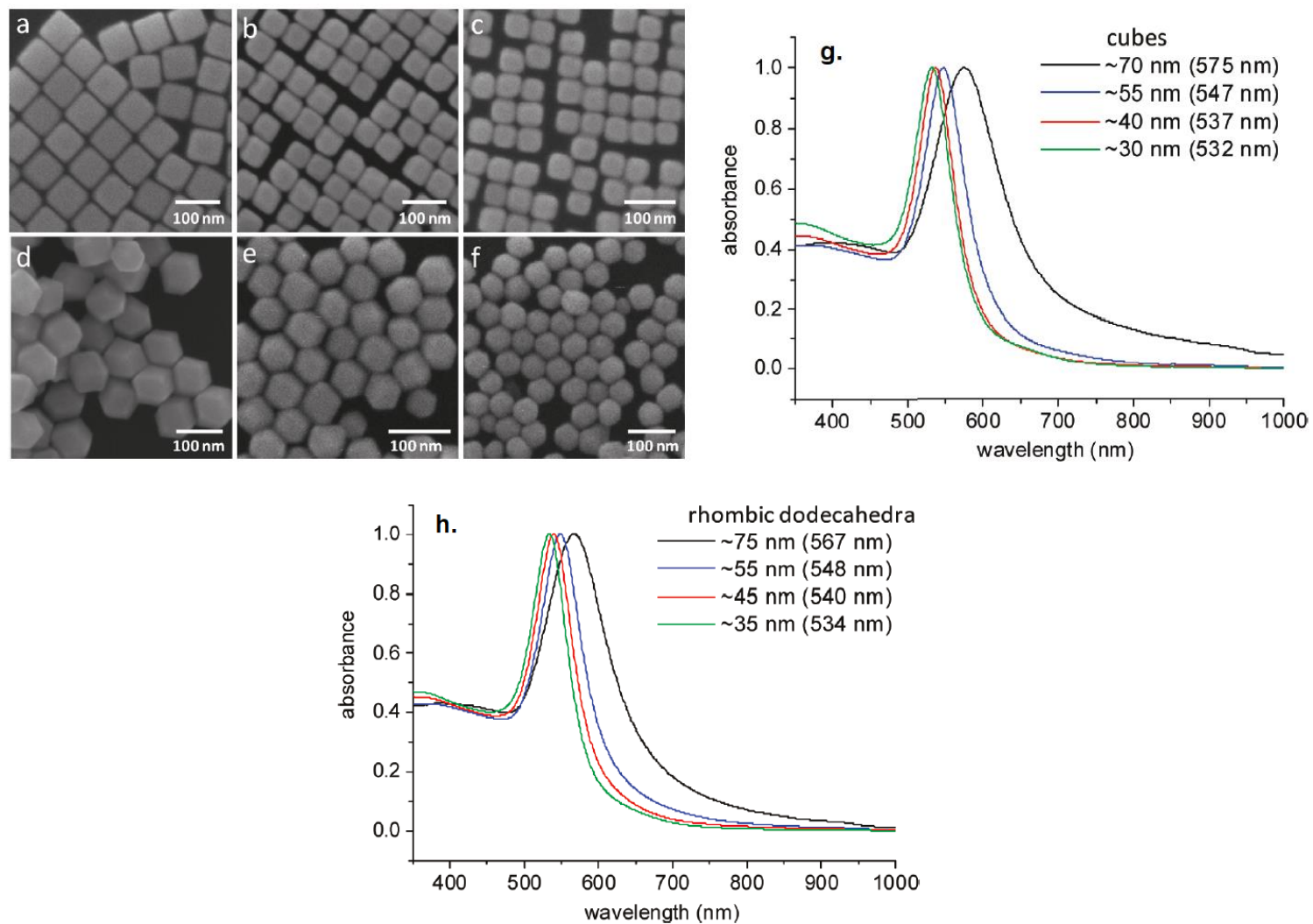


**Fig. 13.** (a-c) SEM images of gold nanocubes synthesized with average sizes of 72, 53, and 40 nm. (d-f) SEM images of rhombic dodecahedral gold nanocrystals with average sizes of 74, 55, and 45 nm. (g). UV-vis absorption spectra of gold nanocubes (h) gold rhombic dodecahedra [105] (Copyright (2010) American Chemical Society).



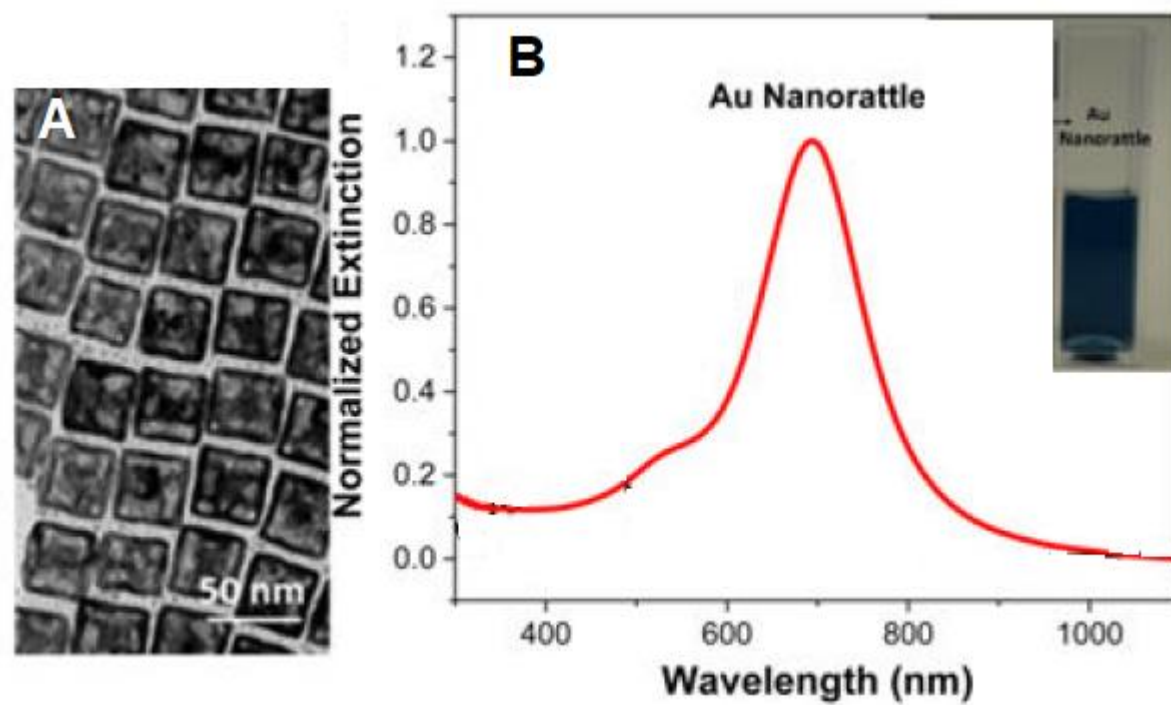


**Fig.14.** TEM image of (A) Au nanorattles. (b) Vis-NIR extinction spectra of aqueous suspension of Au nanorattles. [104](Copyright (2016) American Chemical Society.)

#### 4.2. Dynamic light scattering (DLS)

DLS is another technique used for characterizing size of NPs. The principle of DLS involves measurement of scattered light from a laser passing through the colloid. The intensity of scattered light modulation is studied on the basis of time and it gives us the estimate of hydrodynamic particle size. This technique operates easily and is a faster technique for characterization of particles especially colloidal suspensions. Various advantages of DLS include sensitivity, less measurements time, selectivity of NPs, simplicity of operation and auto calibration which makes it more useful for industrial and scientific research. It also has some limitations when involved in sample measurements having multimodal or large size distribution. Its accuracy for evaluating polydispersed colloids becomes doubtful because small materials might be screened in presence of bigger materials during DLS measurement [108]

#### 4.3. Nuclear magnetic resonance (NMR)

NMR spectroscopy is a transitional molecular characterization tool that needs little perturbation of analyzed system, and gives extensive information regarding chemical nature of atomic nuclei. These properties of NMR make it well-suited for *in-situ* analysis of reactions and chemical structures of metallic NPs. In the synthesis of NPs, analytical target ranges from detecting molecular precursor to recognition of particle surface. In NPs synthesis, presence of interface between particle surface and ligands depends upon various features like ligand shell composition and ligand shell structure. These features are difficult to resolve using electron microscopy or spectroscopy technique; hence, NMR can be used to identify these features. In raw metals, hyperfine coupling of unpaired electrons in the metal leads to change in frequency of NMR known as “Knight shift”. The electronic environment around the nucleus has effect on Knight shift. Extent of shift depends on electronic structure of metals. Examining the change from molecular to metallic structure in NPs is feasible using

NMR techniques. In addition, metallic properties can be determined by evaluating “Korringa” behavior of NPs by NMR measurements. Nuclear magnetic relaxation of material is described as Korringa behavior as it was described by Jan Korringa in 1950. Korringa’s equation ( $k$ ) is related to temperature ( $T$ ). NMR nuclei that show this temperature relation with longitudinal relaxation time constant ( $T_1$ ) exhibit the electronic structure within the material analyzed. Both the slope of  $T_1$  as well as extent of “Knight shift” can give detailed information about particle size, shape, composition and surface chemistry [109]. NPs synthesized by chemical method are capped with organic molecules. Investigation of these capping agents using NMR can provide detail information about nature of particle core (like electronic structure and composition of atom) [109]. Huhn et al. [32] explored the use of NMR to identify the formation of DDT stabilized AuNPs. They analyzed the NMR spectra of poly (isobutylene-alt-maleic anhydride (PMA) before and after the coating of DDT-Au NPs ( $\approx 4$  nm). The  $^1\text{H}$  NMR spectrum of PMA showed non-resolved broad bands due to size distribution of the starting poly (isobutylene-alt-maleic anhydride)-graft-dodecyl and the random distribution of dodecylamine moieties along the polymer chain (Figure 15A). The  $^{13}\text{C}$  NMR spectrum of PMA showed good resolution for nonquaternary carbon atoms due to their higher signal intensity compared to quaternary ones such as  $\text{C}=\text{O}$ , (Fig. 15B).  $^1\text{H}$  NMR of PMA coated Au NPs ( $\approx 4$  nm core diameter) was measured (Fig. 15C). In PMA coated AuNPs, cyclic anhydrides were no longer present and two separate peaks were observed for  $-\text{CH}$  protons. One proton was linked to amide groups and kept inside the hydrophobic core while the other was linked to carboxylic groups and exposed to the water phase. When this spectrum was compared with that of PMA treated with NaOH different pattern was noted. The  $-\text{CH}$  peak was barely visible, and only the  $\text{CH}_2$  and  $\text{CH}_3$  peaks were clearly visible (Fig. 15D).

#### 4.4. Electron microscopy (EM) techniques

EM techniques have gained their wide application for visualizing the AuNPs due to their intrinsic sub-nanometer scale resolution. Scanning electron microscopy (SEM) provides surface (or near surface) image of a sample, while in TEM, the electron beam passes through the sample. Although they have wide application, they fail to analyse non-perturbed samples. Spatial resolution, artefact generation, polydispersion, and disturbances during sample preparation are the major limitations in the characterization of AuNPs using electron microscopy. A suitable spatial resolution is required for ensuring that a significant portion of the sample is imaged. The spatial resolution for SEM is in the range 5–100 nm [110], whereas for TEM it can be  $< 1$  nm [111].

The primary difference in data output between SEM and TEM is the way in which the nanoparticle images are resolved. SEM produces accurate 3D images of particles in the dispersion while TEM produces 2D images that require further interpretation. The images rendered by TEM are two dimensional, but these systems have capacity of delivering much greater resolution. Moreover, internal composition details, such as a particle's crystallinity and lattice structure can be derived by TEM by monitoring electrons as they transmit from the sample. Such information is also provided by SEM, but it is well suited only for analyzing surface characteristics of nanoparticles. Moreover, longer time is required to prepare sample in TEM as compared to SEM, as particles need to be thinly sliced. Furthermore, TEM covers only a very small sample selection. This narrow range combined with longer sample preparation times may result in the presence of aggregates during analysis. Aggregated particulates may result in size distribution measurements being generated from single runs that are unrepresented of the bulk sample. In contrast to this larger amount of sample can be measured at one time using SEM. This improves both the statistical reliability and efficiency of nanoparticle size and shape distribution measurements [112].

Annamalai 2013 *et al.* reported the characterization as well as antimicrobial activity of AuNPs by green method using *Euphorbia hirta* L. leaf extract. TEM imaging revealed that biosynthesized AuNPs were having crystalline nature and spherical shape within a size range of 10-50 nm [113]. As an example, the SEM image of gold nanocubes and rhombic dodecahedral gold nanocrystals is shown in Fig. 13 while TEM images of nanoparticles of different shapes are shown in Figs. 9-12, 14 and 16.

#### **4.5. Atomic force microscopy (AFM)**

AFM is an example of Scanning Probe Microscopy (SPM). In AFM a cantilever scans the sample and allows imaging of AuNPs in their natural environment. AFM can also be applied to non-conductive samples [112]. It is used for 3D characterization of AuNPs. A distinct property of AFM is that it can generate AuNPs images having size between 0.5 nm and 50+ nm. Size distributions of NPs are also calculated from AFM. AFM imaging is based on vibrating tip to explore surface scanning having significant transformation which allows them to go for nanometer-resolution imaging. AFM is a sensitive tool for investigating tip-sample interactions to sub-nm resolution. Therefore, there is a need to develop quantitative method to study different properties of material with better resolution without causing any effect to more soft samples. For any sample to undergo AFM measurements pre-treatment of the sample is not required thus overcoming the limitations involved in electron microscopy. AFM imaging can also be used for characterizing particulate matter depending on organic materials having high spatial resolution. AFM scanning exhibit a good accuracy for obtaining size distributions of NPs as compared to DLS techniques. AFM topography imaging is used for obtaining information on growth mechanism of nanocrystals [114, 115]. Darwich *et al.* [115] reported Manipulation of gold colloidal nanoparticles with atomic force microscopy in dynamic mode: influence of particle–substrate chemistry and morphology, and of operating conditions. Various AFM images of AuNPs reported by them are shown in Fig. 17.

#### **4.6. Mass spectroscopy (MS)**

Use of MS for analysis of small AuNPs is increasing day by day. From mass spectra, the amount of gold atoms can be analyzed. Uses of matrix-assisted laser desorption/ionization (MALDI) provides means to measure the core of ligand stabilized AuNPs. Although these matrices do not affect fragmentation of extensive ligand with the potential to determine intact MPCs, it is now easy to find variations in stoichiometry of different ligands depending upon the mass.

Inductively coupled plasma-mass spectrometry (ICP-MS) is used for elemental characterization of AuNPs. ICP-MS analysis of NPs can be used in biomolecules assays. For characterization of colloidal NPs for bioanalytical applications, there are other extra parameters to be considered like aggregation state, solubility and dissolved metal fractions which could influence ICP-MS measurement. It is one of the most flexible and sensitive technique used for elemental analysis. Detection of very low concentration in picogram range and effective signal are two of its salient features of ICP-MS. Elemental composition of metallic NPs and extraordinary analytical features of ICP-MS for multielemental analysis at very low limits make it suitable for characterization of NPs. It gives information regarding size distribution, composition and chemical state of NPs. Two type of ICP-MS is being used a) Direct ICP-MS b) ICP-MS hyphenated techniques. In case of direct ICP-MS, it provides elemental analysis of both ionic and colloidal solutions. ICP can atomize, vaporize and ionize AuNPs [116].

#### **4.7. X-ray diffraction (XRD)**

XRD is an important role as a powerful nondestructive technique in characterization of metallic NPs. XRD pattern is the fingerprint of periodic atomic arrangements in a given material. The characteristics spectra of X-ray are created when electrons have sufficient energy to dislocate inner shell electrons of target material [117]. Yan et al. [117] reported

successful deposition of ultra-small gold nanoparticles (0.8–1 nm) on titania-modified SBA-15 via a deposition–precipitation method and the deposition was confirmed by comparison of experimental X-ray diffraction (XRD) patterns with theoretical ones. The results showed that gold existed as  $\text{Au}^{3+}$  and  $\text{Au}^0$  in the as-synthesized and reduced catalyst, respectively. The XRD analyses also suggested that Au nanoparticles were more developed along the  $\langle 111 \rangle$  direction forming a raft-type structure (Fig.18). Bathrinarayanan et al. [118] reported the synthesis and characteristics of intracellular AuNPs prepared by green method using *Aspergillus fumigates*. XRD image of the sample after the addition of  $\text{HAuCl}_4$  showed a strong signal was observed at  $31.9^\circ$  that could have been generated from some biomass or media components, while in case of gold nanoparticles, peak position at  $37.8^\circ$  represented the presence of gold and the value was consistent. Moreover, the XRD results also indicated that the produced gold nanoparticles exhibited irregular morphology. XRD patterns clearly showed that both the nanoparticles were crystalline in nature [118].

#### **4.8. Energy dispersive spectroscopy (EDS)**

The energy dispersive spectroscopic analysis is done to get an indication of the amount of gold nanoparticles present in the biomass. Bathrinarayanan et al. [118] reported characterized intracellular AuNPs prepared using *Aspergillus fumigates*. ED spectrum showed a thin film of fungal biomass showing strong signals for gold atoms along with weak signals from oxygen and potassium (Fig.19). The weak signals appearing in the figure indicate the presence of macromolecules like proteins/enzymes and salts of fungal biomass and presence of Au signal indicated gold nanoparticles.

#### **4.9. Thermogravimetric analysis (TGA)**

In TGA, mass of sample is noted with continuous increase in temperature. The sample mass decreases upon its decomposition which allows for analyzing the composition of the sample. Huhn et al utilized TGA for analyzing formation of DDT-Au NPs ( $\approx 4$  nm core diameter).

The TGA curve corresponding to the dodecanethiol-capped Au NPs (Fig. 20A) showed a very slight loss (<1%) in the 25–150 °C range, as expected from metallic NPs. An abrupt loss (around 18%) took place between 150 and 300 °C, which could be due to the decomposition of the DDT. No changes in the mass were observed at higher temperatures. The TGA curve of the DDT-Au NPs overcoated with PMA showed a slight weight loss (around 5%) in the 25–150°C range, which can be due to the release of absorbed water (Fig.20B). Almost no changes in the mass were observed at higher temperatures [32].

#### 4.10. Fourier Transform infra-red spectroscopy (FTIR)

The chemical structure of the organic shell around core of NP nanoparticles can be analyzed through FTIR based on the specific vibrational fingerprint for specific functional groups. Hence, FTIR can be used for qualitative evaluation of the organic shell around NPs and can be employed for following up surface functionalization or ligand exchange. Moreover, deviations in typical vibrational features of adsorbing functional groups on the surface of NPs can be used to describe the type and orientation of organic ligand core interaction. Huhn et al. [32] reported FTIR analysis of DDT-Au NPs ( $\approx 4$  nm core diameter) before and after overcoating with PMA, as well as for free PMA as control. The DDT-Au NPs exhibited only three significant peaks, two strong peaks at 2923 and 2853  $\text{cm}^{-1}$  (corresponding to the asymmetric and symmetric C–H stretching of the alkyl chain) and one peak at 1460  $\text{cm}^{-1}$  (bending vibrations of C–H) (Fig.21). In contrast, the PMA polymer presented more peaks. The strong peaks at 2925 and 2854  $\text{cm}^{-1}$  (corresponding to the asymmetric and symmetric C–H stretching of the alkyl chains), the broad and weak adsorption peak from 3200–3600  $\text{cm}^{-1}$  (corresponding to the presence of the O–H stretching resonance of the carboxylic acids formed after the anhydride opening) and the two peaks at 1780 and 1705  $\text{cm}^{-1}$  (corresponding to the cyclic anhydride with 5-membered rings). Symmetric stretching vibrations of C=O from the carboxylic groups were overlapped at 1705  $\text{cm}^{-1}$ . The N-C=O symmetric stretching



vibrations of the amide groups appeared at  $1583\text{ cm}^{-1}$ . Angular deformation of  $\text{CH}_2$  and  $\text{CH}_3$  was also observed at  $1468$  and  $1375\text{ cm}^{-1}$ . The DDT-Au NPs overcoated with the amphiphilic PMA polymer showed vibrational peaks of both, DDT-Au NPs and PMA. These results indicated the surface modification (overcoating) of DDT-Au NPs with PMA.

Journal Pre-proof

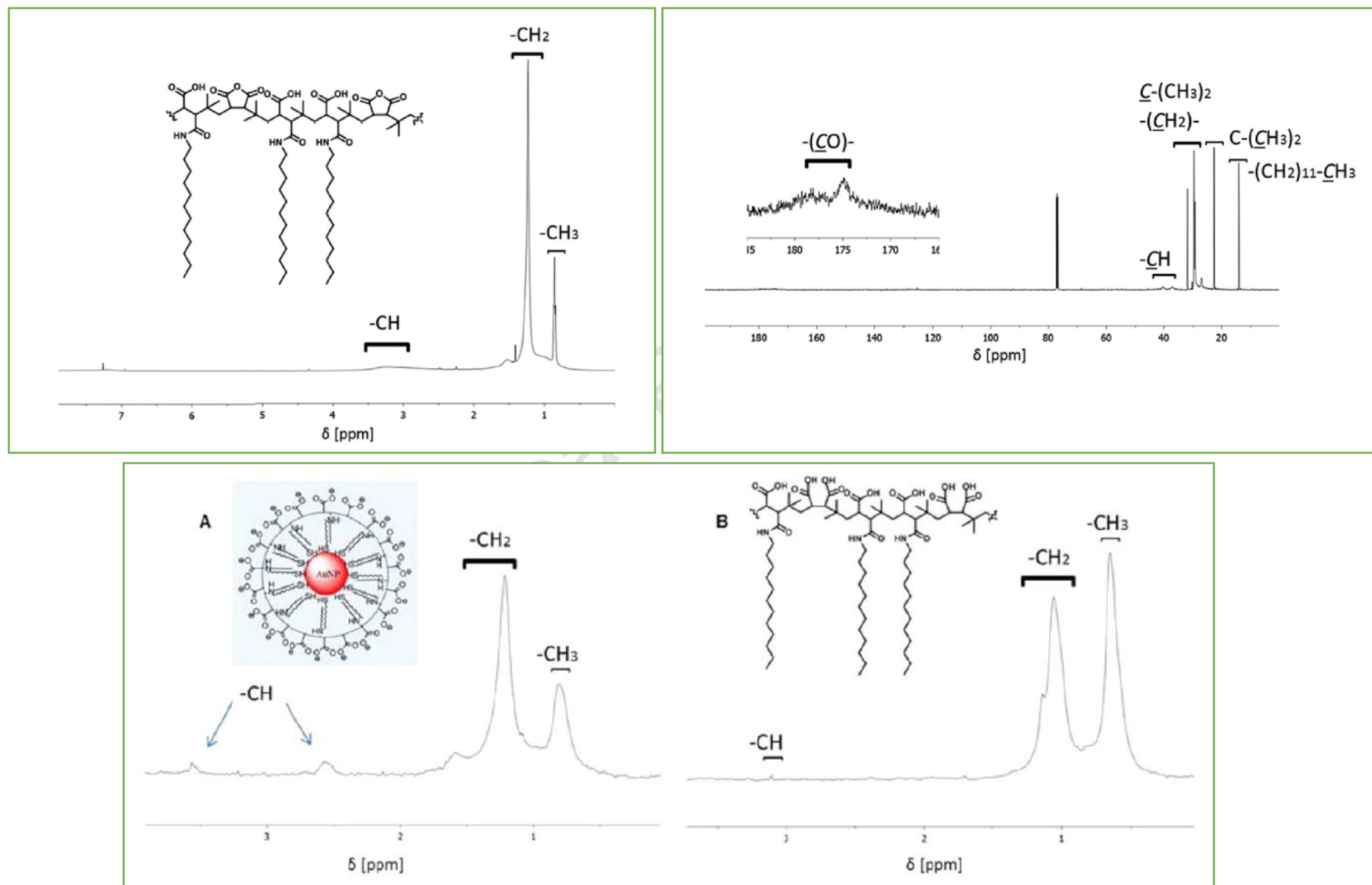


**Fig.15.** (A)  $^1\text{H}$  NMR spectrum of PMA in  $\text{CDCl}_3$ . (B)  $^{13}\text{C}$  NMR spectrum of PMA in  $\text{CDCl}_3$ ; the zoomed area shows the peaks for the carbonyl groups. (C)  $^1\text{H}$  NMR spectrum of PMA coated Au NPs of  $\approx 4$  nm core diameter in 15%  $\text{D}_2\text{O}/\text{H}_2\text{O}$  mixture. (D)  $^1\text{H}$  NMR of PMA in 15%  $\text{D}_2\text{O}/\text{H}_2\text{O}$  mixture after treatment with base to open all anhydride groups. Reprinted with permission from [32]. Copyright 2017, American Chemical Society.

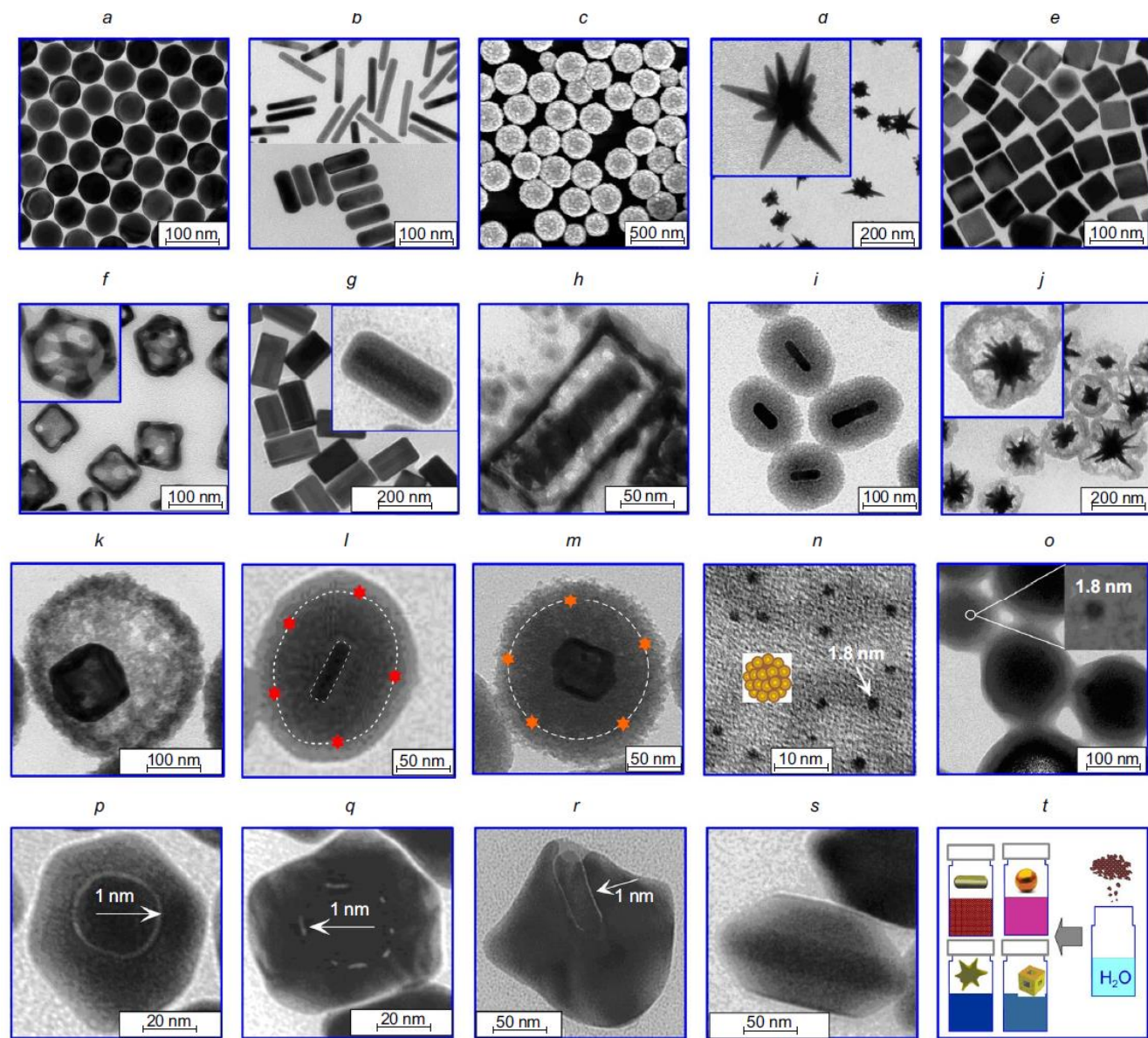


**Fig. 16.** TEM images of gold nanospheres (a); gold nanorods (b); gold nanoshells on silica cores (c); gold nanostars (d); silver nanocubes (e) used as templates for the synthesis of gold nanocages (f); nanocuboids composed of gold nanorods coated by a silver shell (g); anisotropic gold nanocages obtained from nanocuboids (h); gold nanorods (i), nanostars (j) and nanocages (k) coated by a mesoporous silica shell; gold nanorods (l) and nanocages (m) coated by a conventional and mesoporous silica shell and doped with photodynamic agents; fluorescent atomic gold nanoclusters Au<sub>25</sub> stabilized by bovine serum albumin (BSA) molecules (n); human serum albumin (HSA) nanoparticles doped with fluorescent atomic clusters (o); surface enhanced Raman scattering (SERS) gold labels with benzene-1,4-dithiol molecules embedded into a nanometre hollow (p) or bridged (q) gap between the spherical (p) or polygonal (q) core and the shell; anisotropic labels with a gold nanorod as the core and benzene-1,4-dithiol or nitrobenzene-1,4-dithiol embedded into the 1-nm gap between the core and the gold shell (r); SERS labels based on gold nanorods functionalized by 4-aminothiophenol and 4-nitrobenzenethiol molecules coated by a silver shell (s); water-soluble powders of gold nanospheres, nanorods, nanostars and nanocages (t) (powder particles coated by thiolated mPEG-SH molecules, Mw=5000). [60] © 2019 Uspekhi Khimii, Russian Academy of Sciences.



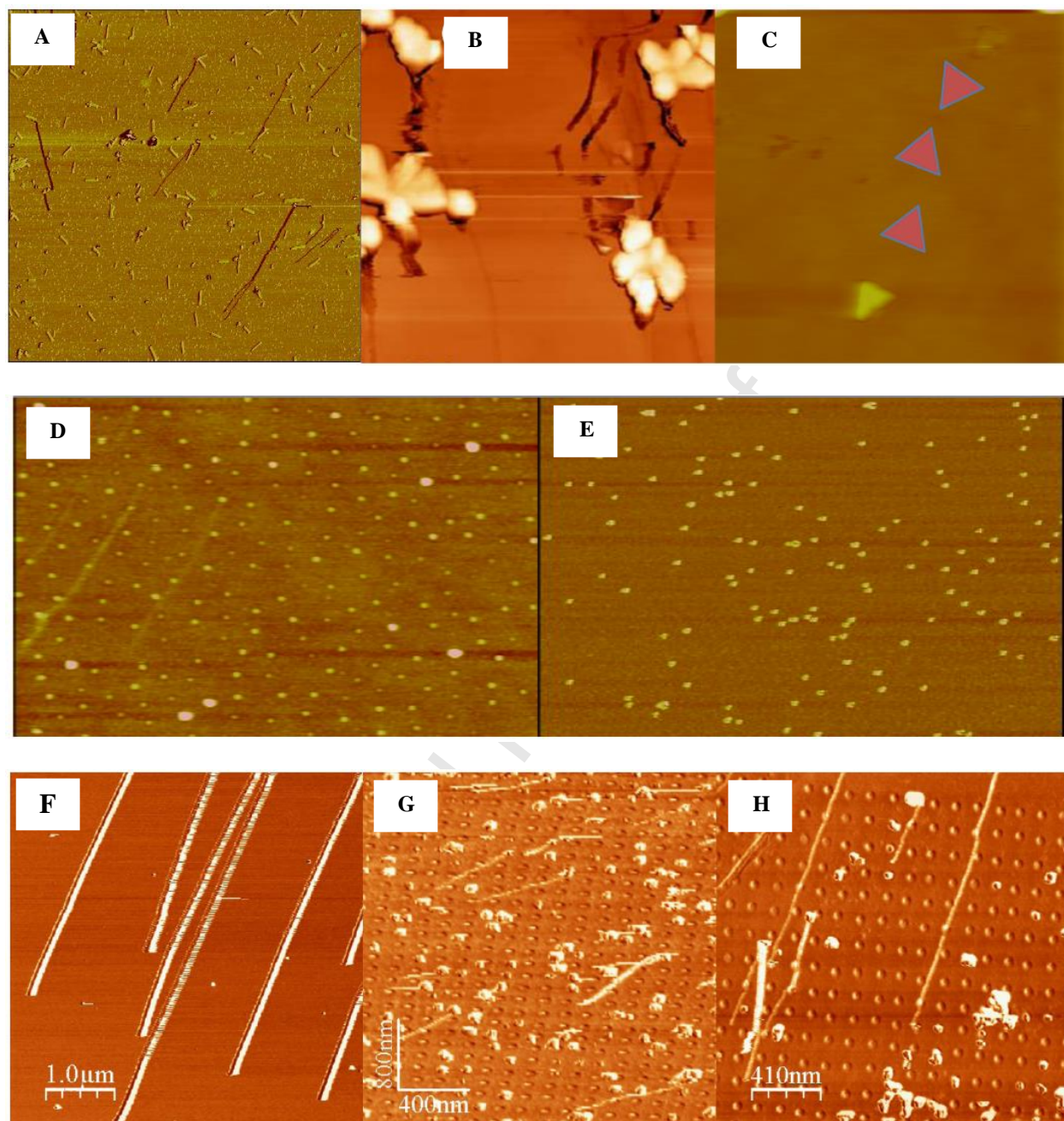


**Fig.17.** AFM images of nanocluster movement during their manipulation (A) gold nanorods deposited onto silicon wafer, scan size: 12  $\mu\text{m}$ ; (B) antimony islands on HOPG, scan size: 1.5  $\mu\text{m}$ ; (C) Au nanotriangles on silicon wafer. Middle triangles have been intentionally coloured in to illustrate the trajectory of the Au nanoparticles during manipulation, scan size: 5  $\mu\text{m}$ . AFM images of 25 nm diameter gold nanoparticles deposited onto a silicon wafer. (D) Ordered organization as described in the Experimental section, (E) random distribution. Frame sizes: 3  $\mu\text{m}$  and 1  $\mu\text{m}$ , respectively. Manipulation of as-synthesized Au nanoparticles on (a) a flat silicon wafer with a spacing of 9.7 nm and (b) a nanopatterned one with a spacing 16 nm, and (c) a patterned wafer with a spacing of 3.9 nm. [115]copyright 2011 Darwich et al; licensee Beilstein-Institute.

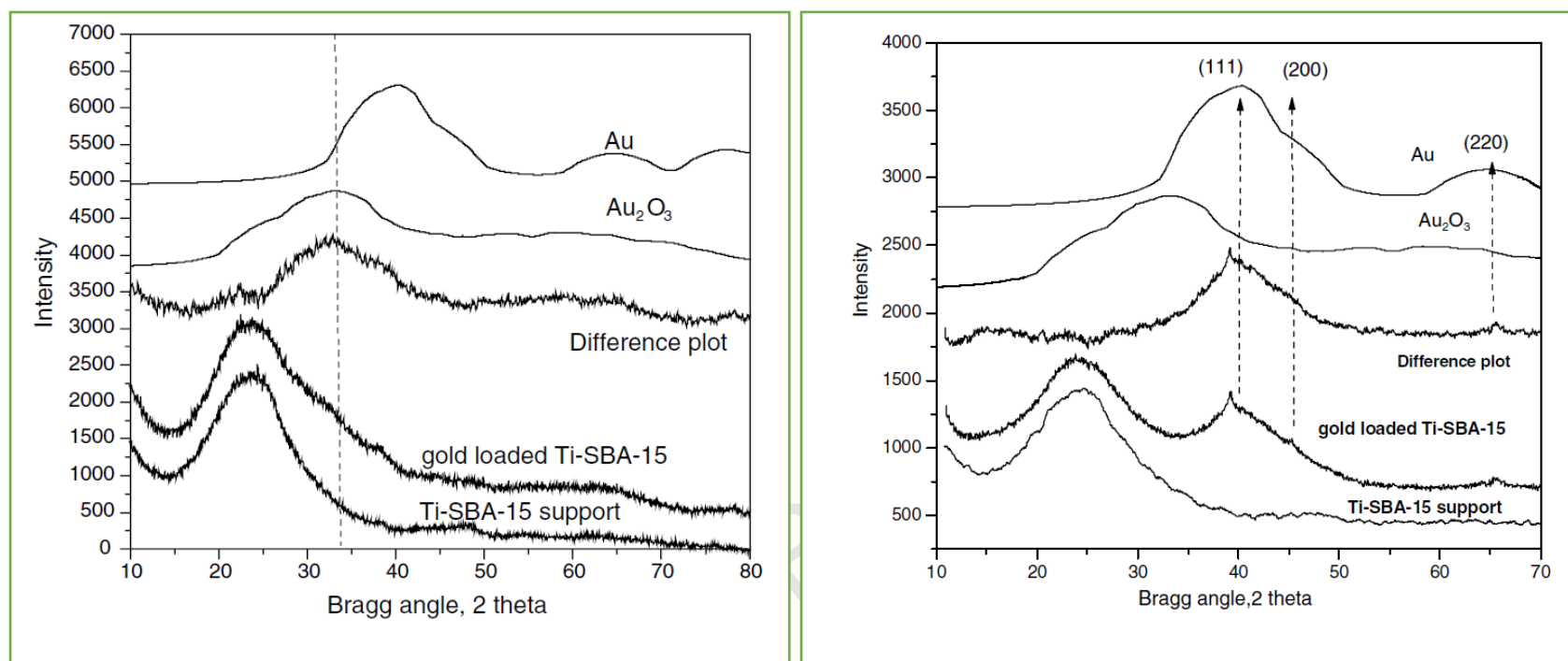


**Fig.18.** A. Experimental powder diffraction spectra for pristine (support) and gold loaded titania-modified SBA-15. The difference between the two experimental spectra is given in the middle. Calculated diffraction spectra for nanocrystalline Au and Au<sub>2</sub>O<sub>3</sub> are given in the upper part. The broken line running through the strongest Bragg peak of Au<sub>2</sub>O<sub>3</sub> is a guide to the eye. B. Experimental powder diffraction spectra for pristine (support) and gold loaded titania-modified SBA-15 reduced in H<sub>2</sub> atmosphere. The difference between the two experimental spectra is given in the middle. Calculated diffraction spectra for nanocrystalline Au and Au<sub>2</sub>O<sub>3</sub> are given in the upper part. First few Bragg peaks of Au are marked with arrows. Reprinted with permission from [117]copyright 2005 Elsevier B.V.

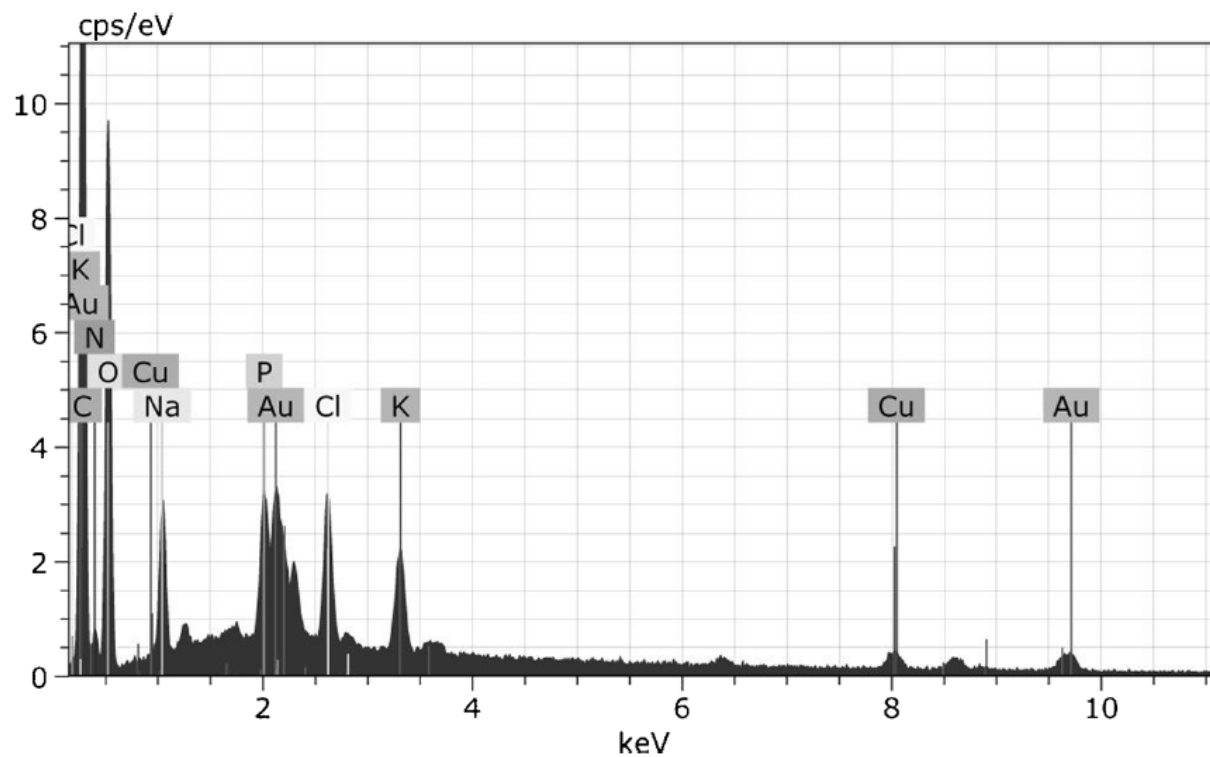


**Fig. 19.** EDS pattern for *A. fumigatus* showing strong signals for gold nanoparticles at three different places. [118]copyright 2013 Indian Academy of Sciences.

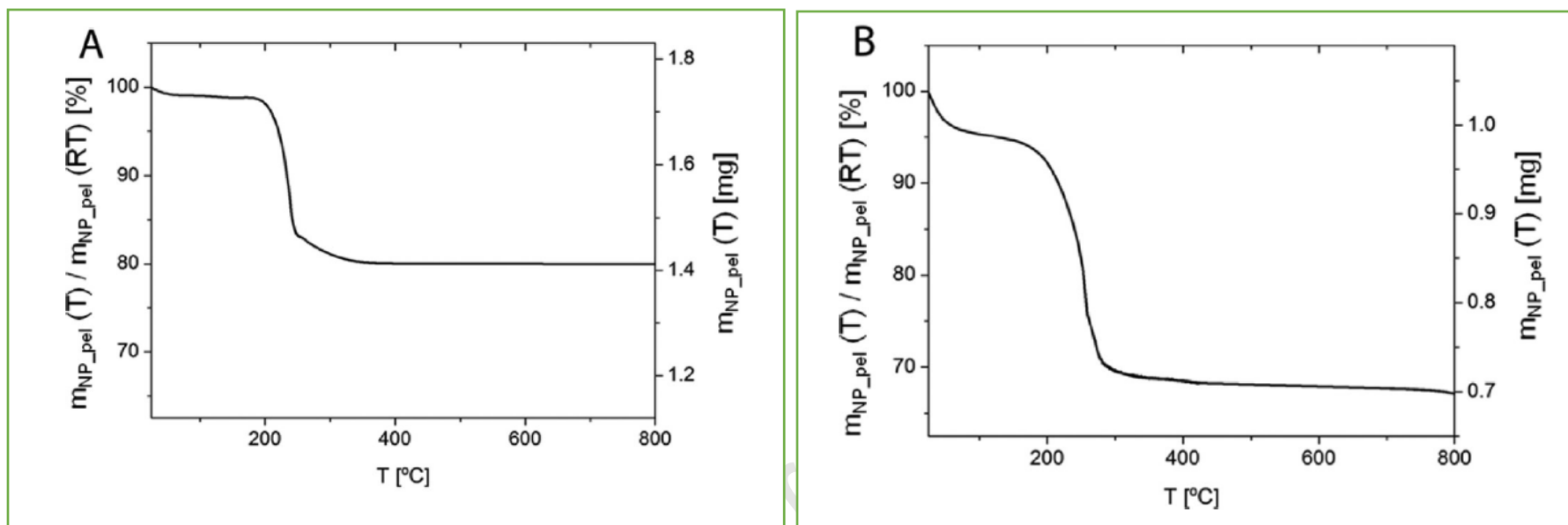


**Fig.20.** TGA analyses of DDT-Au NPs (A) and DDT-Au NPs overcoated with PMA (B). Reprinted with permission from [32]. Copyright 2017, American Chemical Society.

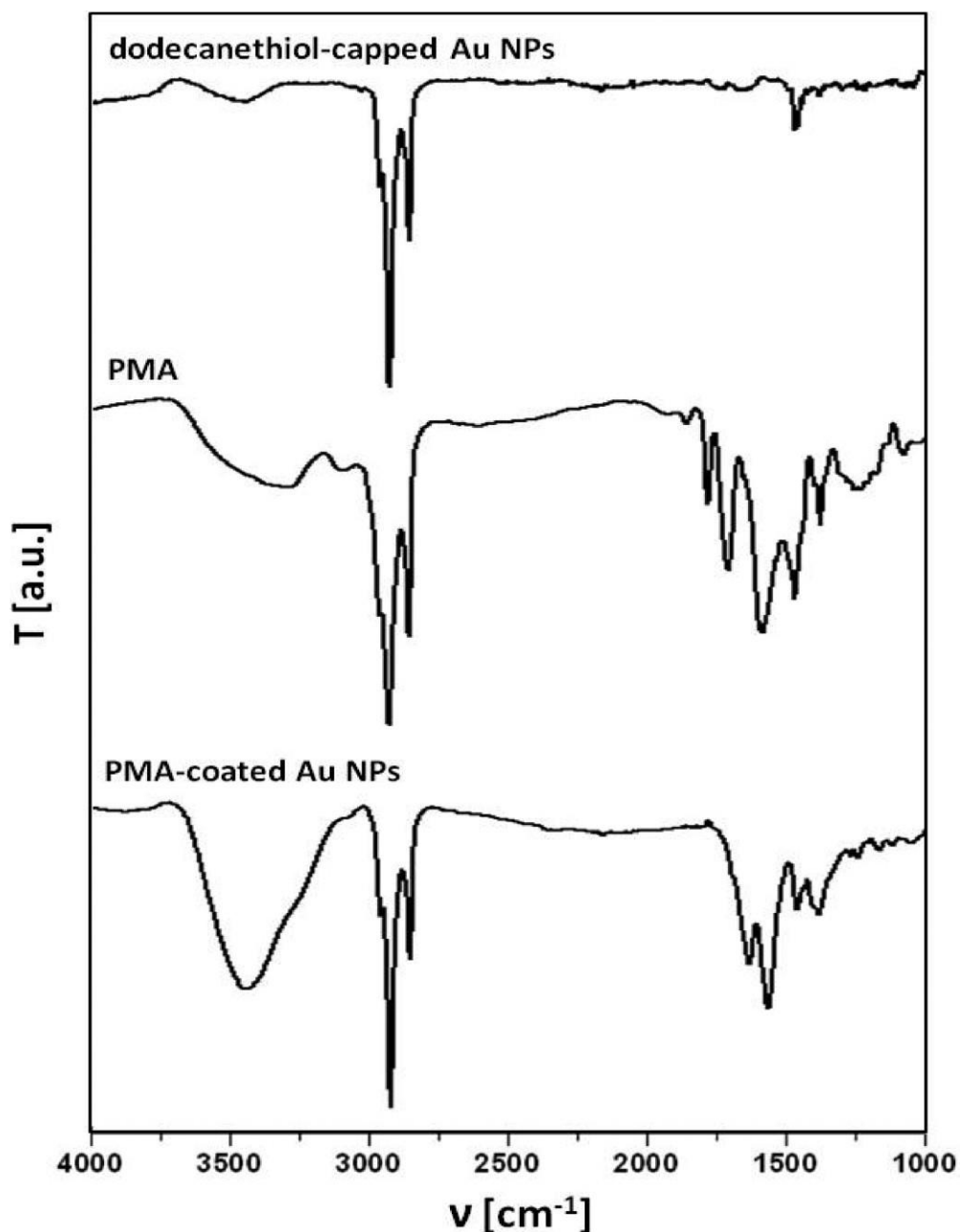


Fig.21. FTIR spectrum of DDT-Au NPs ( $\approx 4$  nm core diameter) before and after overcoating with PMA and spectrum of free PMA. Reprinted with permission from [32]. Copyright 2017, American Chemical Society.

## 5. Application of AuNPs

From past few decades, different forms of gold have been extensively used in the therapeutic treatment throughout the history of medicine. Gold has been described as the elixir of life. In 1925, gold complexes were used for clinical trials to understand its efficacy against rheumatoid arthritis. In 1920s, it was introduced for treatment of tuberculosis as well as to treat the inflammatory skin diseases like urticaria and psoriasis. In recent times, have found a



new application in the form of theranostics. Various applications of AuNPs are discussed below.

### **5.1. Application in delivery of therapeutics**

The unique optical, physicochemical properties, biocompatibility, functional flexibility, tunable monolayers, controlled dispersity, high surface area for loading the density of drugs, stability and nontoxicity make AuNPs an efficient nanocarrier in drug delivery systems (DDSs)[10, 119-122]. These are capable of transferring various drugs such as peptides [123], proteins [124] chemotherapeutic agents, small interfering RNAs (siRNAs), and plasmid DNAs (pDNAs) [125]. The drugs conjugated AuNPs due to their small size exhibit enhanced permeability and retention (EPR) in the tumour cells. These drug conjugated AuNPs, due to the leaky and irregular neo-vasculature of tumour tissues, get accumulated within the tumour while larger particles move ahead [126, 127].

The PEGylation of gold nanorods conjugated with drugs helps them to avoid reticular-endothelial system (RES) clearance. The targeting of cancer cells using biomolecules such as antibodies can be achieved by binding the cancer cell receptors to the surface of nanocages conjugated with bioactive molecule AuNPs conjugating other candidates are called gold nanocages. Verigene (FDA-approved) and Aurimmune (Phase-II) are gold based with application in very niche areas of therapeutics [128]. The specificity and selectivity of active analyte conjugated with AuNPs at the target site could be achieved by active targeting, which depends on a surface functional ligand that is designed for the particular drug to be targeted [129]. Utilizing the principles of site-specific targeting and delivery strategies, gold nanoparticles have been developed for therapeutic applications such as photothermal therapy (PTT) [130] genetic regulation [131], and drug treatment [132]. Use of spherical solid AuNPs (diameter > 50 nm) have been reported in plasmonic PTT due to strong near-infrared (NIR)

absorption of AuNPs [122]. The antibodies conjugated AuNPs have been applied for both diagnosis and PPTT (Fig. 22) [133].

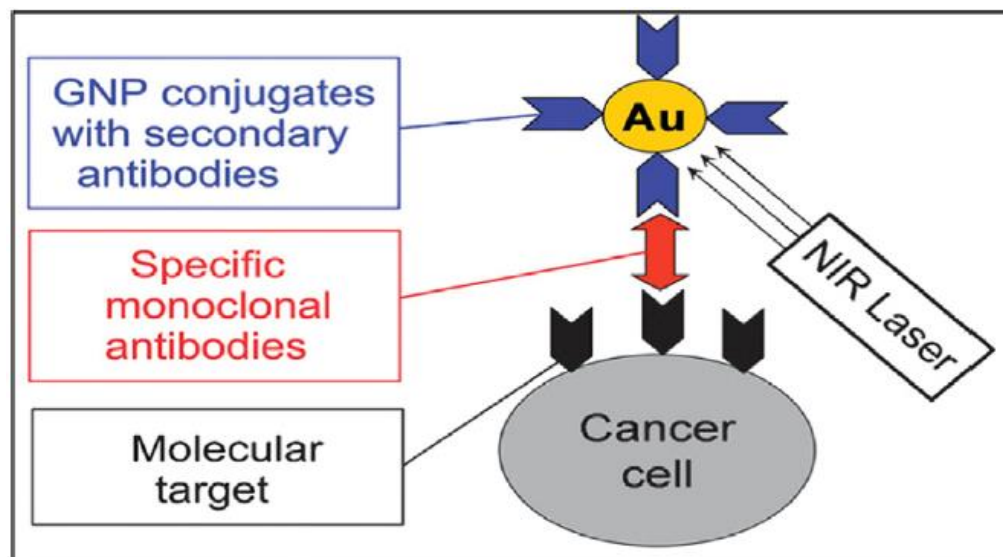


**Fig.22.** Scheme for a PTT employing active delivery of AuNPs to cancer cells. Reprinted with permission from [122]Copyright 2015 Elsevier.

AuNPs play major role in photodynamic therapy (PDT) for the treatment of cancer and certain skin or infectious diseases due to the properties like effective fluorescence quenching and surface plasmon resonance (SPR) absorption. PDT employs photosensitizers as light-sensitizing agents and a laser. Once it is incident on tumour cells, apoptosis or necrosis is induced in them by singlet oxygen and highly active free radicals generated via the energy of photosensitizers [133].

AuNPs scaffolds have been used for creation of transfection agents in gene therapy to cure cancer and genetic disorders. AuNP conjugated oligonucleotide complexes have been used as intracellular gene agents to control protein expression in cells [134]. RNA-conjugated gold nanoparticles have been utilized for knocking down luciferase expression [135]. Cationic amino acid based AuNPs have been utilized for DNA transfection. Lysine conjugated AuNPs

have been used as effective vectors for DNA delivery (about 28 times more effective) as compared to polylysine [136]. The drugs are loaded on AuNPs either through non-covalent interactions or, covalent conjugation (Fig. 23). Non-covalent conjugation of AuNPs with PEG has been reported to provide an amphiphilic environment for capturing silicon phthalocyanine 4 (Pc 4) which is a PDT drug (Fig 24 A and 24 B) for cancer therapy [137]. The Pc 4 conjugated AuNP was observed through passive mechanism. The conjugation yielded deep penetration and rapid release of Pc 4 into tumour cells within few hours [138]. The release of drug covalently bound to AuNPs occurs either through displacement of glutathione (GSH) [139] or through cleavable linkers [140]. For example, enhancement in anti-proliferative effect against K-562 leukaemia cells was observed with GSH-mediated release of 6-mercaptopurine-9- $\beta$ -D-ribofuranoside functionalized AuNPs as compared to the free drug [141]. Similarly, GSH-mediated movement of AuNPs carrying either fluorescein or doxorubicin molecules in a tumour model was investigated and the results indicated better efficacy of cationic AuNPs in delivering payloads to the majority of tumour cells while anionic AuNPs are able to deliver drug deep into tissues [142]. Apart from GSH and cleavable linkers, light controlled external release strategy using photocleavable ligands, pH mediated release strategies and release strategy using reduction of disulfides bonds have also been reported to deliver drugs such as 5-fluorouracil, covalently attached to AuNPs [141, 143-145]. Various applications of AuNPs as theranostic agents is shown in Table 2.

Au salts such as potassium cyanide ( $\text{AuK}(\text{CN})_2$ ), aurous sodium thiosulfate ( $\text{Na}_3[\text{Au}(\text{S}_2\text{O}_3)_2]$ ), aurous sodium thiopropanolsulfonate ( $\text{Na}[\text{Autps}]$ ), aurous sodium thiomalate ( $\text{Na}_2[\text{Autm}]$ ), aurous thioglucose (Autg), and auranofin ( $\text{Et}_3\text{PAupg}$ ) have been reported for the treatment of arthritis and other rheumatic diseases due to their anti-inflammatory (by inhibition of release of lysosomal enzymes by phagocytic cells and modulation of some prostaglandins and antiangiogenic properties (by inhibition of proliferation of synovial cells, as well as synthesis

of collagen) [146]. The anti-inflammatory and anti-angiogenic properties of AuNPs with their possible mechanism are shown in Table 3.

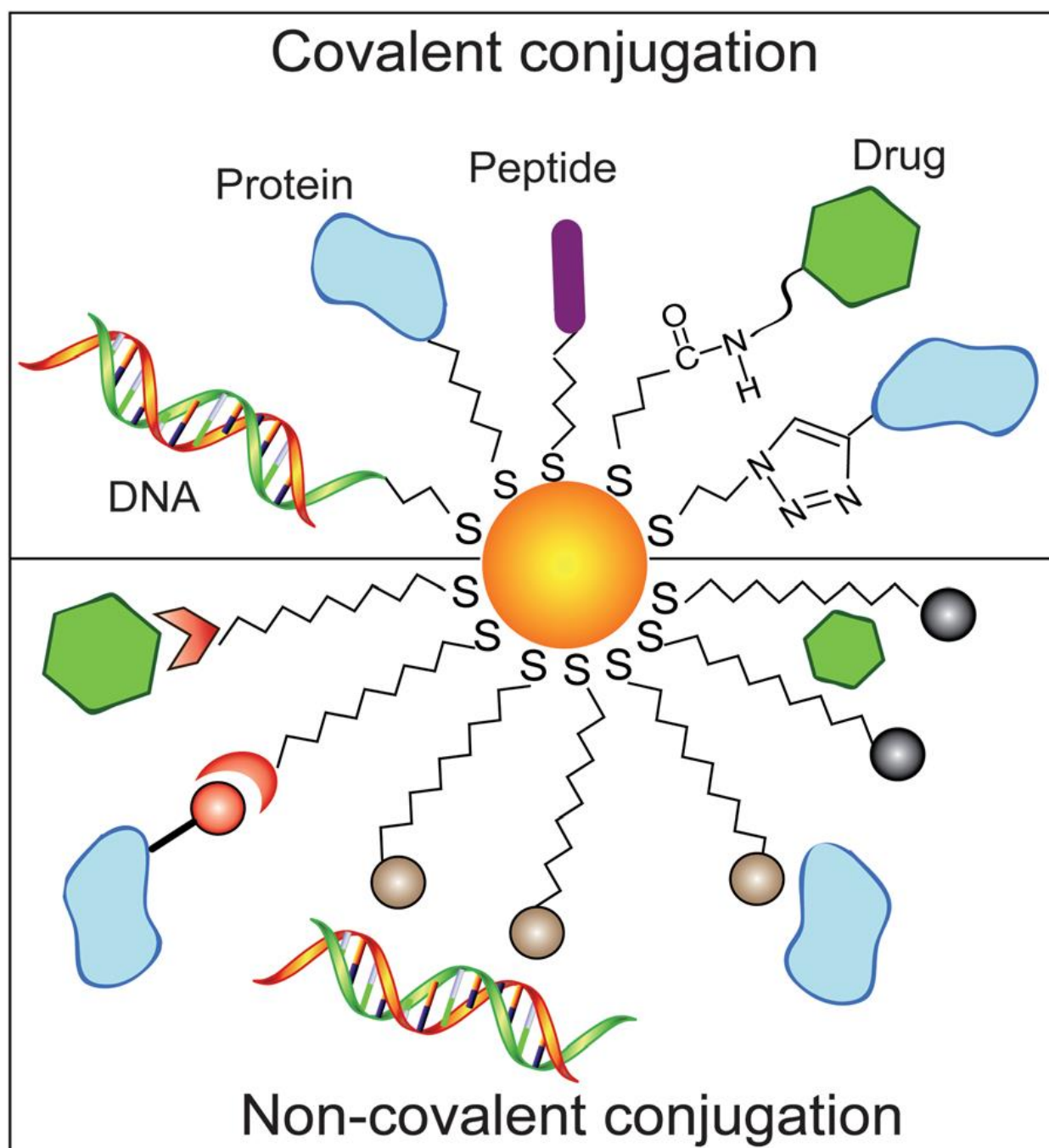


**Fig.23.** Demonstration of covalent and noncovalent conjugation in AuNPs. Reprinted with permission from [10] Copyright 2012 The Royal Society of Chemistry.

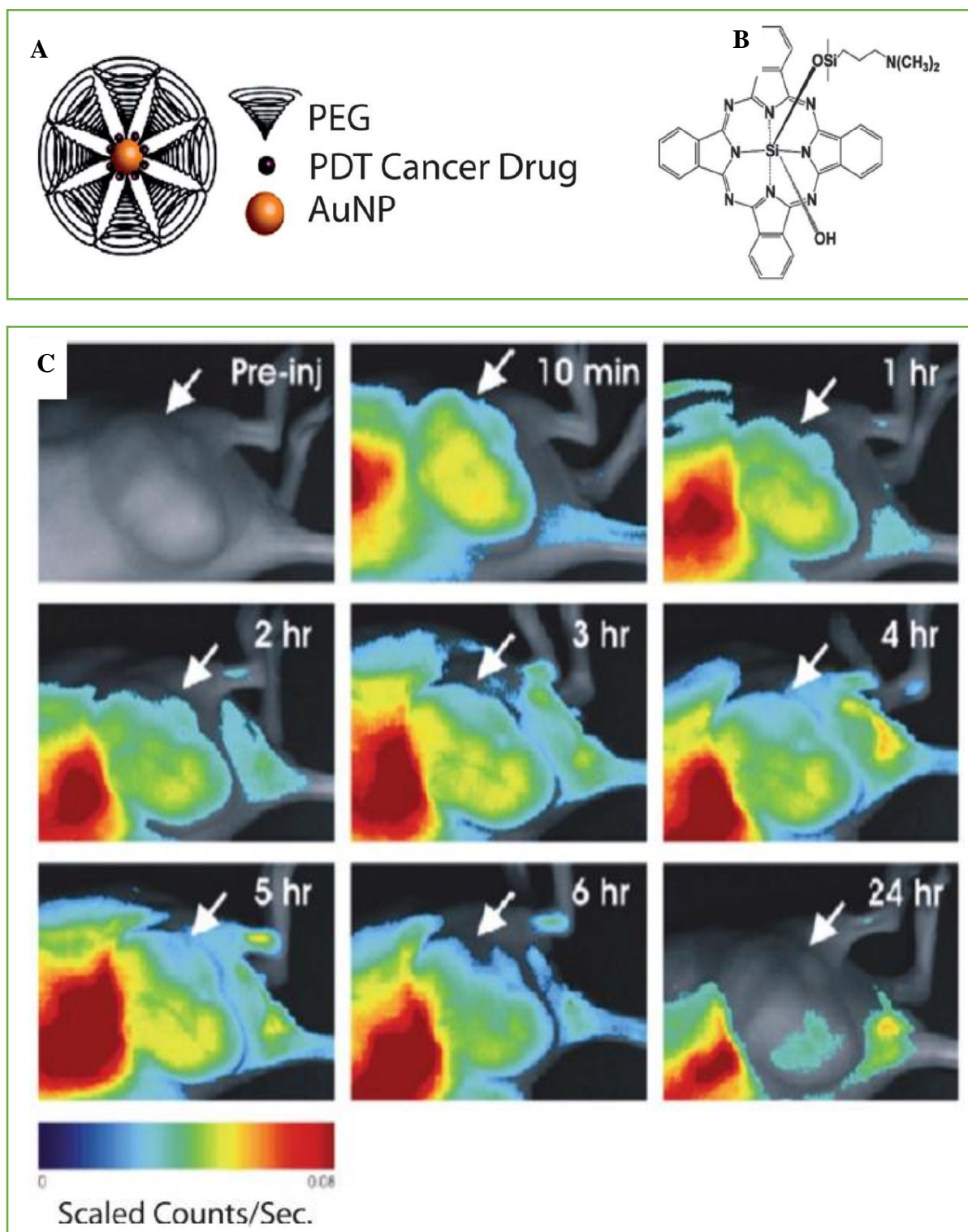


Fig.24. PEG functionalized AuNPs with loading of PDT cancer drug. (B) Chemical structure of the PDT drug Pc 4. (C) In vivo fluorescence imaging of AuNP-Pc 4 conjugates injected mouse at various time points within 24 h. Arrows indicate the tumour location. Reprinted with permission from [138]. Copyright 2015 Elsevier.

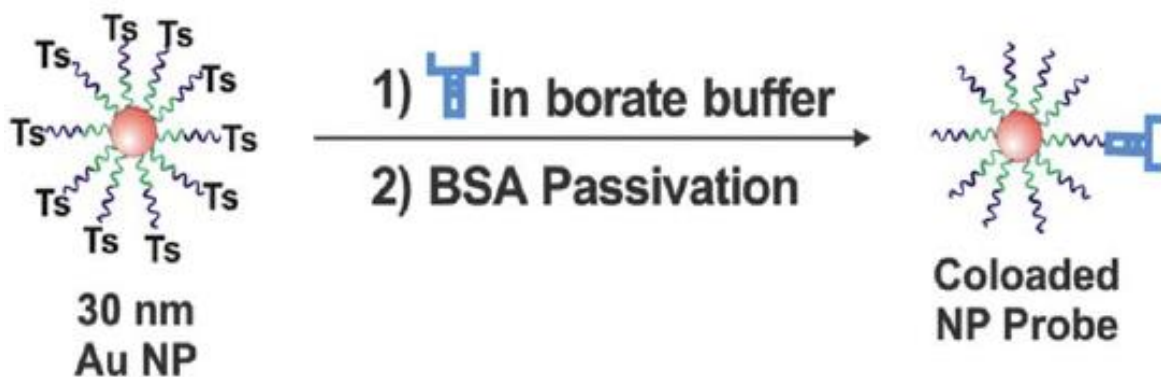
## 5.2. AuNPs as sensors

AuNPs have been used as efficient sensors for the detection of different analytes such as metal ions, anions, and molecules like, saccharides, nucleotides, proteins and toxins [122]. Table 4 shows various nano biosensors based on AuNPs features and their application. The sensors are designed based on the intent of detection and various properties of AuNPs. These include colorimetric, fluorescence-based, electrical and electrochemical, surface plasmon resonance, surface enhanced Raman scattering (SERS)-based, quartz crystal microbalance based and Bio-Barcode assay sensors [147]. Colorimetric sensing is based on visible color change due to the aggregation of AuNPs, fluorescence-based sensing is based on the fluorescence quenching feature of AuNPs. On the other hand, electrical and electrochemical sensors conductivity is based on high surface area and catalytic properties of AuNPs. Au NP-based SPR sensors are based on the optical properties (SPR) of AuNPs [122]. Surface-enhanced Raman scattering (SERS)-based sensors are based on the inelastic scattering of photons by AuNPs due to quantized vibrational level/signature. Au NPs in Quartz crystal microbalance-based sensing is based on the high surface area of AuNPs for enhancing detection sensitivity. Au NP-Based Bio-Barcode Assay (AuNP BBBA) is based on strong binding affinity of AuNPs to thiols and visible color change due to aggregation of AuNPs. AuNP BBBA is an ultrasensitive method for detecting target proteins and nucleic acids. The basic principle involved in AuNP BBBA is conjugation of AuNPs with both barcode oligonucleotides and target-specific antibodies, as well as magnetic microparticles (MMPs) functionalized with monoclonal antibodies for the target moiety [118]. A sandwich complex is produced upon detection of the target molecule which releases a large amount of barcode oligonucleotides, providing both identification and quantification of the target (Fig.25). This technique was used to detect prostate specific antigen



(PSA) [10, 148]. High resolution multicolour AuNPs containing a silver alloy (gold nanoshells rods) have also been used as for visual observation of alkaline phosphatase (ALP) activity through naked-eyes (Fig.26). The method is based on enzymatic reaction, assisted silver deposition on gold nanorods to produce colour change, which was dependent on ALP activity. Upon target incubation with the substrate, ascorbic acid 2-phosphate was hydrolysed to produce ascorbic acid, which in turn reduced silver ion to metallic silver coating the gold nanorods, thereby resulting in a colour change [149]. Colorimetric AuNPs methods that have been developed for conducting plasmonic ELISA and immunoassays for understanding activities of PSA, Urease, Horse Radish, Peroxidase, Tyrosinase and matrix metallo proteinase [150]. Gold nanorods are elongated AuNPs that possess two plasmon resonance absorptions in the visible and NIR regions due to their anisotropic shape [151] that are produced by transverse (TSPR), short axis, and longitudinal (LSPR), long axis, oscillation of electrons [151, 152]. These unique optical and physiochemical properties play a key role in various biomedical applications of Au NRs such as photothermal therapy, and near-infrared imaging, X-ray computed tomography, photoacoustic imaging, biosensing, drug/gene delivery, and thermal therapy of tumour [152, 153]. Some of the applications of gold nanorods as sensors are shown in Fig. 27.

## Gold Nanoparticle (Au NP) Probes



## Bio-Barcode Assay

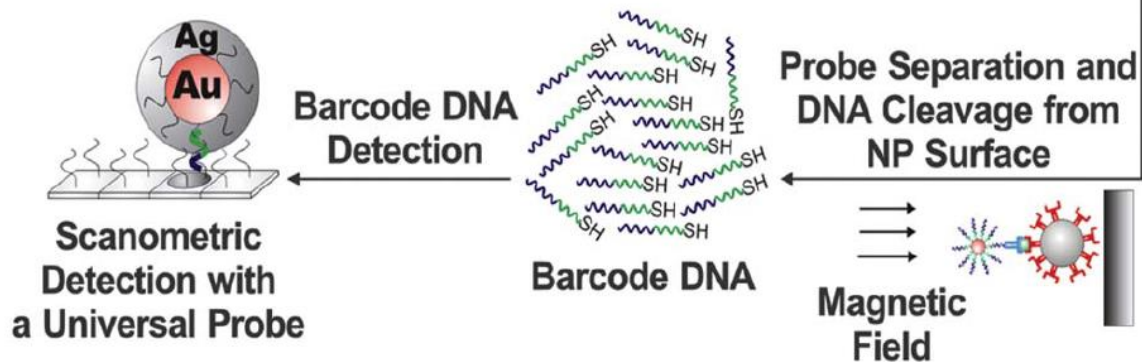
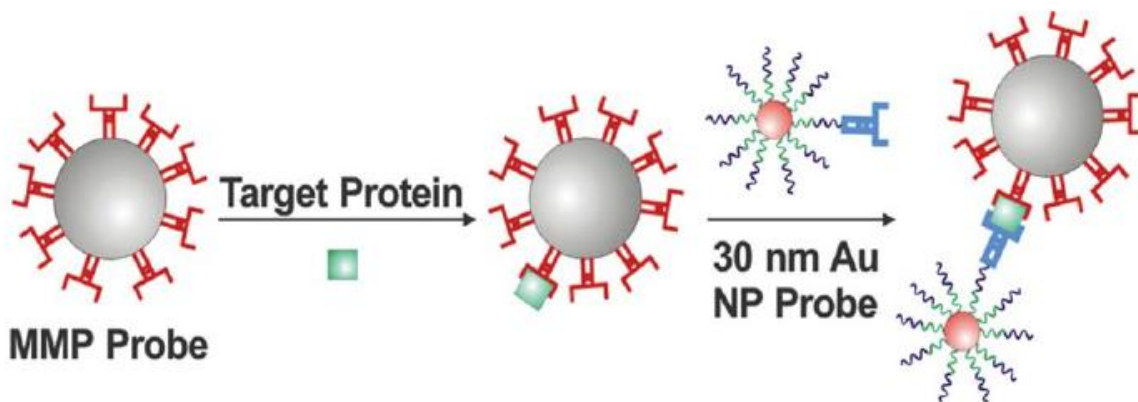




Fig. 25. AuNP-based bio-barcode detection strategy. Reprinted with permission from [10] Copyright 2012 The Royal Society of Chemistry.

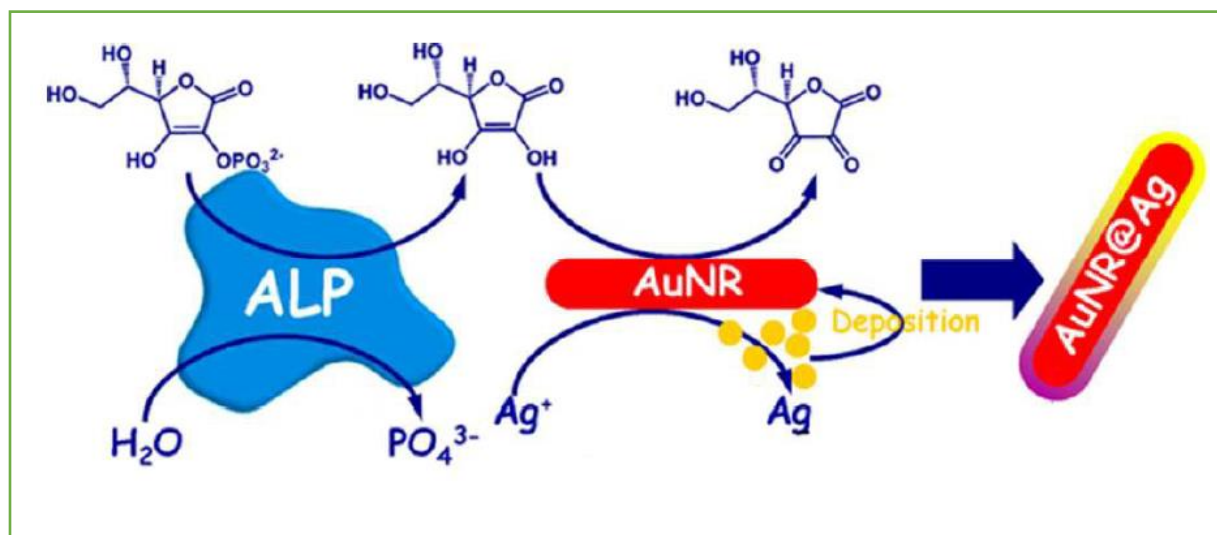
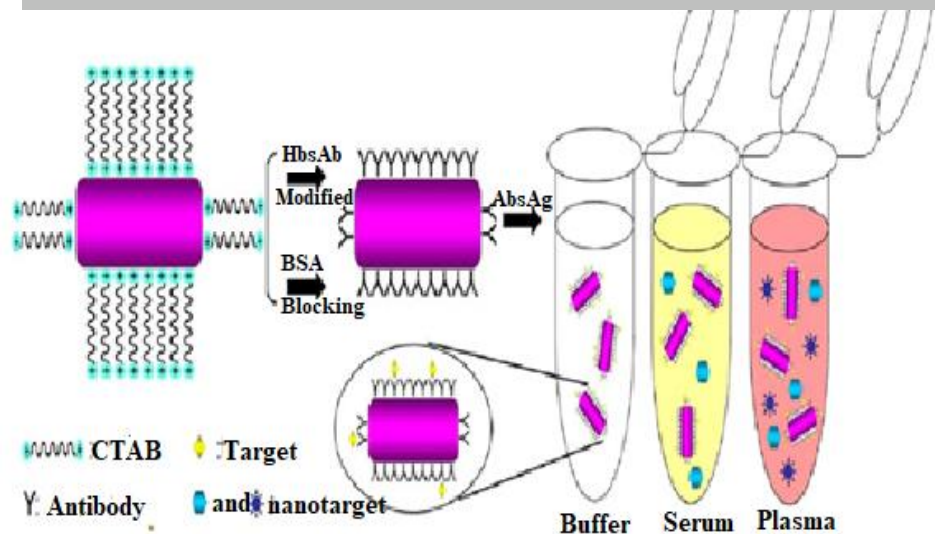
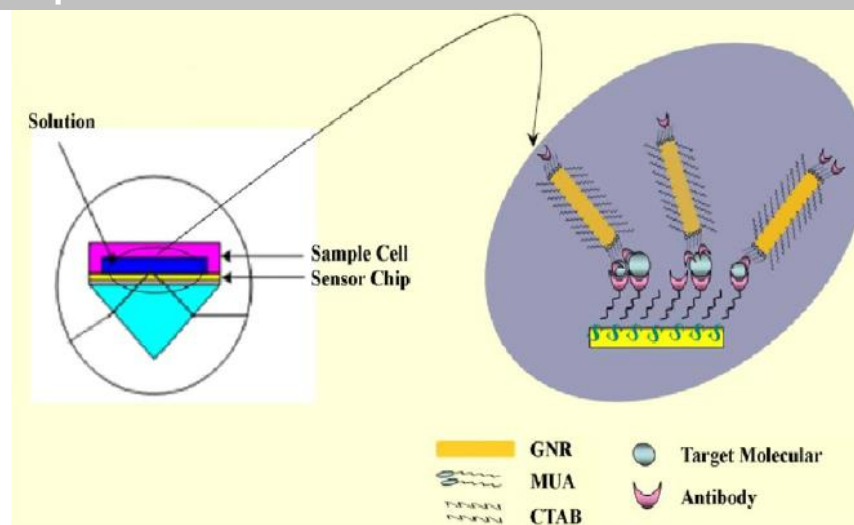


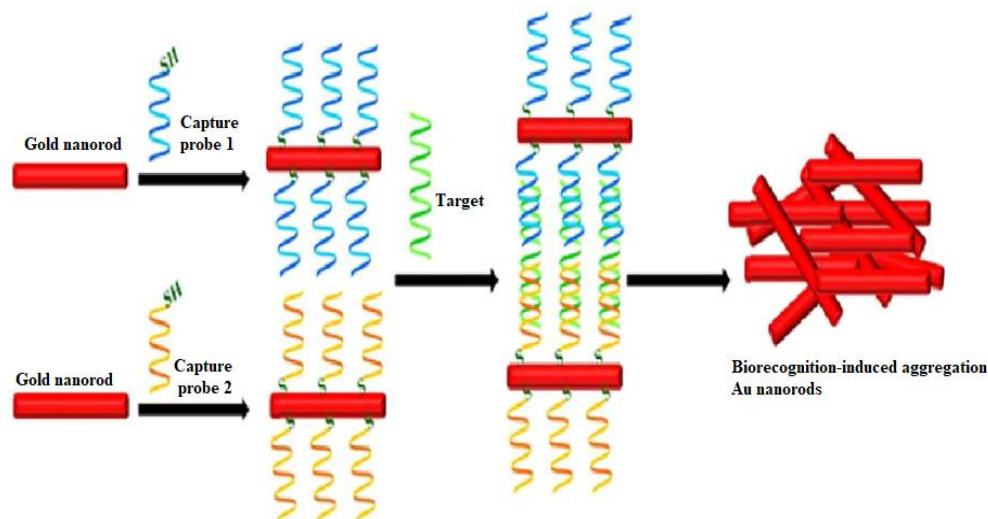
Fig. 26. High-resolution colorimetric assay for sensitive visual readout of phosphatase activity based on gold/silver core/shell nanorod. Reprinted with permission from reference [170]. Copyright (2014) American Chemical Society.



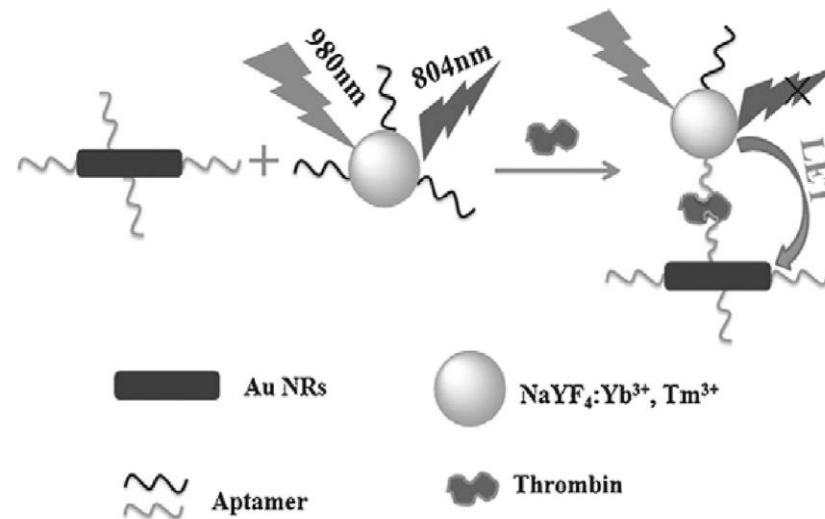
A. The LSPR based Au NRs biosensor to detect the hepatitis B surface antigen (HBsAg) which indicates active viral replication of hepatitis B virus (HBV).



B. Combined target molecular to antibody with AUNRs in SPR sensor; AU NRs were used to enhance the sensitivity of the biosensor for *Escherichia coli O157:H7* in SPR system.



C. Detection of DNA hybridization with Au NRs. Aggregation of AuNRs is induced by specific target recognition.



D. Two probes (UCNPs-TBA15 and Au NRs-TBA29) were obtained by functionalization of the poly (acrylic acid) (PAA)-modified NaYF<sub>4</sub>:Yb<sup>3+</sup>, Tm<sup>3+</sup> UCNPs and the CTAB stabilized Au NRs with thrombin aptamers.

### 5.3. AuNPs as diagnostic agents

SPR, magnetic resonance and fluorescence properties of AuNPs lead to their application in clinical diagnosis and different biological studies (Fig.28). SPR of AuNPs is being utilized for measurement of real-time kinetics of ligand-receptor interactions, DNA hybridization, screening of lead compound in pharmaceutical drug development as well as in detection of small molecules, antibody characterization, studying antigen-antibody interaction, enzyme substrate interactions, characterization of antibody orientations, epitope mapping, label free immunoassays and protein conformational studies [137, 154]. The magnetic resonance properties of AuNPs is helpful in magnetic resonance imaging (MRI) measurement of biological processes at cellular and molecular level. This helps in quantification of molecular changes associated with the onset and development of pathological states, thereby, providing early diagnosis and prognosis of diseases like cancer. The imaging of cells, cellular and subcellular structures, requires imaging agents of high relaxivity and density, endowed with targeting ability to specific cellular receptors. In the field of MRI, AuNPs can be used as a template agent in place of Gadolinium (*Gd*) chelates for use as MRI contrast agents due to their high sensitivity and also in clinical diagnosis. Several types of AuNPs such as core-shell structured iron-gold (*Fe-Au*) NPs (prepared by reverse micelle method having size 19 nm), PEG-coated iron oxide gold core-shell nanoparticles (measuring approximately 25 nm in diameter), and AuNPs coated with by *Gd*-chelate, have been used as a potential CT/MRI Bimodal contrast agent to detect cancerous tumours [155-157]. The anti-photobleaching under the presence of strong light illumination causes AuNPs to exhibit strong native fluorescence under relatively high excitation energy state. AuNP stained cells illuminate strong fluorescent light on cell membrane or inside cells which helps in cell imaging [158]. Au nanoprobe immobilized with fluorescein-hyaluronic acid (HA)

conjugates have been utilized for monitoring intracellular reactive oxygen species (ROS) generation in live cells via NP surface energy transfer [159]. AuNPs as fluorescent labels have been found helpful for optical imaging and sensing for analytical genomics and proteomics, with particular emphasis on the outlook for different strategies of using NPs for bioimaging and quantitative bioanalytical applications [160]. Fluorescence resonance energy transfer (FRET) is a spectroscopic technique whereby the excitation energy of the donor electron is transferred to the acceptor via an induced-dipole movement interaction [6]. DNA hybridization, and cleavage of DNA by nucleobases after hybridization by varying the DNA length have been monitored using AuNP-based FRET. AuNPs (20 nm size) stabilized by Cy5.5-Gly-Po- Leu-Gly-Val-Arg-Gly-Cys-(amide) were used to sense macromolecules such as proteins [161]. Using the principle of SPR, magnetic resonance and fluorescent properties AuNPs have been utilized for diagnosis of cancer (Fig.29) and HIV/AIDS. There are three basic approaches through which AuNPs are utilized as diagnostic agent. These include, (i) colorimetric sensing for specific DNA hybridization, depending upon inter-AuNP distance for the detection of specific nucleic acid sequences in biological samples, (ii) surface functionalization with different coating materials resulting in highly selective nanoprobe, and (iii) electrochemical-based methods for signal enhancement detection [162]. Immunotargeted AuNPs have been used for imaging of overexpression of transmembrane glycoprotein and epithelial growth factor (EGFR) in cancer cell lines (SiHa cells) to diagnose pericervical cancer [163]. PEGylated AuNPs conjugated with monoclonal antibody (Herceptin) enables the detection of breast cancer. Colloidal AuNPs conjugated to EGFR and self-assembled surface enhanced-Raman-Scattering (SERS) activated AuNPs have been used for imaging cancer cells [164]. AuNPs conjugated aptamer has been utilized for the detection of leukemia, liver cancer, lung cancer and lymphoma. In a study,

multifunctional oval shaped AuNPs were prepared by conjugating AuNPs with monoclonal antibody (Anti-HER2) and S6RNA aptamer. Upon mixing these functionalized AuNPs with SK-BR-3 breast cancer cell lines, a distinct colour change with thirteen times increase in two-photon scattering intensity was observed (Fig.30a).

AuNPs are used for optical imaging in biological studies by majorly using the three techniques

- 1) Direct visualization of AuNPs inside the biosystems using i) dark field (DF) microscopy, ii) differential interference contrast (DIC) microscopy, iii) interferometric scattering (iSCAT) microscopy and photothermal imaging, iv). optical imaging methods in the rotational and orientation tracking of AuNPs.
- 2) Monitoring of biomolecular events and physiological processes using i) surface-enhanced Raman spectroscopy (SERS) and ii) plasmon enhanced fluorescence (PEF) for ultra-sensitive detection of biomolecules, including proteins, metabolites, DNA, RNA, etc.
- 3) In vivo deep tissue imaging using i) two-photon and/or multi-photon imaging, ii) optical coherence tomography (OCT), and iii) photoacoustic (PA) imaging for disease diagnoses, such as detecting tumors and other diseases in eye, brain, and bone [154]. As an example, the melanoma cells contain melanin that absorbs natural light and induces photoacoustic waves for tumor cell detection in non-pigmented prostate cancer cell line (PC-3). The non-pigmented tumor cells do not produce photoacoustic waves for their detection. The photoacoustic response over wavelengths (470-570 nm) was recorded by tagging PC-3 cell lines with functionalized AuNPs. SER tagged AuNPs conjugated with EGF peptides have been reported for direct measurement of targeted circulating tumor cells (Fig.30b) present in blood of patients with squamous cell carcinoma of head and neck (SCCHN) [165]. Dark field microscopy (DFM) has been used to track the intracellular locations and behavior of AuNPs inside cells, such as the examination of AuNP uptake [166]. The color change in cells indicated the evolution

of AuNP clusters in live cells, that was dependent upon size and cellular location of cluster and the endocytosis followed by their transport along the microtubules [Fig.31A] [167]. The tracking of trafficking of AuNPs along microtubules was reported by Nan et al., who developed a novel strategy to track AuNPs in 2D with 1.5 nm spatial precision and 25  $\mu$ s time resolution through utilization of a quadrant photodiode to record the positions of the AuNPs [168]. DFM incorporated AuNPs can be used for understanding biological processes. For example, AuNP functionalized nanospheres have been used for imaging cell division [169]. AuNPs localized in the nuclear region were tracked in real time during the mitosis of the HSC-3 cancer cell (Fig.31B). The real time tracking of virus-cell interactions were assisted by AuNPs in order to understand the respiratory syncytial virus infection of Hep-2 cells (Fig.31C). Different optical imaging techniques and their application is shown in Fig.32.

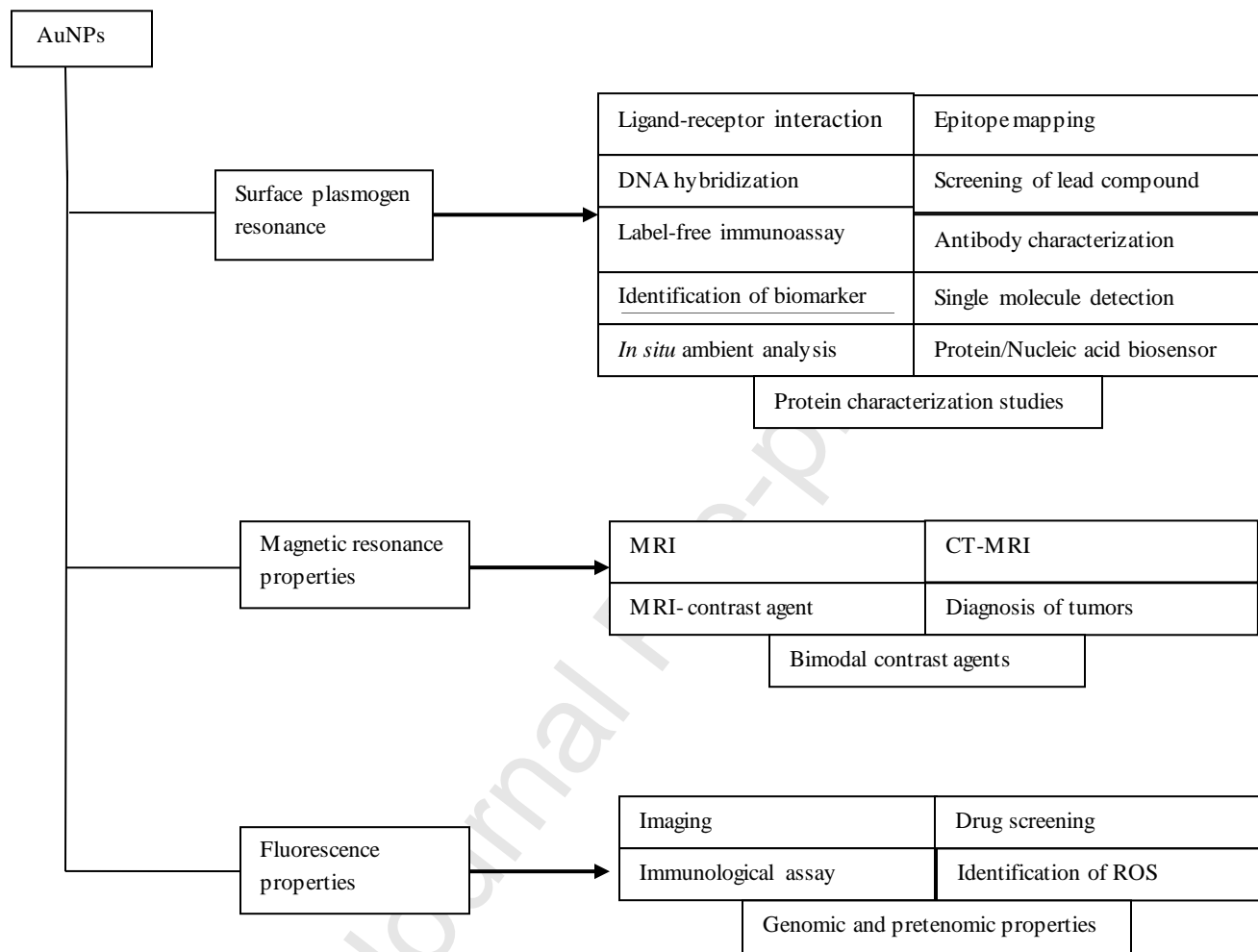


**Fig.28.** Unique properties of AuNPs and their application in diagnosis [137].



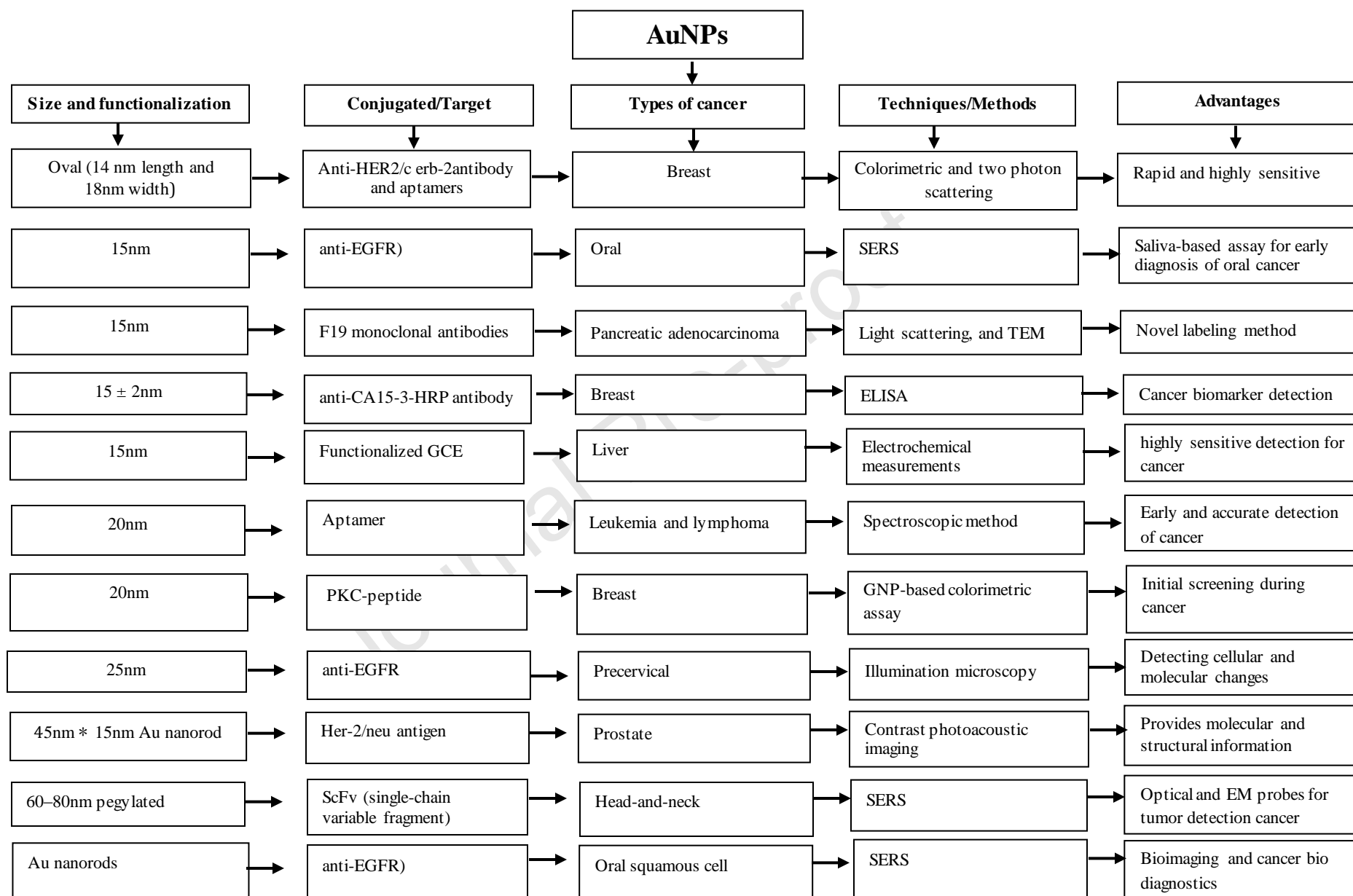


**Fig.29.** Application of AuNPs in diagnosis of cancer.

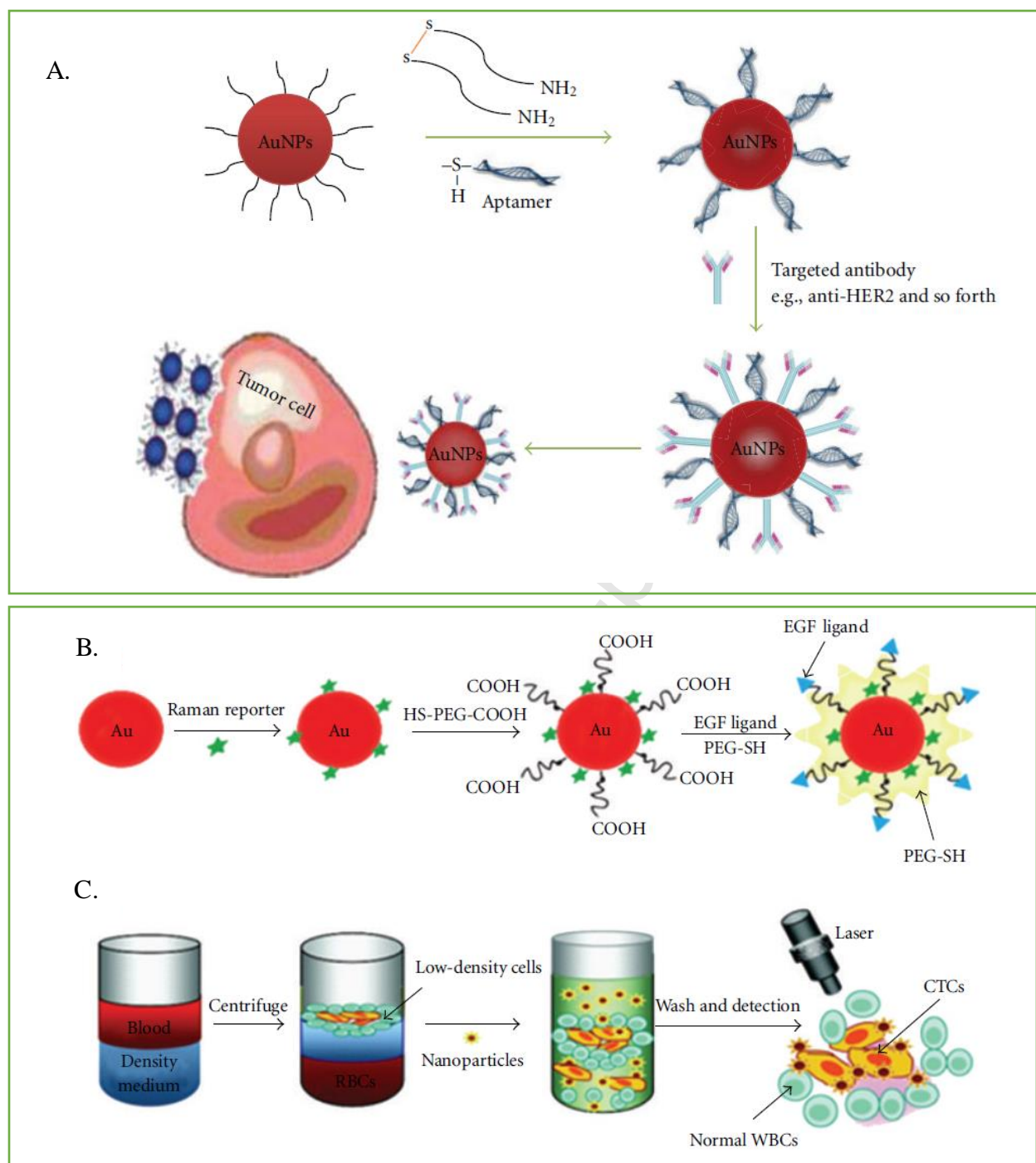


**Fig.30** (A). Synthesis of monoclonal anti-HER2 antibody and S6 RNA aptamer-conjugated oval-shaped AuNPs (steps one and two). Third step shows multifunctional oval-shaped AuNP-based sensing of the breast cancer cell lines. Schematic design of EGF-SERS NPs for labelling and detection of CTCs [137]; (B) Raman-encoded, PEG-stabilized, and EGF-peptide functionalized SERS nanoparticle. (C) Assay principle of CTC detection from whole blood using EGF-SERS nanoparticles [165] © 2011 American Association for Cancer Research.

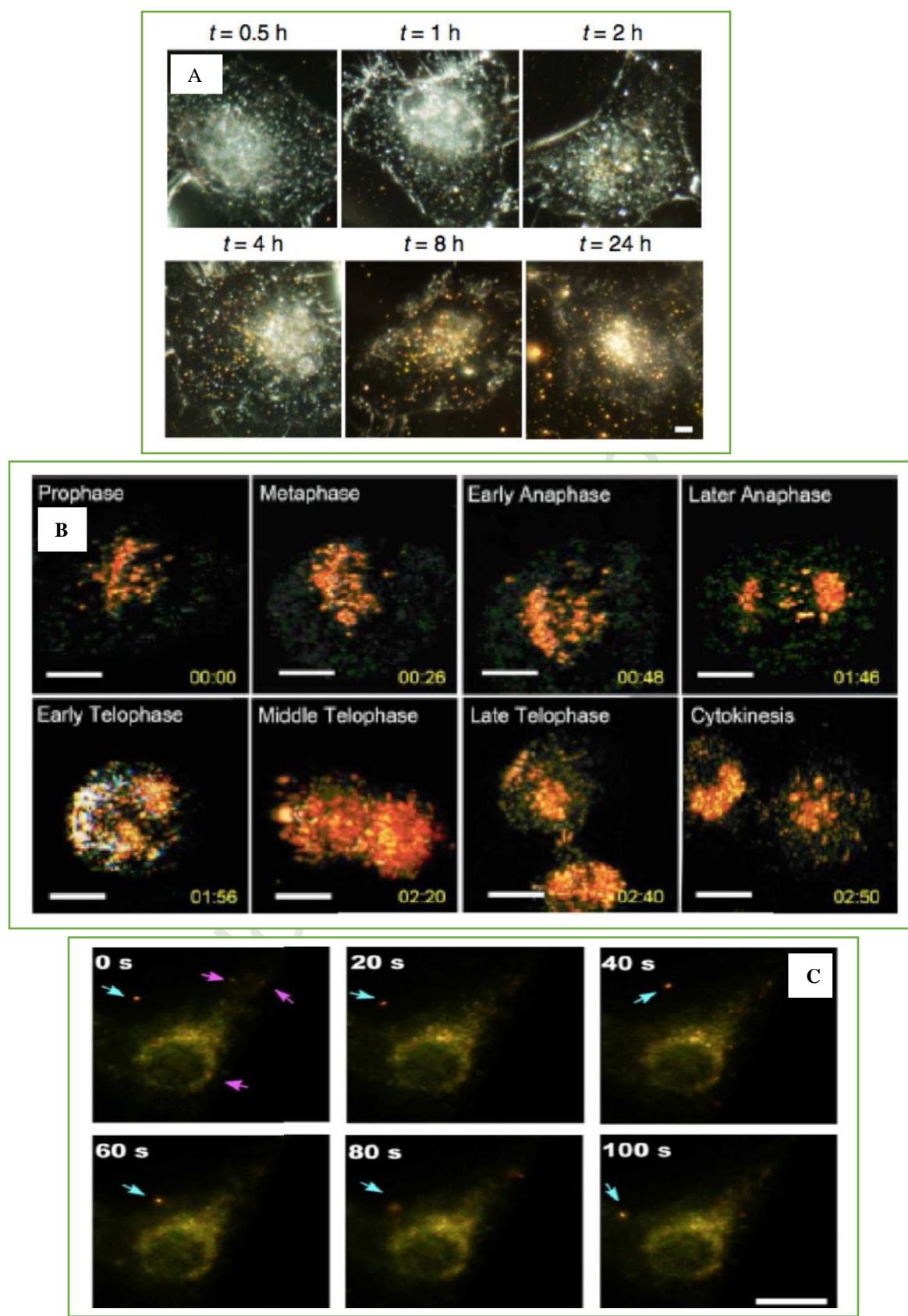
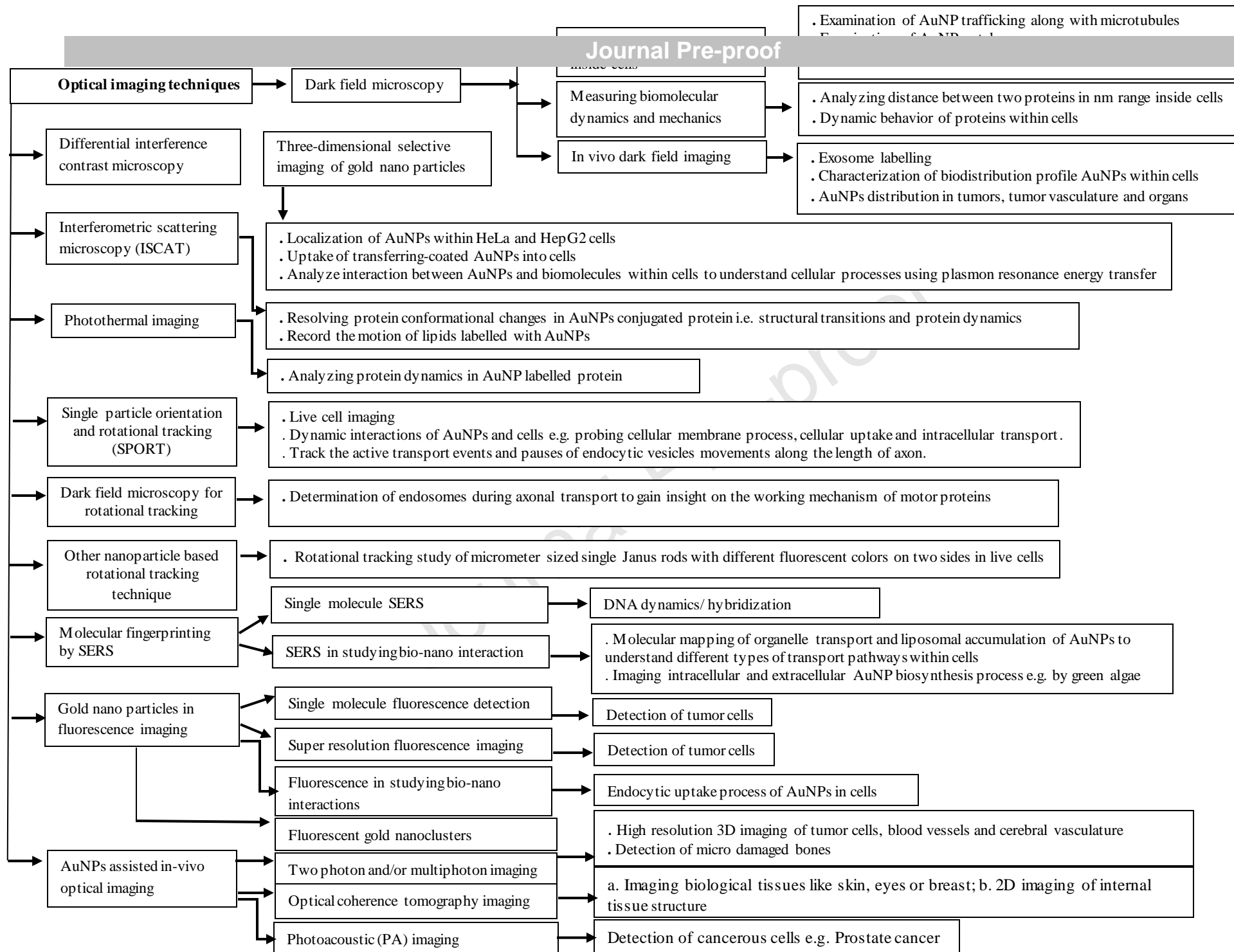


Fig. 31. (A) Dark field (DF) microscopy showing the evolution of AuNP color in HeLa cells at the different durations (0.5–24 h) of incubation [167]. (B) Human oral squamous cell carcinoma (HSC-3) cell division process (prophase to cytokinesis) visualized by the AuNPs [169]. (C) Real-time tracking (0–100 s) of AuNPs labeled respiratory syncytial virus (indicated by blue and red arrows) infecting HEp-2 cells [171]. Reprinted with permission from [154]. Copyright 2019 Elsevier.



**Table 2.** Theranostic applications of AuNPs

Types of AuNPs	Size and Shape	Therapeutic	Diagnostic	References
Therapeutic based AuNPs				
5-fluorouracil conjugated AuNPs	2nm, spherical	Photo cleavable ligand used for conjugation of AuNPs which gets dissociates when exposed to UV rays and releases drug to the targeted site	For SERS imaging of pH in living NIH 3T3 cells	[172]
P-mercaptobenzoic acid-conjugated Au nano aggregates	Spherical	-	For SERS imaging of pH in living NIH 3T3 cells	[173]
Cisplatin-glucose conjugated AuNPs	20 nm	-	. Bio-imaging and Cell labelling . bypass surgeries . Theranostic agent for head and neck cancer	[174]
Polymer based AuNPs				
PEG-modified AuNPs	26nm, spherical	-	Delivery of anticancer drug paclitaxel	[175]
PEG-modified AuNPs conjugated with herceptin	Spherical	Treatment of breast cancer	-	[176]
Biopolymers and Sugars as Reducing Agent based AuNPs	1-40nm	-	immobilization of enzymes (in biosensor) for the detection of pathogens, virus and bacteria	[177]
Doxorubicin conjugated AuNPs	12.1 nm	Cytotoxic effect on Cancer cells	. Bio-imaging . Bio-sensors	[178]

Pacitaxel conjugated AuNPs	50nm	Photo-thermal activity	Bio-imaging	[179]
PEG-b-P	63nm	As a multicarrier in cancer treatment	.Bio-imaging .Cell labelling	[180]
Polypyrrole and gold shell	65nm	As a photo thermal agent	Cell labelling	[181]
Biomolecules based AuNPs				
Antibody conjugated AuNPs	35nm, spherical	-	For imaging anatomic location and molecular sensing	[182]
Anti-EGFR conjugated AuNPs	25nm, spherical	For paracervical cancer	-	[176]
Hollow Au nanospheres conjugated with antibodies	45 ±12nm, spherical	-	. Used for MCF7 cells . quantitative immune analysis of cancer biomarkers	[183]
AuNPs functionalized with peptides	7-13 nm, spherical	Induction of cancer cell apoptosis	-	[184]
TNF- $\alpha$ conjugated PEG coated gold nanoparticle	-	Enhance the activity of anticancer activity	Bio-imaging	[153]
AuNPs coated with phospholipids	30nm, spherical	-	Used as a delivery vehicle for nucleic acid cargoes	[186]
CYT-6091	27nm	Enhanced the activity of anticancer drugs	Bio-imaging	[187]
Plant based AuNPs				
Plumbago zeylanica	> 100nm,spherical, triangles, hexagons	Antibacterial activity against Gram-negative and Gram-positive bacteria	-	[188]

Abelmoschus esculentus	45-75nm,spherical	Antifungal activity against Puccinia graminis tritici, Aspergillus flavus, Aspergillus niger and Candida albicans	-	[172]
Eucommia ulmoides	~20nm,spherical		Excellent catalytic activity	[189]
Terminalia arjuna	20-50nm,spherical	Enhance the mitotic cell division and pollen germination activity	-	[190]
Mentha piperita	> 100nm,spherical	Antibacterial activity against clinically isolated pathogens		[191]
Rosa hybrida	10nm,cubic		High potential for use in biological applications	[192]
Microbes based AuNPs				
Bacteria				
Klebsiella pneumoniae (MTCC-4030)	10-15nm, spherical	Antibacterial activity against Escherichia coli	-	[193]
Klebsiella pneumoniae	35-65nm, spherical		Medical and pharmaceutical applications	[194]
Bacillus stearothermophilus	5-30 nm, spherical, triangular		Detect toxin A (TOA) of Clostridium difficile based on an aptamer	[195]
Bacillus Subtilis	10-15nm, cubic	Antimicrobial agents in packaging applications	-	[196]
Fungi				
Penicillium citrinum	60-80 nm, spherical	Antioxidant activity in pharmaceutical and cosmetic industries	-	[197]



Algae					
Sargassum swartzii	35nm, spherical	Anticancer for HeLa cells	-		[198]
Cystoseira baccata (CB)	8.4 ± 2.2nm, spherical	Activity in colon cancer cells (cytotoxic effect against colon cancer cells)	-		[199]
Yeast					
Instant high-sugar dry yeasts	Dependent on PH, triangle, truncated triangle, hexagon Nano	-		Plasmonic Properties	[200]
Baker's yeast (Saccharomyces cerevisiae)	~5.0 ± 2.0nm, spherical	Anticancer evaluation against Ehrlich ascites carcinoma cells	-		[201]

**Table 3:** Overview of report on anti-inflammatory and angiogenic potential of nanogold [146].

Nanogold	Size (nm)	Biological system	Route of administration	Dose and Exposure time	Outcome	Mechanism of action
<b>Anti-inflammatory effect of nanogold</b>						
AuNP <sub>a</sub>	5,15, and 35	Male C57BL/6 mice at 4 wk	Intraperitoneal	100 nmol Au/kg, Acute (evaluation after 4 h)	Downregulation of cellular responses induced by IL-1 $\beta$	Decreased expression of HIF-1 $\alpha$ , and decreased levels of TNF- $\alpha$ and PI3 K in blood cells
AuNP <sub>a</sub>	10–50	Jurkat cell line	In-vitro	Au-Gal (containing 40 $\mu$ g of galectin-1 and 360 $\mu$ g of Au), Acute (evaluation after 48 h)	Amelioration of clinical symptoms of arthritis	Apoptosis of CD4 <sup>+</sup> T cells and reduced IFN- $\gamma$ , IL-4, IL-17 and TNF- $\alpha$ levels in the ankle joints
AuNP and PEG coated AuNP (both spherical)	13	CIA male Sprague-Dawley rats at 8 wk	Intra-articular	27 $\mu$ g AuNP, Acute (on d 7 after CIA; evaluation within the 9 subsequent d)	Attenuation of CIA	Decreased edema, levels of TNF- $\alpha$ , IL1 $\beta$ . and macrophage infiltration in the ankle joint
Galectin-1 AuNP (Au-Gal) (spherical) Spherical AuNP	13 and 50	CIA male Wistar rats at 10 wk	Intra-articular	20 $\mu$ l of 50 $\mu$ g Au/ml solution (13 nm; 1 $\mu$ g of Au) and 180 $\mu$ g Au/ml solution (50 nm; 3.76 $\mu$ g of Au), 5 times/wk, 12 injections (evaluation 14 d after CIA)	Inflammation, joint edema, and polyarthritis regression	Less pathomorphological changes in internal organs and higher levels of catalase <sup>b</sup>
Spherical AuNP	20	Male Wistar rats (250–350g) carragenan administered	Subcutaneous	10, 25 and 50 mg/kg AuNP, Acute (evaluation 4 h after	Reversal of carrageenan-induced inflammation	Decreased levels of TNF $\alpha$ , IL-1 $\beta$ , and myeloperoxidase; reversal of redox state b

in pleural  
cavity

administration  
of carragenan)

n and  
oxidative  
stress

### Anti-angiogenic effect of nanogold

Naked and positively charged AuNP <sup>a</sup>	5,10, and 20	HUVEC and NIH3T3 cells (preincubated with VEGF165 and HB-GF, respectively)	In vitro	1 nmol/L, 24 h	Antiangiogenic potential due to a direct inhibitory effect of AuNP to binding with the of pro angiogenic cytokines probably leading to conformational changes in the proteins structure	Inhibition of KDR phosphorylation and Ca <sup>2+</sup> release due to blockage of VEGF165 by AuNP, in a concentration dependent manner; no effect considering positively charged AuNP
Spherical AuNP and AuNP coated with PEG	15	Human umbilical vein endothelial cells (HUVEC)	In vitro	125 or 250 nM AuNP, 24/48 h	Anti-angiogenesis (endothelial cell proliferation, migration, and tube formation)	Inhibition of VEGF165-induced cell migration and tube formation by Akt pathway
Spherical AuNP	15	HUVEC cultured with conditioned medium (CM) from the HepG2	In vitro	1–4 nM AuNP, 24/48 h	Inhibition of HUVECs proliferation and migration induced by HepG2-CM; obvious pseudopodia, larger membrane particle sizes and much rougher	Reduced levels of active VEGF due to direct inhibition by AuNP; inhibition of actin filaments disruption by AuNP

Spherical AuNP	5	HUVEC (incubated with VEGF165)	In vitro	670,335, and 67 nM, 24 h	surface Antiangiogenic effect by binding to angiogenesis mediator	Inhibited VEGF receptor-2 phosphorylation, intracellular calcium release, cell migration and RhoA activation
Spherical diaminopyridinyl (DAP)derivatized heparin (HP) polysaccharides conjugated AuNP and glucose conjugated AuNP	10–25	Male mice (C57BL/6N Cr) at 6–8 wk injected with 0.1 µg FGF-2; 0.1 µg FGF-2 + 10 µg Au-DAPHP/Au glucose	Subcutaneous	10 µg Au DAPHP 10 µg Au glucose, 3injections (evaluation on d 12 after last injection)	More pronounced antiangiogenic and anticoagulant activity of Au-DAP-HP than Au glucose	Inhibition of basic fibroblast growth factor induced angiogenesis
Spherical biosynthesized Hamelia patens (HaP) leaf extract- Au NPs and AuNP coated with PEG	25–50	HUVEC	In vitro	5–20 µg/ml, 4/24 h	Pro-angiogenic activity of HP-AuNP x antiangiogenic potential of AuNP PEG coated	Formation of ROS and activation of p-Akt (for angiogenesis)

Table 4. AuNPs-Based Sensors [122].

S.No.	Types	Applications
1.	Colorimetric Sensing	a. Detection of metal ions b. Detection of small organic molecules d. Detection of proteins e. Detection of oligonucleotides f. Detection of anions
2.	Fluorescence-Based Sensors	a. Chemical Nose “Approach for the detection of cancerous and circulating tumor cells b. Proteins, Pathogens and Mammalian Cells c. Sensors based on FRET between QDs and AuNPs d. AuNP-based molecular beacons e. FRET-based detection of metal ions and small molecules
3.	Electrical And Electrochemical Sensors	a. AuNP-based electrochemical immunosensors b. AuNP-based electrochemical detection of oligonucleotides c. AuNP-based electrochemical enzymatic biosensors d. AuNPs as platforms for electrocatalytic and electrochemical sensors e. Electronic AuNP sensors employing macrocyclic complex at ion f. Vapor sensing
4.	Au NP-Based Surface Plasmon Resonance Sensors	a. Sensors based on AuNP plasmon scattering resonance b. AuNP-mediated SPR signal amplification c. Sensors based on change in LSPR AuNPs absorption of
5.	Surface Enhanced Raman Scattering (SERS)-Based Sensors	a. Detection of proteins b. Detection of oligonucleotides c. Detection of small organic molecules
6.	Au NPs in Quartz Crystal Microbalance-Based Sensors	a. Detection of proteins b. Detection of oligonucleotides
7.	Au NP-Based Bio-Barcode Assay Sensors	-

## 6. Toxicity aspects of AuNPs

Nanotoxicology refers to toxicological evaluation of structured nanomaterial and nanodevices. The need of investigation for this area became prominent after expansion of nanotechnology, which in past two decades has been used extensively in the area of medicine, pharmaceutical industry. Different nanoparticles may have different optical, structural and chemical properties and also have differential toxicity profiles [202]. Global demand of nanomaterials is increasing year by year, and it is related with penetration of NPs into the environment. As per the economic and social committee, monitoring the number of NPs in environment is a technical challenge. Toxicity of NPs would be specific to the

material type, shape, size and coatings. Due to their small size, nanoparticles have large surface area. These may result into better biological activity, due to their interactions with cells and its components. Nanoparticles favor the formation of oxidants upon exposure to day light, UV light or transition metals; thereby, destabilizing the balance between the production of reactive oxygen species (ROS) and biological system's ability to detoxify or repair the system. Manufactured nanomaterials may enter into the environment through intentional or unintentional releases for e.g. atmospheric emission and solid or liquid waste releasing from industries. The size and shape of AuNPs has been suggested to influence their uptake and cytotoxicity profile [203, 204].

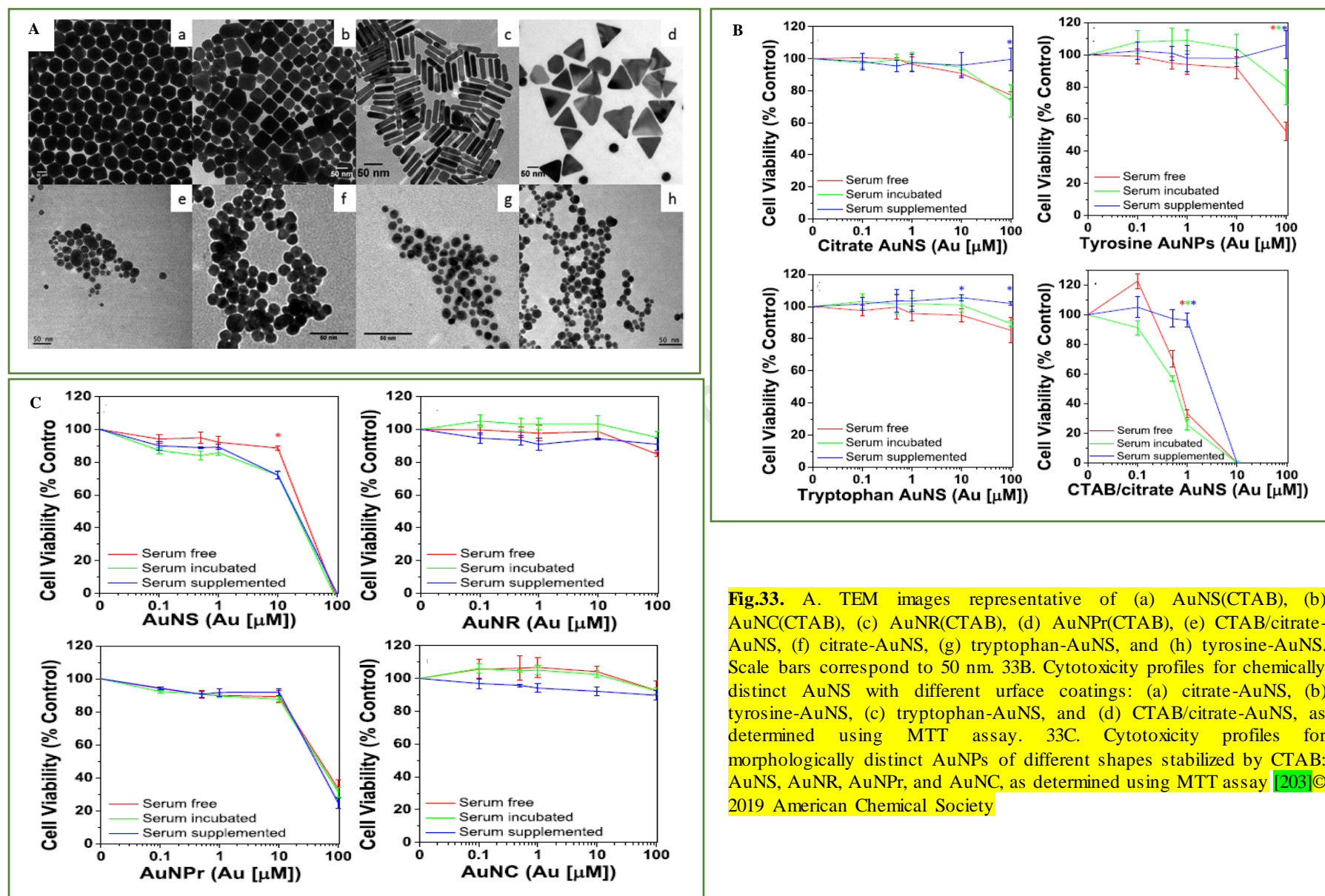
Connor et.al., investigated the uptake and toxicity of AuNPs in human leukemia cells. Results revealed that spherical AuNPs along with different surface modifiers are not toxic to human cells. Shape of AuNPs also influences the toxicity. Among all the shapes, AuNPs having rod shaped have been reported to show more toxicity as compared to spherical shape AuNPs [205]. Niidome et.al, reported that cetyl trimethyl ammonium bromide (CTAB) stabilized gold nanorods were toxic, as evaluated by MTT assay using HeLa cell line. Furthermore, it was found that toxicity can be decreased by coating AuNPs with polyethylene glycol (PEG), which reduces binding of biological molecules non-specifically to surfaces. Apart from shape, toxic potential of AuNPs rely on surface chemistry and charge [206]. Kim et al. [207], investigated the role of size and surface charge on toxicity of AuNPs using zebrafish embryonic model. This zebrafish model was exposed to 1.3 nm AuNPs and functionalized with cationic ligand. It was found toxic and caused lethality to embryos. Author reported that N,N,N-trimethylammonium ethanethiol (TMAT)-AuNPs caused significant increase in apoptotic cell death in the eye. Embryos exposed to TMAT-AuNPs exhibited hypo activity and inhibition of axonal growth. In order to understand the effect of size, shape, and capping ligand on toxicity of AuNPs, Carnovale et al [203] prepared eight different AuNPs. Four

AuNPs of different shapes viz. spherical (AuNS), cubical (AuNC), rod shaped (AuNR), and prismatic (AuNPr) particles were prepared using CTAB alone in order to understand the effect of shape on toxicity and cellular uptake. In order to understand the effect of size on toxicity and cellular uptake of AuNPs, citrate (Cit) stabilized CTAB-coated quasi-spherical AuNPS (CTAB/citrate-AuNS) were prepared. The size of CTAB/citrate-AuNS was smaller than CTAB-AuNS. In order to understand the effect of capping ligand another three AuNS were prepared. These were citrate capped-AuNS, tryptophan capped-AuNS (TRP-AuNS) and tyrosine capped AuNS (TYR-AuNS). The TEM images of all the eight AuNPs are shown in Fig. 33A. The study was carried out for 16 h using optical microscopy and 3-(4,5-dimethylthiazol-2-yl)-2,5-diphenyltetrazolium bromide (MTT) assays on PC-3 cells. The cytotoxicity profiles (Fig.33B) for AuNS with different coating in different serum conditions showed no significant difference between citrate AuNS and tyrosine-AuNS at lower doses at different serum conditions. However, the difference in cytotoxicity was observed at their higher doses. In contrast to that, tryptophan-AuNS significant toxicity profile at different serum conditions i.e. 10 and 100  $\mu\text{M}$  gold concentrations. For all the ligand capped AuNS, highest cell viability with no toxicity was found at 100  $\mu\text{M}$  gold concentration. In contrast to the above observations, significantly different behavior was noted for citrate-AuNS functionalized with CTAB (CTAB/citrate-AuNS). The tolerance was observed for PC-3 cells only at a dose of 1  $\mu\text{M}$  gold concentration. Above to this concentration, complete loss of cellular viability was observed. It is important to note that very little variation was observed in cellular toxicity for the four morphologically different AuNPs prepared and solely stabilized with CTAB (Fig.33C) as compared to the smaller spherical AuNPS stabilized using other reducing agents (Fig.33B). The results revealed that use of CTAB as capping agent superseded any potential effect caused by biological corona. This negligible influence of

serum proteins on the cytotoxicity of these AuNPs may be attributed to surfactant properties of CTAB.

Journal Pre-proof





The cellular uptake studies were also performed by Carnovale et al [203] for the same AuNPs, produced by different stabilizers (Figs. 34a, b) and using same stabilizer (CTAB) of different shapes (Figs.34c, d). It was observed that AuNPs were taken up in greater numbers [the mass of gold taken up per cell and average numbers of AuNPs (Figs.34a, c) and taken up by each cell (Figs.34b, d)] in serum free conditions as compared to serum supplemented media. No significant difference was observed between serum-free and serum pre-incubated conditions for citrate AuNS, tryptophan AuNS, CTAB/citrate AuNS, AuNC and AuNPr. Whereas, an intermediate uptake behavior was noted for tyrosine-AuNS and AuNS (CTAB). In terms of number of particles taken per cell, AuNR were most readily taken up, followed by AuNC, AuNS, and AuNPr. In contrast to this, the total gold accessible per cell was found highest for AuNS, followed by AuNC, AuNR, and AuNPr [203]. List of various in vivo and in vitro cytotoxicity studies of AuNPs are listed in Fig.35.

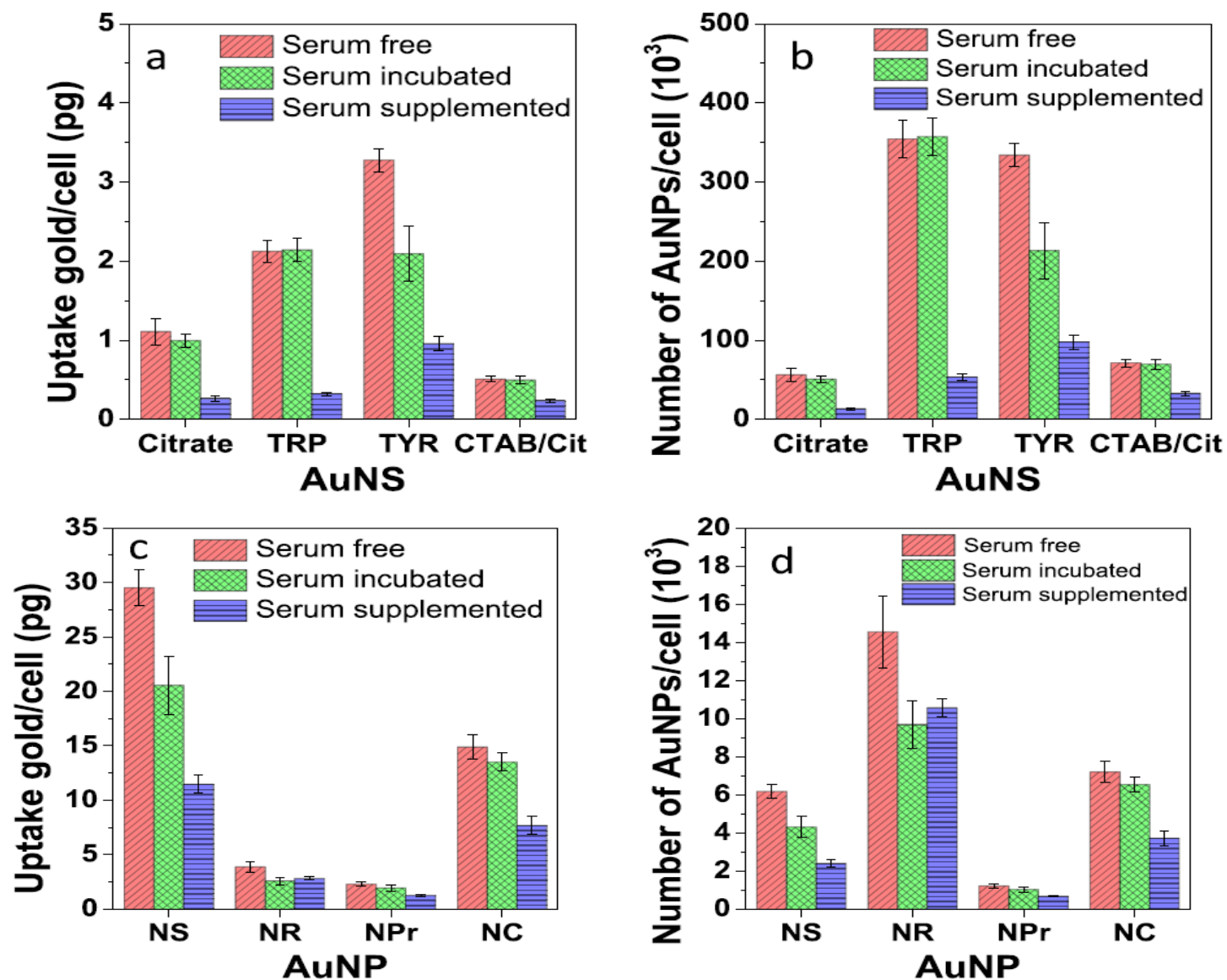


**Fig.34.** Cellular uptake of (a,b) AuNS produced by employing various chemical stabilizers and (c,d) various shaped AuNPs stabilized solely with CTAB under different serum conditions. Data are presented both as (a,c) uptake of gold in picograms per cell and (b,d) number of AuNPs taken up per cell. [203]© 2019 American Chemical Society.

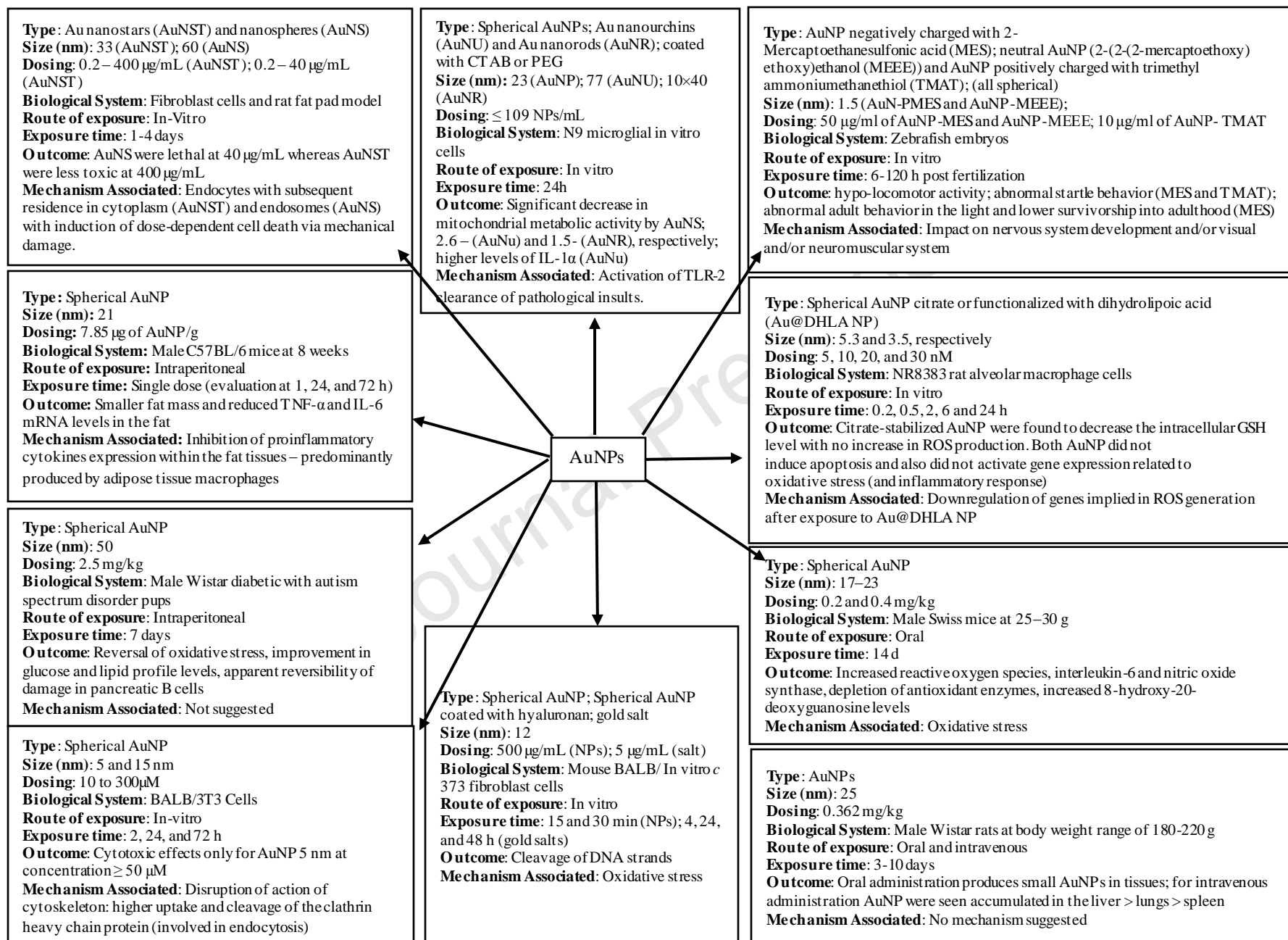


**Fig.35.** Toxicity of gold nanoparticles in respect to their size and shape [146, 208-217].

## 7. Conclusion

With day to day, increase in the burden of chronic diseases which is rapidly increasing worldwide, there is a need for modification of conventional treatment strategies. Nanotechnology has gained innumerable advancements in theranostic field using nanomedicine approaches. Gold being a costly biomaterial, gained attention by the researchers as potential theranostic for the treatment of various diseases such as cancer and rheumatoid arthritis. It is being used as potential nano-carrier (AuNPs) to target various drugs to their site of action. Despite having various biomedical applications of AuNPs, synthesis of stable NPs with desired size and charge is a consistent challenge. In the present review various synthetic, plant based and biological processes that are used to synthesize AuNPs along with their merits and limitations and different factors that affect shapes and size of AuNPs have been discussed. These include reaction conditions (temperature, time, pH, stirring speed), stoichiometry of reagents and addition of additives. Various advanced techniques that are used to characterize these AuNPs are also discussed. The role of AuNPs in biomedical applications and the effect of shape, size and capping ligand on their toxicity and cellular uptake are also highlighted. Taking all the aspects together, in order to make AuNPs as versatile nanomaterial for biomedical application it is important to understand the various factors that affect their size, shape and stability. A systematic understanding of these factors could offer better optimization of AuNPs and this will help in placing them to market potential theranostic for biomedical applications.

**Conflict of interest:** Declared none

## References

- [1] Shukla R, Bansal V, Chaudhary M, Basu A, Bhonde RR, Sastry M. Biocompatibility of gold nanoparticles and their endocytotic fate inside the cellular compartment: a microscopic overview. *Langmuir*. 2005;21(23):10644-54.
- [2] Judy JD, Unrine JM, Rao W, Wirick S, Bertsch PM. Bioavailability of gold nanomaterials to plants: importance of particle size and surface coating. *Environmental science & technology*. 2012;46(15):8467-74.
- [3] Zhou J, Ralston J, Sedev R, Beattie DA. Functionalized gold nanoparticles: synthesis, structure and colloid stability. *Journal of colloid and interface science*. 2009;331(2):251-62.
- [4] Cordeiro M, Ferreira Carlos F, Pedrosa P, Lopez A, Baptista P. Gold nanoparticles for diagnostics: advances towards points of care. *Diagnostics*. 2016;6(4):43.
- [5] Hall JB, Dobrovolskaia MA, Patri AK, McNeil SE. Characterization of nanoparticles for therapeutics. *Nanomedicine* 2007;2(6):789-803.
- [6] Boisselier E, Astruc D. Gold nanoparticles in nanomedicine: preparations, imaging, diagnostics, therapies and toxicity. *Chem Soc Rev* 2009;38(6):1759-82.
- [7] Ghosh P, Han G, De M, Kim CK, Rotello VM. Gold nanoparticles in delivery applications. *Adv Drug Deliv Rev* 2008;60(11):1307-15.
- [8] Chowdhury A, Kunjiappan S, Panneerselvam T, Somasundaram B, Bhattacharjee C. Nanotechnology and nanocarrier-based approaches on treatment of degenerative diseases. *Int Nano Lett* 2017;7(2):91-122.
- [9] Xia, Y.; Xiong, Y.; Lim, B.; Skrabalak, S.E. Shape-controlled synthesis of metal nanocrystals: simple chemistry meets complex physics? *Angew Chem Int Ed Engl* 2009;48:60-103.
- [10] Yeh Yi-C, Czeran B, Rotello VM. Gold Nanoparticles: Preparation, Properties, and Applications in Bionanotechnology. *Nanoscale* 2012;4(6):1871-80.
- [11] Huang X, El-Sayed IH, El-Sayed MA. Applications of gold nanorods for cancer imaging and photothermal therapy. *Methods Mol Biol* 2010;624:343-357.
- [12] Thambiraj S, Hema S, Ravi Shankaran D. Functionalized gold nanoparticles for drug delivery applications. *Materials Today: Proceedings*. 2018;5(8):16763-73.
- [13] Pal K, Al-Suraih F, Gonzalez-Rodriguez R, Dutta SK, Wang E, Kwak HS, et al. Multifaceted peptide assisted one-pot synthesis of gold nanoparticles for plectin-1 targeted gemcitabine delivery in pancreatic cancer. *Nanoscale*. 2017;9(40):15622-34.



- [14] Lopez N, Janssens TV, Clausen BS, Xu Y, Mavrikakis M, Bligaard T, et al. On the origin of the catalytic activity of gold nanoparticles for low-temperature CO oxidation. *J Catal* 2004;223(1):232-5.
- [15] Arvizo R, Bhattacharya R, Mukherjee P. Gold nanoparticles: Opportunities and Challenges in Nanomedicine. *Expert Opin Drug Deliv* 2010;7(6):753-763.
- [16] Goel R, Shah N, Visaria R, Paciotti GF, Bischof JC. Biodistribution of TNF- $\alpha$ -coated gold nanoparticles in an in vivo model system. *Nanomedicine*. 2009;4(4):401-10.
- [17] James LR, Xu ZQ, Sluyter R, Hawksworth EL, Kelso C, Lai B, et al. An investigation into the interactions of gold nanoparticles and anti-arthritis drugs with macrophages, and their reactivity towards thioredoxin reductase. *J Inorg biochem* 2015;142:28-38.
- [18] Arvizo R, Bhattacharya R, Mukherjee P. Gold NPs: opportunities and challenges in nanomedicine. *Expert Opin Drug Deliv* 2010;7(6):753-63.
- [19] Dykman L, Khlebtsov N. Gold nanoparticles in biomedical applications: recent advances and perspectives. *Chem Soc Rev* 2012;41(6):2256-82.
- [20] Jain PK, Lee KS, El-Sayed IH, El-Sayed MA. Calculated absorption and scattering properties of gold nanoparticles of different size, shape, and composition: applications in biological imaging and biomedicine. *J Phys Chem B* 2006;110(14):7238-48.
- [21] Daniel MC, Astruc D. Gold nanoparticles: assembly, supramolecular chemistry, quantum-size-related properties, and applications toward biology, catalysis, and nanotechnology. *Chem Rev* 2004;104(1):293-346.
- [22] Fernández JR, Perej-Juste J, de Abajo, FJG, Liz-Marzán LM. Seeded Growth of Submicron Au Colloids with Quadrupole Plasmon Resonance Modes. *Langmuir*. 2006;22(16):7007-10.
- [23] Ghosh SK, Pal T. Interparticle coupling effect on the surface plasmon resonance of gold nanoparticles: from theory to applications. *Chem Rev* 2007;107(11):4797-862.
- [24] El-Brollosy TA, Abdallah T, Mohamed MB, Abdallah S, Easawi K, Negm S, et al. Shape and size dependence of the surface plasmon resonance of gold nanoparticles studied by Photoacoustic technique. *Eur Phys J Spec Top* 2008;153(1):361-64.
- [25] Swierczewska M, Lee S, Chen X. The design and application of fluorophore-gold nanoparticle activatable probes. *Phys Chem Chem Phys* 2011;13(21):9929-41.
- [26] Jiang C, Zhao T, Yuan P, Gao N, Pan Y, Guan Z, et al. Two-photon induced photoluminescence and singlet oxygen generation from aggregated gold nanoparticles. *ACS Appl Mater Interfaces* 2013 May 30;5(11):4972-7.

- [27] Ahmed S, Ahmad M, Swami BL, Ikram S. A review on plants extract mediated synthesis of silver NPs for antimicrobial applications: a green expertise. *J Adv Res* 2016;7(1):17-28.
- [28] Turkevich J, Stevenson PC, Hillier J. A study of the nucleation and growth processes in the synthesis of colloidal gold. *Discuss Faraday Soc* 1951; 11:55-75.
- [29] Brust M, Walker M, Bethell D, Schiffrin DJ, Whyman R. Synthesis of thiol-derivatised gold nanoparticles in a two-phase liquid-liquid system. *J Chem Soc Chem Commun*. 1994;(7):801-2.
- [30] Kharissova OV, Dias HR, Kharisov BI, Pérez BO, Pérez VM. The greener synthesis of nanoparticles. *Trends Biotechnol* 2013;31(4):240-48.
- [31] Sharma N, Bhatt G, Kothiyal P. Gold NPs synthesis, properties, and forthcoming applications-A review. *Indian J Pharm Biol Res* 2015;3(2):13-27.
- [32] Hühn J, Carrillo-Carrion C, Soliman MG, Pfeiffer C, Valdeperez D, Masood A, et al. Selected standard protocols for the synthesis, phase transfer, and characterization of inorganic colloidal nanoparticles. *Chem Mater* 2016;29:399-461.
- [33] Frens G. Controlled nucleation for the regulation of the particle size in monodisperse gold suspensions. *Nat Phys Sci* 1973;241:20-24.
- [34] Ojea-Jiménez I, Bastús NG, Puentes V. Influence of the sequence of the reagents addition in the citrate-mediated synthesis of gold nanoparticles. *J Phys Chem C* 2011;115:15752-7.
- [35] Zhao P, Li N, Astruc D. State of the art in gold nanoparticle synthesis. *Coord Chem Rev* 2013;257:638-65.
- [36] Biju V. Chemical modifications and bioconjugate reactions of nanomaterials for sensing, imaging, drug delivery and therapy. *Chem Soc Rev* 2014;43:744-64.
- [37] Polte J. Fundamental growth principles of colloidal metal nanoparticles—a new perspective. *CrystEngComm* 2015;17:6809-30.
- [38] Piella J, Bastús NG, Puentes V. Size-Controlled Synthesis of Sub-10-nanometer Citrate-Stabilized Gold Nanoparticles and Related Optical Properties. *Chem Mater* 2016;28:1066-75.
- [39] Schulz F, Homolka T, Bastús NG, Puentes V, Weller H, Vossmeier T. Little adjustments significantly improve the Turkevich synthesis of gold nanoparticles. *Langmuir* 2014;30:10779-84.



- [40] Bastús NG, Comenge J, Puentes V. Kinetically controlled seeded growth synthesis of citrate-stabilized gold nanoparticles of up to 200 nm: size focusing versus Ostwald ripening. *Langmuir* 2011;27:11098-105.
- [41] Perala SRK, Kumar S. On the mechanism of metal nanoparticle synthesis in the Brust–Schiffrin method. *Langmuir* 2013;29:9863-73.
- [42] Brust M, Fink J, Bethell D, Schiffrin DJ, Kiely C. Synthesis and Reactions of Functionalised Gold Nanoparticles. *J Chem Soc Chem Commun* 1995 (16) 1655-1656.
- [43] Ziegler C, Eychmüller A. Seeded growth synthesis of uniform gold nanoparticles with diameters of 15– 300 nm. *J Phys Chem C* 2011;115:4502-6.
- [44] Jana NR, Gearheart L, Murphy CJ. Wet chemical synthesis of high aspect ratio cylindrical gold nanorods. *J Phys Chem B* 2001;105:4065-67.
- [45] Ye X, Jin L, Caglayan H, Chen J, Xing G, Zheng C, et al. Improved size-tunable synthesis of monodisperse gold nanorods through the use of aromatic additives. *ACS Nano* 2012;6:2804-17.
- [46] Nikoobakht B, El-Sayed MA. Preparation and growth mechanism of gold nanorods (NRs) using seed-mediated growth method. *Chem Mater* 2003;15:1957-62.
- [47] Ye X, Zheng C, Chen J, Gao Y, Murray CB. Using binary surfactant mixtures to simultaneously improve the dimensional tunability and monodispersity in the seeded growth of gold nanorods. *Nano Lett* 2013;13:765-71.
- [48] Iravani S. Green synthesis of metal nanoparticles using plants. *Green Chem* 2011;13:2638-50.
- [49] Vaseghi Z, Nematollahzadeh A, Tavakoli O. Green methods for the synthesis of metal nanoparticles using biogenic reducing agents: a review. *Rev Chem Eng* 2018;34:529-59.
- [50] Mukherjee S, Nethi SK, Patra CR. Green synthesized gold nanoparticles for future biomedical applications. *Particulate Technology for Delivery of Therapeutics*: Springer; 2017. p. 359-93.
- [51] Muralikrishna T, Pattanayak M, Nayak P. Green synthesis of gold nanoparticles using (Aloe vera) aqueous extract. *World J Nano Sci Technol* 2014;3:45-51.
- [52] Rajeshkumar S, Malarkodi C, Gnanajobitha G, Paulkumar K, Vanaja M, Kannan C, et al. Seaweed-mediated synthesis of gold nanoparticles using *Turbinaria conoides* and its characterization. *J Nanostructure Chem* 2013;3(44):1-7.

- [53] Sujitha MV, Kannan S. Green synthesis of gold nanoparticles using Citrus fruits (Citrus limon, Citrus reticulata and Citrus sinensis) aqueous extract and its characterization. *Spectrochim Acta A Mol Biomol Spectrosc* 2013;102:15-23.
- [54] Chandran K, Song S, Yun S-I. Effect of size and shape controlled biogenic synthesis of gold nanoparticles and their mode of interactions against food borne bacterial pathogens. *Arab. J. Chem* 2014. doi.org/10.1016/j.arabjc.2014.11.041
- [55] Xin Lee K, Shamel K, Miyake M, Kuwano N, Khairudin BA, Bahiyah N, et al. Green synthesis of gold nanoparticles using aqueous extract of *Garcinia mangostana* fruit peels. *Journal of Nanomaterials*. 2016. doi.org/10.1155/2016/8489094
- [56] Yasmin A, Ramesh K, Rajeshkumar S. Optimization and stabilization of gold nanoparticles by using herbal plant extract with microwave heating. *Nano Converg.* 2014;1(12):1-7. Doi.org/10.1186/s40580-014-0012-8
- [57] Mukherjee S, Sushma V, Patra S, Barui AK, Bhadra MP, Sreedhar B, et al. Green chemistry approach for the synthesis and stabilization of biocompatible gold nanoparticles and their potential applications in cancer therapy. *Nanotechnology* 2012;23(45):455103. doi.org/10.1088/0957-4484/23/45/455103
- [58] Das RK, Gogoi N, Bora U. Green synthesis of gold nanoparticles using *Nyctanthes arbortristis* flower extract. *Bioprocess Biosyst Eng* 2011;34(5):615-9.
- [59] Sadeghi B. *Zizyphus mauritiana* extract-mediated green and rapid synthesis of gold nanoparticles and its antibacterial activity. *J Nanostructure Chem* 2015;5(3):265-73.
- [60] Dykman LA, Khlebtsov NG. Methods for chemical synthesis of colloidal gold. *Russ Chem Rev* 2019;88(3). doi.org/10.1070/RCR4843
- [61] Tan Y, Dai X, Li Y, Zhu D. Preparation of gold, platinum, palladium and silver nanoparticles by the reduction of their salts with a weak reductant–potassium bitartrate. *J Mater Chem* 2003;13(5):1069-75.
- [62] Jeon S-H, Xu P, Zhang B, Mack NH, Tsai H, Chiang LY, et al. Polymer-assisted preparation of metal nanoparticles with controlled size and morphology. *J Mater Chem* 2011;21:2550–4. doi:10.1039/C0JM02340J.
- [63] Sakura T, Takahashi T, Kataoka K, Nagasaki Y. One-pot preparation of mono-dispersed and physiologically stabilized gold colloid. *Colloid Polym Sci* 2005;284(1):97-101.
- [64] Sato S, Toda K, Oniki S. Kinetic study on the formation of colloidal gold in the presence of acetylenic glycol nonionic surfactant. *J Colloid Interface Sci* 1999;218(1):504-10.

- [65] Hussain I, Brust M, Papworth AJ, Cooper AI. Preparation of acrylate-stabilized gold and silver hydrosols and gold– polymer composite films. *Langmuir* 2003;19(11):4831-35.
- [66] Njoki PN, Luo J, Kamundi MM, Lim S, Zhong C-J. Aggregative growth in the size-controlled growth of monodispersed gold nanoparticles. *Langmuir* 2010;26(16):13622-9.
- [67] Aslam M, Fu L, Su M, Vijayamohan K, Dravid VP. Novel one-step synthesis of amine-stabilized aqueous colloidal gold nanoparticles. *J Mater Chem* 2004;14:1795-7.
- [68] Polavarapu L, Xu Q-H. A simple method for large scale synthesis of highly monodisperse gold nanoparticles at room temperature and their electron relaxation properties. *Nanotechnology* 2009;20(18):185606. doi.org/10.1088/0957-4484/20/18/185606
- [69] Sakai T, Alexandridis P. Size- and shape-controlled synthesis of colloidal gold through autoreduction of the auric cation by poly (ethylene oxide)–poly (propylene oxide) block copolymers in aqueous solutions at ambient conditions. *Nanotechnology* 2005;16(7):S344-53.
- [70] Richardson MJ, Johnston JH, Borrmann T. Monomeric and polymeric amines as dual reductants/stabilisers for the synthesis of gold nanocrystals: A mechanistic study. *Eur J Inorg Chem* 2006;2006(13):2618-23.
- [71] Sardar R, Park J-W, Shumaker-Parry JS. Polymer-induced synthesis of stable gold and silver nanoparticles and subsequent ligand exchange in water. *Langmuir* 2007;23(23):11883-89.
- [72] Premkumar T, Kim D, Lee K, Geckeler KE. A facile and efficient “one-step” synthesis of Au<sub>0</sub> with tunable size. *Gold Bull.* 2007;40(4):321-27.
- [73] Peveler WJ, Parkin IP. Rapid synthesis of gold nanostructures with cyclic and linear ketones. *RSC Adv* 2013;3(44):21919-27.
- [74] Sanna V, Pala N, Dessì G, Manconi P, Mariani A, Dedola S, et al. Single-step green synthesis and characterization of gold-conjugated polyphenol nanoparticles with antioxidant and biological activities. *Int J Nanomedicine.* 2014;9:4935-51
- [75] Han G, Wu S, Wang J, Geng X, Liu G. Poly-L-lysine mediated synthesis of gold nanoparticles and biological effects. *J Nanosci Nanotechnol* 2015;15(9):6503-8.
- [76] Alinejad Z, Khakzad F, Mahdavian AR. Efficient approach to in-situ preparation of anisotropic and assemblable gold nanoparticles mediated by stimuli-responsive PDMAEMA. *Eur Polym J* 2018;104:106-14.

- [77] Porta F, Krpetić Ze, Prati L, Gaiassi A, Scari G. Gold-ligand interaction studies of water-soluble aminoalcohol capped gold nanoparticles by NMR. *Langmuir* 2008;24(14):7061-64.
- [78] Nalawade P, Mukherjee T, Kapoor S. Green synthesis of gold nanoparticles using glycerol as a reducing agent, *Adv Nanopart* 2013;2:78-86.
- [79] Larm NE, Essner JB, Pokpas K, Canon JA, Jahed N, Iwuoha EI, et al. Room-temperature turkevich method: formation of gold nanoparticles at the speed of mixing using cyclic oxocarbon reducing agents. *J Phys Chem C* 2018;122(9):5105-18.
- [80] Goswami N, Saha R, Pal SK. Protein-assisted synthesis route of metal nanoparticles: exploration of key chemistry of the biomolecule. *J Nanopart Res* 2011;13:5485. Doi.org/10.1007/s11051-011-0536-3
- [81] Njagi JI, Goia DV. Nitritotriacetic acid: A novel reducing agent for synthesizing colloidal gold. *J Colloid Interface Sci* 2014;421:27-32.
- [82] Baymiller M, Huang F, Rogelj S. Rapid one-step synthesis of gold nanoparticles using the ubiquitous coenzyme NADH. *Matters* 2017. Doi.org/10.19185/matters.201705000007
- [83] Esumi K, Takei N, Yoshimura T. Antioxidant-potentiality of gold–chitosan nanocomposites. *Colloids Surf B Biointerfaces* 2003;32(2):117-23.
- [84] Chamundeeswari M, Sobhana SL, Jacob JP, Kumar MG, Devi MP, Sastry TP, et al. Preparation, characterization and evaluation of a biopolymeric gold nanocomposite with antimicrobial activity. *Biotechnol Appl Biochem* 2010;55(1):29-35.
- [85] Bhumkar DR, Joshi HM, Sastry M, Pokharkar VB. Chitosan reduced gold nanoparticles as novel carriers for transmucosal delivery of insulin. *Pharm Res* 2007;24(8):1415-26.
- [86] Krpetic Ze, Nativo P, Porta F, Brust M. A multidentate peptide for stabilization and facile bioconjugation of gold nanoparticles. *Bioconjug Chem* 2009;20(3):619-24.
- [87] Pal A. Preparation of ultrafine colloidal gold particles using a bioactive molecule. *J Nanopart Res* 2004;6(1):27-34.
- [88] Li G, Li D, Zhang L, Zhai J, Wang E. One-step synthesis of folic acid protected gold nanoparticles and their receptor-mediated intracellular uptake. *Chem Eur J* 2009;15(38):9868-73.
- [89] Rai A, Prabhune A, Perry CC. Antibiotic mediated synthesis of gold nanoparticles with potent antimicrobial activity and their application in antimicrobial coatings. *J Mater Chem* 2010;20(32):6789-98.

- [90] Cho H-J, Oh J, Choo M-K, Ha J-I, Park Y, Maeng H-J. Chondroitin sulfate-capped gold nanoparticles for the oral delivery of insulin. *Int J Biol Macromol* 2014;63:15-20.
- [91] Baranwal A, Mahato K, Srivastava A, Maurya PK, Chandra P. Phytofabricated metallic nanoparticles and their clinical applications. *RSC Adv* 2016;6(107):105996-6010.
- [92] Harkness KM, Cliffel DE, McLean JA. Characterization of thiolate-protected gold nanoparticles by mass spectrometry. *Analyst* 2010;135(5):868-74.
- [93] Amendola V, Pilot R, Frascioni M, Marago OM, Iati MA. Surface plasmon resonance in gold nanoparticles: a review. *J Phys Condens Matter* 2017;29:203002. doi.org/10.1088/1361-648X/aa60f3
- [94] Zuber A, Purdey M, Schartner E, Forbes C, van der Hoek B, Giles D, et al. Detection of gold nanoparticles with different sizes using absorption and fluorescence based method. *Sens Actuators B Chem* 2016;227:117-27.
- [95] Zeng S, Yu X, Law W-C, Zhang Y, Hu R, Dinh X-Q, et al. Size dependence of Au NP-enhanced surface plasmon resonance based on differential phase measurement. *Sens Actuators B Chem*. 2013;176:1128-33.
- [96] Xia Y, Halas NJ. Shape-controlled synthesis and surface plasmonic properties of metallic nanostructures. *MRS Bull* 2005;30(5):338-48.
- [97] Zijlstra P, Chon JW, Gu M. Five-dimensional optical recording mediated by surface plasmons in gold nanorods. *Nature*. 2009;459:410-13.
- [98] Bonaccorso F, Zerbetto M, Ferrari AC, Amendola V. Sorting nanoparticles by centrifugal fields in clean media. *J Phys Chem C* 2013;117(25):13217-29.
- [99] Park J, Kang H, Kim YH, Lee S-W, Lee TG, Wi J-S. Physically-synthesized gold nanoparticles containing multiple nanopores for enhanced photothermal conversion and photoacoustic imaging. *Nanoscale* 2016;8(24):15514-20.
- [100] Wang H, Brandl DW, Nordlander P, Halas NJ. Plasmonic nanostructures: artificial molecules. *Acc Chem Res* 2007;40(1):53-62.
- [101] Poletti A, Fracasso G, Conti G, Pilot R, Amendola V. Laser generated gold nanocorals with broadband plasmon absorption for photothermal applications. *Nanoscale* 2015;7(32):13702-14.
- [102] Soares L, Csáki A, Jatschka J, Fritzsche W, Flores O, Franco R, et al. Localized surface plasmon resonance (LSPR) biosensing using gold nanotriangles: detection of DNA hybridization events at room temperature. *Analyst* 2014;139(19):4964-73.

- [103] Barbosa S, Agrawal A, Rodríguez-Lorenzo L, Pastoriza-Santos I, Alvarez-Puebla R A, Kornowski A, et al. Tuning Size and Sensing Properties in Colloidal Gold Nanostars. *Langmuir* 2010;26(18):14943-50.
- [104] Luan J, Liu K, Tadepalli S, Jiang Q, Morrissey J J, Kharasch E D, et al. PEGylated Artificial Antibodies: Plasmonic Biosensors with Improved Selectivity. *ACS Appl Mater Interfaces* 2016;8(36):23509-16.
- [105] Wu H-L, Kuo C-H, Huang MH. Seed-mediated synthesis of gold nanocrystals with systematic shape evolution from cubic to trisoctahedral and rhombic dodecahedral structures. *Langmuir* 2010;26(14):12307-313.
- [106] Wang C, Luan J, Tadepalli S, Liu K-K, Morrissey JJ, Kharasch ED, et al. Silk-encapsulated plasmonic biochips with enhanced thermal stability. *ACS Appl Mater Interfaces*. 2016;8(40):26493-500.
- [107] Gomes Silva C, Juárez R, Marino T, Molinari R, García H. Influence of excitation wavelength (UV or visible light) on the photocatalytic activity of titania containing gold nanoparticles for the generation of hydrogen or oxygen from water. *J Am Chem Soc* 2010;133(3):595-602.
- [108] Jans H, Liu X, Austin L, Maes G, Huo Q. Dynamic light scattering as a powerful tool for gold nanoparticle bioconjugation and biomolecular binding studies. *Anal Chem* 2009;81(22):9425-32.
- [109] Guo C, Yarger JL. Characterizing gold nanoparticles by NMR spectroscopy. *Magn Reson Chem* 2018;56(11):1074-82.
- [110] Lopez-Sanz S, Bernardo FJG, Martín-Doimeadios RCR, Rios A. Analytical metrology for nanomaterials: Present achievements and future challenges. *Anal Chim Acta* 2019;1059:1-15.
- [111] Lapresta-Fernández A, Salinas-Castillo A, Anderson De La Llana S, Costa-Fernández JM, Domínguez-Meister S, Cecchini R, et al. A general perspective of the characterization and quantification of nanoparticles: imaging, spectroscopic, and separation techniques. *CRIT REV SOLID STATE*. 2014;39(6):423-58.
- [112] Wang ZL. Characterization of nanophase materials. *Part Part Syst Charact*. 2001;18(3):142-65.
- [113] Annamalai A, Christina V, Sudha D, Kalpana M, Lakshmi P. Green synthesis, characterization and antimicrobial activity of Au NPs using *Euphorbia hirta* L. leaf extract. *Colloids Surf B Biointerfaces* 2013;108:60-5.

- [114] Rao A, Schoenenberger M, Gnecco E, Glatzel T, Meyer E, Brändlin D, et al. Characterization of nanoparticles using atomic force microscopy. *J Phys Conf Ser* 2007;61(61):971.
- [115] Darwich S, Mougín K, Rao A, Gnecco E, Jayaraman S, Haidara H. Manipulation of gold colloidal nanoparticles with atomic force microscopy in dynamic mode: influence of particle–substrate chemistry and morphology, and of operating conditions. *Beilstein J Nanotechnol* 2011;2:85-98.
- [116] Trapiella-Alfonso L, Costa-Fernández JM, Encinar JR, Pereiro R, Sanz-Medel A. Chapter 8 - Mass Spectrometry for the Characterization of Gold Nanoparticles. In: Valcárcel M, López-Lorente ÁI, (editors). *Comprehensive Analytical Chemistry*. Vol. 66: Elsevier; 2014. p. 329-56.
- [117] Yan W, Petkov V, Mahurin SM, Overbury SH, Dai S. Powder XRD analysis and catalysis characterization of ultra-small gold nanoparticles deposited on titania-modified SBA-15. *Catal Commun* 2005;6(6):404-8.
- [118] Vasanthi Bathrinarayanan P, Thangavelu D, Muthukumarasamy VK, Munusamy C, Gurunathan B. Biological synthesis and characterization of intracellular gold nanoparticles using biomass of *Aspergillus fumigatus*. *Bull Mater Sci* 2013;36(7):1201-5.
- [119] Wang Y, Black KC, Luehmann H, Li W, Zhang Y, Cai X, et al. Comparison study of gold nanohexapods, nanorods, and nanocages for photothermal cancer treatment. *ACS Nano* 2013;7(3):2068-77.
- [120] Wang J, Zhu G, You M, Song E, Shukoor MI, Zhang K, et al. Assembly of aptamer switch probes and photosensitizer on gold nanorods for targeted photothermal and photodynamic cancer therapy. *ACS Nano* 2012;6(6):5070-7.
- [121] Luo P, Liu Y, Xia Y, Xu H, Xie G. Aptamer biosensor for sensitive detection of toxin A of *Clostridium difficile* using gold nanoparticles synthesized by *Bacillus stearothermophilus*. *Biosens Bioelectron* 2014;54:217-21.
- [122] Elahi N, Kamali M, Baghersad MH. Recent biomedical applications of gold nanoparticles: A review. *Talanta* 2018;184:537-56.
- [123] Lu X, Dong X, Zhang K, Han X, Fang X, Zhang Y. A gold nanorods-based fluorescent biosensor for the detection of hepatitis B virus DNA based on fluorescence resonance energy transfer. *Analyst* 2013;138(2):642-50.
- [124] Lohse SE, Murphy CJ. The Quest for Shape Control: A History of Gold Nanorod Synthesis. *Chem Mater* 2013;25(8):1250-61.



- [125] Liu J, Detrembleur C, De Pauw-Gillet MC, Mornet S, Jérôme C, Duguet E. Gold nanorods coated with mesoporous silica shell as drug delivery system for remote near infrared light activated release and potential phototherapy. *Small* 2015;11(19):2323-32.
- [126] Perrault SD, Walkey C, Jennings T, Fischer HC, Chan WC. Mediating tumor targeting efficiency of nanoparticles through design. *Nano Lett* 2009;9(5):1909-15.
- [127] Kennedy LC, Bear AS, Young JK, Lewinski NA, Kim J, Foster AE, et al. T cells enhance gold nanoparticle delivery to tumors in vivo. *Nanoscale Res Lett* 2011;6(1):283. doi: 10.1186/1556-276X-6-283.
- [128] Liu H, Lian T, Liu Y, Hong Y, Sun D, Li Q. Plant-mediated synthesis of Au nanoparticles: separation and identification of active biomolecule in the water extract of *Cacumen Platycladi*. *Ind Eng Chem Res* 2017;56(18):5262-70.
- [129] Li X, Zhou H, Yang L, Du G, Pai-Panandiker AS, Huang X, et al. Enhancement of cell recognition in vitro by dual-ligand cancer targeting gold nanoparticles. *Biomaterials* 2011;32(10):2540-5.
- [130] Van de Broek B, Devoogdt N, D'Hollander A, Gijs H, Jans K, Lagae L, et al. Specific Cell Targeting with Nanobody Conjugated Branched Gold Nanoparticles for Photothermal Therapy. *ACS Nano* 2011;5(6):4319-28.
- [131] McMahon KM, Mutharasan RK, Tripathy S, Veliceasa D, Bobeica M, Shumaker DK, et al. Biomimetic high density lipoprotein nanoparticles for nucleic acid delivery. *Nano Lett* 2011;11(3):1208-14.
- [132] Brown SD, Nativo P, Smith J-A, Stirling D, Edwards PR, Venugopal B, et al. Gold nanoparticles for the improved anticancer drug delivery of the active component of oxaliplatin. *J Am Chem Soc* 2010;132(13):4678-84.
- [133] Narang J, Malhotra N, Singh G, Pundir C. Electrochemical impedimetric detection of anti-HIV drug taking gold nanorods as a sensing interface. *Biosens Bioelectron* 2015;66:332-7.
- [134] Rosi NL, Giljohann DA, Thaxton CS, Lytton-Jean AK, Han MS, Mirkin CA. Oligonucleotide-modified gold nanoparticles for intracellular gene regulation. *Science* 2006;312(5776):1027-30.
- [135] Giljohann DA, Seferos DS, Prigodich AE, Patel PC, Mirkin CA. Gene regulation with polyvalent siRNA–nanoparticle conjugates. *J Am Chem Soc* 2009;131(6):2072-3.
- [136] Ghosh P, Kim C, Han G, Forbes N, Rotello V. Efficient gene delivery vectors by tuning the surface charge density of amino acid-functionalized gold nanoparticles. *ACS Nano* 2008;2(11):2213–18.



- [137] Kumar A, Boruah B M, Liang X-J. Gold Nanoparticles: Promising Nanomaterials for the Diagnosis of Cancer and HIV/AIDS. *J Nanomater* 2011 doi.org/10.1155/2011/202187
- [138] Cheng Y, Meyers JD, Broome A-M, Kenney ME, Basilion JP, Burda C. Deep penetration of a PDT drug into tumors by noncovalent drug-gold nanoparticle conjugates. *J Am Chem Soc* 2011;133(8):2583-91.
- [139] Hong R, Han G, Fernández JM, Kim B-j, Forbes NS, Rotello VM. Glutathione-mediated delivery and release using monolayer protected nanoparticle carriers. *J Am Chem Soc* 2006;128(4):1078-9.
- [140] Nakanishi J, Nakayama H, Shimizu T, Ishida H, Kikuchi Y, Yamaguchi K, et al. Light-regulated activation of cellular signaling by gold nanoparticles that capture and release amines. *J Am Chem Soc* 2009;131(11):3822-23.
- [141] Podsiadlo P, Sinani VA, Bahng JH, Kam NWS, Lee J, Kotov NA. Gold nanoparticles enhance the anti-leukemia action of a 6-mercaptopurine chemotherapeutic agent. *Langmuir* 2008;24(2):568-74.
- [142] Kim B, Han G, Toley BJ, Kim C-k, Rotello VM, Forbes NS. Tuning payload delivery in tumour cylindroids using gold nanoparticles. *Nat Nanotechnol* 2010;5:465-72
- [143] Agasti SS, Chompoosor A, You C-C, Ghosh P, Kim CK, Rotello VM. Photoregulated release of caged anticancer drugs from gold nanoparticles. *J Am Chem Soc* 2009;131(16):5728-9.
- [144] Saito G, Swanson JA, Lee K D. Drug delivery strategy utilizing conjugation via reversible disulfide linkages: role and site of cellular reducing activities. *Adv Drug Deliv Rev* 2003;55(2):199-215.
- [145] Wang F, Wang Y C, Dou S, Xiong M H, Sun T M, Wang J. Doxorubicin-tethered responsive gold nanoparticles facilitate intracellular drug delivery for overcoming multidrug resistance in cancer cells. *ACS Nano* 2011;5(5):3679-92.
- [146] Hornos Carneiro MF, Barbosa Jr F. Gold nanoparticles: A critical review of therapeutic applications and toxicological aspects. *J Toxicol Environ Health B Crit Rev* 2016;19(3-4):129-48.
- [147] Yeo ELL, Joshua U, Cheah J, Neo DJH, Goh WI, Kanchanawong P, et al. Exploiting the protein corona around gold nanorods for low-dose combined photothermal and photodynamic therapy. *J Mater Chem B* 2017;5(2):254-68.
- [148] Thaxton CS, Elghanian R, Thomas AD, Stoeva SI, Lee J-S, Smith ND, et al. Nanoparticle-based bio-barcode assay redefines “undetectable” PSA and biochemical

- recurrence after radical prostatectomy. *Proc Natl Acad Sci U S A* 2009;106(44):18437-42.
- [149] Gao Z, Deng K, Wang X-D, Miró M, Tang D. High-Resolution Colorimetric Assay for Rapid Visual Readout of Phosphatase Activity Based on Gold/Silver Core/Shell Nanorod. *ACS Appl Mater Interfaces* 2014;6(20):18243-50.
- [150] Aldewachi H, Chalati T, Woodroffe M, Bricklebank N, Sharrack B, Gardiner P. Gold nanoparticle-based colorimetric biosensors. *Nanoscale* 2018;10(1):18-33.
- [151] Zeng S, Yong K-T, Roy I, Dinh X-Q, Yu X, Luan F. A review on functionalized gold nanoparticles for biosensing applications. *Plasmonics* 2011;6:491. [Doi .org/10.1007/s11468-011-9228-1](https://doi.org/10.1007/s11468-011-9228-1)
- [152] Yuan F, Chen H, Xu J, Zhang Y, Wu Y, Wang L. Aptamer-based luminescence energy transfer from near-infrared-to-near-infrared upconverting nanoparticles to gold nanorods and its application for the detection of thrombin. *Chemistry* 2014;20(10):2888-94.
- [153] Li N, Niu D, Jia X, He J, Jiang Y, Gu J, et al. Multiple gold nanorods@hierarchically porous silica nanospheres for efficient multi-drug delivery and photothermal therapy. *J Mater Chem B* 2017;5(8):1642-49.
- [154] Wu Y, Ali MRK, Chen K, Fang N, El-Sayed MA. Gold nanoparticles in biological optical imaging. *Nano Today* 2019;24:120-40.
- [155] Moriggi L, Cannizzo C, Dumas E, Mayer CR, Ulianov A, Helm L. Gold Nanoparticles Functionalized with Gadolinium Chelates as High-Relaxivity MRI Contrast Agents. *J Am Chem Soc* 2009;131(31):10828-89.
- [156] Cho S-J, Jarrett BR, Louie AY, Kauzlarich SM. Gold-coated iron nanoparticles: a novel magnetic resonance agent for T1 and T2 weighted imaging. *Nanotechnology* 2006;17(3):640. [doi.org/10.1088/0957-4484/17/3/004](https://doi.org/10.1088/0957-4484/17/3/004)
- [157] Md N-Sk, Kim H-K, Park J-A, Chang Y-M, Kim T-J. Gold Nanoparticles Coated with Gd-Chelate as a Potential CT/MRI Bimodal Contrast Agent. *Bull Korean Chem Soc* 2010;31(5):1177-81.
- [158] He H, Xie C, Ren J. Nonbleaching Fluorescence of Gold Nanoparticles and Its Applications in Cancer Cell Imaging. *Anal Chem* 2008;80(15):5951-57.
- [159] Lee H, Lee K, Kim I-K, Park TG. Fluorescent Gold Nanoprobe Sensitive to Intracellular Reactive Oxygen Species. *Adv Funct Mater* 2009;19(12):1884-90.

- [160] Coto-García AM, Sotelo-González E, Fernández-Argüelles MT, Pereiro R, Costa-Fernández JM, Sanz-Medel A. Nanoparticles as fluorescent labels for optical imaging and sensing in genomics and proteomics. *Anal Bioanal Chem* 2011;399(1):29-42.
- [161] Lee S, Cha E-J, Park K, Lee S-Y, Hong J-K, Sun I-C, et al. A Near-Infrared-Fluorescence-Quenched Gold-Nanoparticle Imaging Probe for In Vivo Drug Screening and Protease Activity Determination. *Angew Chem Int Ed Engl* 2008;47(15):2804-7.
- [162] Baptista P, Pereira E, Eaton P, Doria G, Miranda A, Gomes I, et al. Gold nanoparticles for the development of clinical diagnosis methods. *Anal Bioanal Chem* 2008;391(3):943-50.
- [163] Rahman M, Abd-El-Barr M, Mack V, Tkaczyk T, Sokolov K, Richards-Kortum R, et al. Optical imaging of cervical pre-cancers with structured illumination: An integrated approach. *Gynecol Oncol* 2005;99(3-1):S112-S5.
- [164] Kah JC, Kho KW, Lee CG, James C, Sheppard R, Shen ZX, et al. Early diagnosis of oral cancer based on the surface plasmon resonance of gold nanoparticles. *Int J Nanomedicine* 2007;2(4):785-98.
- [165] Wang X, Qian X, Beitler JJ, Chen ZG, Khuri FR, Lewis MM, et al. Detection of Circulating Tumor Cells in Human Peripheral Blood Using Surface-Enhanced Raman Scattering Nanoparticles. *Cancer Res* 2011;71(5):1526-32.
- [166] Rosman C, Pierrat S, Henkel A, Tarantola M, Schneider D, Sunnick E, et al. A New Approach to Assess Gold Nanoparticle Uptake by Mammalian Cells: Combining Optical Dark-Field and Transmission Electron Microscopy. *Small* 2012;8(23):3683-90.
- [167] Liu M, Li Q, Liang L, Li J, Wang K, Li J, et al. Real-time visualization of clustering and intracellular transport of gold nanoparticles by correlative imaging. *Nat Commun* 2017;8:15646. doi.org/10.1038/ncomms15646
- [168] Nan X, Sims PA, Xie XS. Organelle tracking in a living cell with microsecond time resolution and nanometer spatial precision. *Chemphyschem* 2008;9(5):707-12.
- [169] Qian W, Huang X, Kang B, El-Sayed MA. Dark-field light scattering imaging of living cancer cell component from birth through division using bioconjugated gold nanoprobe. *J Biomed Opt* 2010;15(4):046025. doi.org/10.1117/1.3477179
- [170] Baron R, Zayats M, Willner I. Dopamine-, L-DOPA-, adrenaline-, and noradrenaline-induced growth of Au nanoparticles: assays for the detection of neurotransmitters and of tyrosinase activity. *Anal Chem* 2005;77(6):1566-71.

- [171] Wan X-Y, Zheng L-L, Gao P-F, Yang X-X, Li C-M, Li YF, et al. Real-time light scattering tracking of gold nanoparticles-bioconjugated respiratory syncytial virus infecting HEP-2 cells. *Scientific reports*. 2014;4. doi.org/10.1038/srep04529
- [172] Terentyuk G, Panfilova E, Khanadeev V, Chumakov D, Genina E, Bashkatov A, et al. Gold nanorods with a hematoporphyrin-loaded silica shell for dual-modality photodynamic and photothermal treatment of tumors in vivo. *Nano Res* 2014;7(3):325-37.
- [173] Kneipp J, Kneipp H, Wittig B, Kneipp K. One-and two-photon excited optical pH probing for cells using surface-enhanced Raman and hyper-Raman nanosensors. *Nano Lett* 2007;7(9):2819-23.
- [174] Davidi ES, Dreifuss T, Motiei M, Shai E, Bragilovski D, Lubimov L, et al. Cisplatin-conjugated gold nanoparticles as a theranostic agent for head and neck cancer. *Head Neck*. 2018;40(1):70-78.
- [175] Paciotti GF, Myer L, Weinreich D, Goia D, Pavel N, McLaughlin RE, et al. Colloidal gold: a novel nanoparticle vector for tumor directed drug delivery. *Drug Deliv* 2004;11(3):169-83.
- [176] Eghtedari M, Liopo AV, Copland JA, Oraevsky AA, Motamedi M. Engineering of hetero-functional gold nanorods for the in vivo molecular targeting of breast cancer cells. *Nano Lett*. 2008;9(1):287-91.
- [177] Ayala G, de Oliveira Vercik LC, Menezes TAV, Vercik A. A simple and green method for synthesis of Ag and Au nanoparticles using biopolymers and sugars as reducing agent. *MRS Online Proceedings Library Archive*. 2012;1386. DOI: 10.1557/opl.2012.645
- [178] Kim K, Oh KS, Park DY, Lee JY, Lee BS, San Kim I, et al. Doxorubicin/gold-loaded core/shell nanoparticles for combination therapy to treat cancer through the enhanced tumor targeting. *J Control Release* 2016;228:141-49.
- [179] Zhang N, Xu X, Zhang X, Qu D, Xue L, Mo R, et al. Nanocomposite hydrogel incorporating gold nanorods and paclitaxel-loaded chitosan micelles for combination photothermal-chemotherapy. *Int J Pharm* 2016;497(1-2):210-21.
- [180] Ghorbani M, Hamishehkar H. Redox and pH-responsive gold nanoparticles as a new platform for simultaneous triple anti-cancer drugs targeting. *Int J Pharm* 2017;520(1-2):126-38.

- [181] Han L, Zhang Y, Zhang Y, Shu Y, Chen X-W, Wang J-H. A magnetic polypyrrole/iron oxide core/gold shell nanocomposite for multimodal imaging and photothermal cancer therapy. *Talanta* 2017;171:32-38.
- [182] El-Sayed IH, Huang X, El-Sayed MA. Surface plasmon resonance scattering and absorption of anti-EGFR antibody conjugated gold nanoparticles in cancer diagnostics: applications in oral cancer. *Nano Lett* 2005;5(5):829-34.
- [183] Chon H, Lee S, Son SW, Oh CH, Choo J. Highly sensitive immunoassay of lung cancer marker carcinoembryonic antigen using surface-enhanced Raman scattering of hollow gold nanospheres. *Anal Chem* 2009;81(8):3029-34.
- [184] Cormode DP, Skajaa T, van Schooneveld MM, Koole R, Jarzyna P, Lobatto ME, et al. Nanocrystal core high-density lipoproteins: a multimodality contrast agent platform. *Nano Lett* 2008;8(11):3715-23.
- [185] Raghavendra R, Arunachalam K, Annamalai SK, Aarrthy AM. Diagnostics and therapeutic application of gold nanoparticles. *Int J Pharm Pharm Sci* 2014;6(2):74-87.
- [186] Lee SE, Sasaki DY, Perroud TD, Yoo D, Patel KD, Lee LP. Biologically functional cationic phospholipid– gold nanoplasmonic carriers of RNA. *J Am Chem Soc* 2009;131(39):14066-74.
- [187] Koonce NA, Quick CM, Hardee ME, Jamshidi-Parsian A, Dent JA, Paciotti GF, et al. Combination of gold nanoparticle-conjugated tumor necrosis factor- $\alpha$  and radiation therapy results in a synergistic antitumor response in murine carcinoma models. *Int J Radiat Oncol Biol Phys* 2015;93(3):588-96.
- [188] Thakkar KN, Mhatre SS, Parikh RY. Biological synthesis of metallic nanoparticles. *Nanomedicine* 2010;6(2):257-62.
- [189] Suman T, Rajasree SR, Ramkumar R, Rajthilak C, Perumal P. The Green synthesis of gold nanoparticles using an aqueous root extract of *Morinda citrifolia* L. *Spectrochim Acta A Mol Biomol Spectrosc* 2014;118:11-16.
- [190] Singh M, Harris-Birtill DC, Zhou Y, Gallina ME, Cass AE, Hanna GB, et al. Application of gold nanorods for photothermal therapy in ex vivo human oesophagogastric adenocarcinoma. *J Biomed Nanotechnol* 2016;12(3):481-90.
- [191] Singh C, Sharma V, Naik PK, KHandelwal V, Singh H. A green biogenic approach for synthesis of gold and silver nanoparticles using *Zingiber officinale*. *Dig J Nanomater Biostruct* 2011;6(2):535-42.

- [192] Stasyuk N, Gayda G, Serkiz R, Gonchar M. The green” synthesis of gold nanoparticles by the yeast *Hansenula polymorpha*. Вісник Львівського університету Серія біологічна. 2016;73:96-102.
- [193] Seo S-H, Kim B-M, Joe A, Han H-W, Chen X, Cheng Z, et al. NIR-light-induced surface-enhanced Raman scattering for detection and photothermal/photodynamic therapy of cancer cells using methylene blue-embedded gold nanorod@ SiO<sub>2</sub> nanocomposites. *Biomaterials* 2014;35(10):3309-18.
- [194] Sengani M, Grumezescu AM, Rajeswari VD. Recent trends and methodologies in gold nanoparticle synthesis—a prospective review on drug delivery aspect. *OpenNano* 2017;2:37-46.
- [195] Salunke GR, Ghosh S, Kumar RS, Khade S, Vashisth P, Kale T, et al. Rapid efficient synthesis and characterization of silver, gold, and bimetallic nanoparticles from the medicinal plant *Plumbago zeylanica* and their application in biofilm control. *Int J Nanomedicine* 2014;9:2635-53
- [196] Saha K, Agasti SS, Kim C, Li X, Rotello VM. Gold nanoparticles in chemical and biological sensing. *Chem Rev* 2012;112(5):2739-79.
- [197] Ramakrishna M, Babu DR, Gengan RM, Chandra S, Rao GN. Green synthesis of gold nanoparticles using marine algae and evaluation of their catalytic activity. *J Nanostructure Chem* 2016;6(1):1-13.
- [198] Prema P, Iniya P, Immanuel G. Microbial mediated synthesis, characterization, antibacterial and synergistic effect of gold nanoparticles using *Klebsiella pneumoniae* (MTCC-4030). *RSC Adv* 2016;6(6):4601-7.
- [199] Pissuwan D, Niidome T, Cortie MB. The forthcoming applications of gold nanoparticles in drug and gene delivery systems. *J Control Release* 2011;149(1):65-71.
- [200] Park K, Hsiao M-s, Yi Y-J, Izor S, Koerner H, Jawaid A, et al. Highly concentrated seed-mediated synthesis of monodispersed gold nanorods. *ACS Appl Mater Interfaces* 2017;9(31):26363-71.
- [201] Parida S, Maiti C, Rajesh Y, Dey KK, Pal I, Parekh A, et al. Gold nanorod embedded reduction responsive block copolymer micelle-triggered drug delivery combined with photothermal ablation for targeted cancer therapy. *Biochim Biophys Acta Gen Subj* 2017;1861(1-A):3039-52.
- [202] Vega-Villa KR, Takemoto JK, Yáñez JA, Remsberg CM, Forrest ML, Davies NM. Clinical toxicities of nanocarrier systems. *Adv Drug Deliv Rev* 2008;60(8):929-38.

- [203] Carnovale C, Bryant G, Shukla R, Bansal V. Identifying Trends in Gold Nanoparticle Toxicity and Uptake: Size, Shape, Capping Ligand, and Biological Corona. *ACS Omega* 2019;4(1):242-56.
- [204] Schmid G, Kreyling WG, Simon U. Toxic effects and biodistribution of ultrasmall gold nanoparticles. *Arch Toxicol* 2017;91(9):3011-37.
- [205] E Connor E, Mwamuka J, Gole A, Murphy C, Wyatt M. Gold Nanoparticles Are Taken Up by Human Cells but Do Not Cause Acute Cytotoxicity. *Small* 2005;1(3):325-27.
- [206] Niidome T, Yamagata M, Okamoto Y, Akiyama Y, Takahashi H, Kawano T, et al. PEG-modified gold nanorods with a stealth character for in vivo applications. *J Control Release* 2006;114(3):343-47.
- [207] Kim KT, Zaikova T, Hutchison JE, Tanguay RL. Gold nanoparticles disrupt zebrafish eye development and pigmentation. *Toxicol Sci* 2013;133:275-288.
- [208] Favi PM, Gao M, Johana Sepúlveda Arango L, Ospina SP, Morales M, Pavon JJ, et al. Shape and surface effects on the cytotoxicity of nanoparticles: gold nanospheres versus gold nanostars. *J Biomed Mater Res A* 2015;103(11):3449-62.
- [209] Hutter E, Boridy S, Labrecque S, Lalancette-Hébert M, Kriz J, Winnik FM, et al. Microglial response to gold nanoparticles. *ACS Nano*. 2010;4(5):2595-606.
- [210] Chen H, Wang Z, Ma X, Zong S, Cui Y. Magnetically controllable dual-mode nanoprobe for cell imaging with an onion-like structure. *Talanta* 2013;116:978-84.
- [211] Selim ME, Abd-Elhakim YM, Al-Ayadhi LY. Pancreatic response to gold nanoparticles includes decrease of oxidative stress and inflammation in autistic diabetic model. *Cell Physiol Biochem* 2015;35(2):586-600.
- [212] Coradeghini R, Gioria S, García CP, Nativo P, Franchini F, Gilliland D, et al. Size-dependent toxicity and cell interaction mechanisms of gold nanoparticles on mouse fibroblasts. *Toxicol Lett* 2013;217(3):205-16.
- [213] Truong L, Sali KS, Miller JM, Hutchison JE, Tanguay RL. Persistent adult zebrafish behavioral deficits results from acute embryonic exposure to gold nanoparticles. *Comp Biochem Physiol C Toxicol Pharmacol* 2012;155(2):269-74.
- [214] Guglielmo CD, Lapuente JD, Porredon C, Ramos-López D, Sendra J, Borràs M. In vitro safety toxicology data for evaluation of gold nanoparticles—chronic cytotoxicity, genotoxicity and uptake. *J Nanosci Nanotechnol* 2012;12(8):6185-91.
- [215] Shrivastava R, Kushwaha P, Bhutia YC, Flora S. Oxidative stress following exposure to silver and gold nanoparticles in mice. *Toxicol Ind Health* 2016;32(8):1391-404.

- [216] Bednarski M, Dudek M, Knutelska J, Nowiński L, Sapa J, Zygmunt M, et al. The influence of the route of administration of gold nanoparticles on their tissue distribution and basic biochemical parameters: in vivo studies. *Pharmacol Rep* 2015;67(3):405-9.
- [217] Tournebize J, Boudier A, Joubert O, Eidi H, Bartosz G, Maincent P, et al. Impact of gold nanoparticle coating on redox homeostasis. *Int J Pharm* 2012;438(1-2):107-16.

Journal Pre-proof

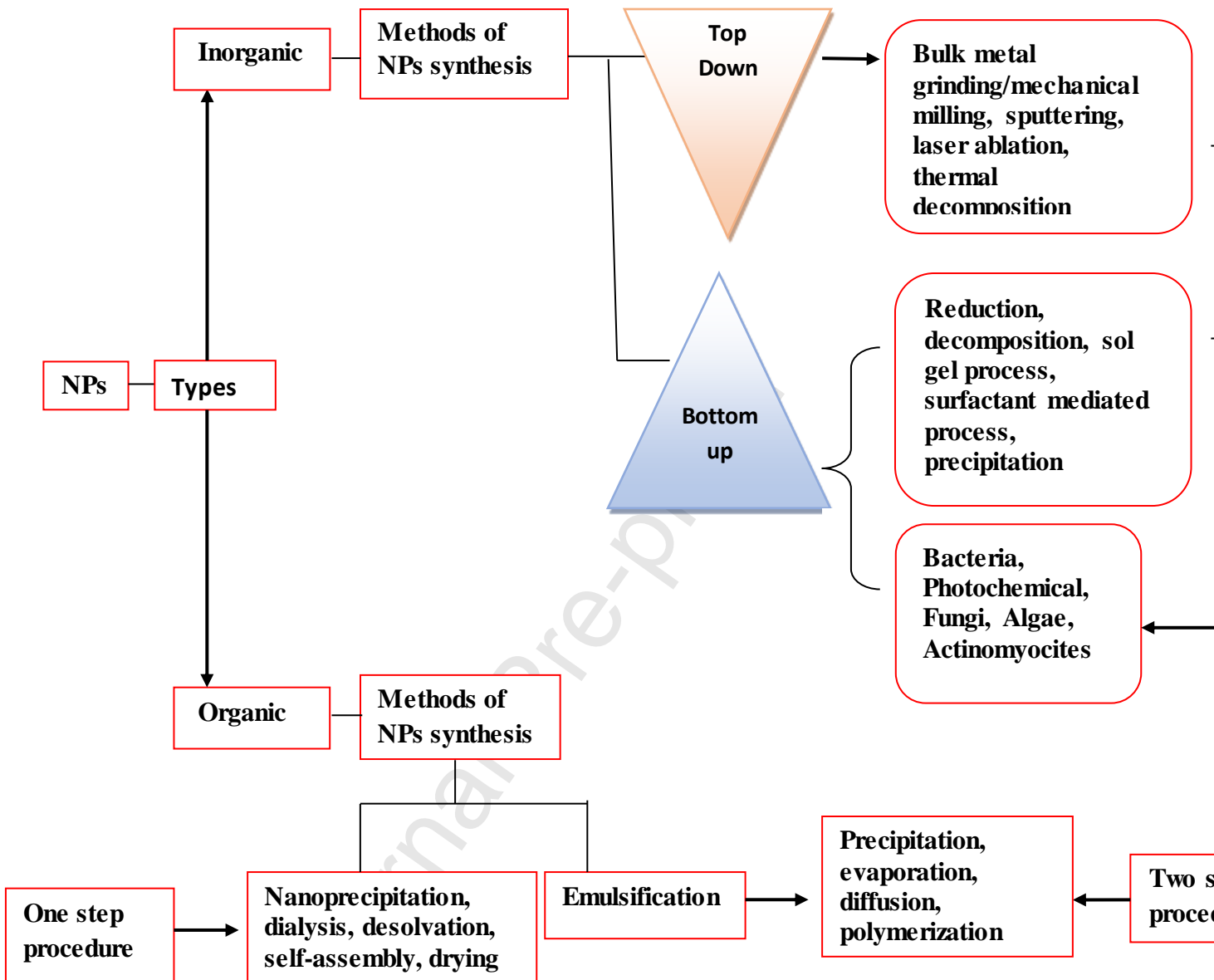


**Conflict of interest**

This review did not receive any specific grant from funding agencies in the public, commercial, or not-for-profit sectors. Authors declare no conflict of interest.

\*Sachin Kumar Singh

Journal Pre-proof



Overall scheme for synthesis of AuNPs involving top down and bottom up approach

**Article highlights**

- Turkevich, Brust-Schiffrin, seeded growth, sonochemical and green methods are mainly used to prepare AuNPs.
- UV-Visible, NMR and mass spectroscopy are used for chemical characterization of AuNPs
- Dynamic light scattering, TEM and AFM and X-ray diffraction studies are used for physical characterization.
- Optical and physio-chemical properties of AuNPs offer their application in targeted therapies and imaging.
- Toxicity of nanoparticles depends upon their size, shape and capping ligand.